UNIVERSIDADE DE LISBOA
FACULDADE DE CIÊNCIAS
DEPARTAMENTO DE BIOLOGIA ANIMAL

The molecular mechanisms of Autosomal Dominant Polycystic Kidney Disease

Inês Matos de Oliveira

Mestrado em Biologia Humana e Ambiente

Dissertação orientada por:
Doutora Mónica Roxo-Rosa
Prof.ª Doutora Ana Maria Crespo

2018

AGRADECIMENTOS

Em primeiro lugar, gostaria de agradecer à Doutora Mónica Roxo-Rosa por ter aceite ser minha orientadora e pela oportunidade de poder trabalhar neste projeto que me permitiu elaborar a tese de mestrado. Mais que isso, obrigada por todo o conhecimento transmitido, conselhos profissionais e de vida, por toda a ajuda, apoio e dedicação que nunca faltaram durante todo este processo. Por toda a paciência durante as revisões e pelas palavras de força e apoio nas alturas mais difíceis. Na função de orientadora, as minhas expectativas foram excedidas e sinto-me verdadeiramente afortunada por ter podido trabalhar e ser orientada por uma cientista tão trabalhadora, empenhada e talentosa.

Gostava também de agradecer à Doutora Susana Lopes por me ter aceite como aluna de mestrado no seu laboratório, *Cilia Regulation and Disease*, pelas palavras amigas e por todo o apoio prestado.

À Sociedade Portuguesa de Nefrologia pelo apoio financeiro no projeto.

À Professora Doutora Ana Crespo por ter aceite ser a minha co-orientadora e por toda a disponibilidade e apoio dispensados.

A todo o *staff* da *Fish Facility*, Fábio V., Petra P. e Andreia C., por toda a ajuda durante as experiências, pelo esclarecimento de quaisquer dúvidas que tivesse e por todos os conselhos.

À Cláudia A. pela disponibilidade e por todo o auxílio incansável nas experiências de citometria de fluxo.

A todos os outros elementos do laboratório, à Raquel J. por todos os conselhos e ajuda sempre que precisei; à Margarida R., à Catarina B., ao Filipe T., ao Pedro S., à Sara P., à Bárbara T. por toda a ajuda e pelos momentos divertidos nas pausas das experiências e do trabalho.

Por último, mas não menos importante, gostava de agradecer à minha família, em especial ao meu pai, à minha mãe e à minha irmã, por todo o seu apoio durante esta etapa da minha vida. Aos meus amigos, em particular à Rita M. pela ajuda e partilha das suas experiências enquanto também aluna de mestrado. E ao Ricardo G., o meu pilar, pelo encorajamento, por nunca me deixar desistir e por todo o apoio incondicional em qualquer que fosse o momento.

Esta foi uma etapa de grande aprendizagem, de grande crescimento profissional e pessoal, pela qual estou muito grata e que não teria sido possível sem todos vocês.

SUMÁRIO

A Doença Poliquística Renal Autossómica Dominante (ADPKD do inglês *Autosomal Dominant Polycystic Kidney Disease*) é a causa genética mais comum e a 4ª principal causa de insuficiência renal no mundo, com uma prevalência de 1 em cada 400 a 1000 indivíduos[1]. Esta doença é causada por mutações nos genes *PKD1* (em 85% dos casos) ou *PKD2* (nos restantes 15%), os quais codificam as proteínas policistina-1 (PKD1) e policistina-2 (PKD2), respetivamente[2]. Ambas estão presentes nos cílios (em cílios primários, nos humanos), funcionando a PKD1 como um mecanosensor dos estímulos extracelulares[3] e a PKD2 como canal não seletivo de Ca^{2+} [4]. Estas interagem uma com a outra, formando um complexo mecanosensitivo que é essencial para a regulação da homeostase do Ca^{2+} [5]. Quando afetadas, o processo de cistogénese é desencadeado[6].

A principal manifestação clínica desta doença é o desenvolvimento de múltiplos quistos renais cheios de fluído que vão crescendo em número e tamanho ao longo da vida dos pacientes. Os quistos vão substituindo o parênquima saudável do rim levando ao decréscimo da função renal[7]. As manifestações extra-renais mais comuns são o desenvolvimento de quistos no fígado e pâncreas e problemas vasculares[8]. A severidade da doença varia consoante o gene afetado, sendo que geralmente, os doentes com mutações associadas no gene PKD1 têm os fenótipos mais graves[9,10].

Na ADPKD existem diversas vias de sinalização alteradas, sendo as principais a do Ca^{2+} e do AMP cíclico (cAMP). A homeostase do Ca^{2+} encontra-se alterada, sendo que os seus níveis intracelulares são bastante mais baixos que os fisiológicos. Estas modificações provocam por sua vez um aumento dos níveis de cAMP, quando comparados com os níveis fisiológicos[8]. Os níveis elevados de cAMP levam à hiperestimulação da proteína responsável pelo insuflamento dos quistos, a CFTR (do inglês *Cystic Fibrosis Transmembrane conductance Regulator*). Esta é uma proteína membranar que atua como um canal de Cl^- e que nas células epiteliais dos quistos promove a secreção de Cl^-, funcionando como força motriz para a entrada de água para o lúmen dos mesmos[11,12]. Contudo, o impacto da falta das policistinas na CFTR não está ainda bem clarificado, conduzindo-nos à questão: poderá o impacto ser apenas ao nível da atividade da CFTR ou também afetará os níveis de expressão ou ainda estabilidade da proteína na membrana? Assim, o principal objetivo deste trabalho foi contribuir para o conhecimento dos mecanismos subjacentes a este processo.

Para responder a esta questão o modelo usado foi a Vesícula de *Kupffer* (KV do inglês *Kupffer's Vesicle*) do peixe-zebra, órgão que foi anteriormente sugerido pelo nosso grupo como sendo um modelo adequado para estudar os mecanismos moleculares através dos quais os reduzidos níveis de PKD2 levam à anormal ativação da CFTR. Apesar de não ser um órgão relacionado com o rim ou com a função renal, a KV tem algumas semelhanças com um quisto de ADPKD. Como por exemplo o facto de a falta de PKD2 causar um aumento do seu volume e este ser devido à anormal estimulação da CFTR[13]. Em embriões de peixe-zebra, para efetuar o *knockdown* de uma proteína, estes são injetados (no estadio de uma célula) com oligómeros específicos, designados por *morpholinos*, que bloqueiam a tradução do mRNA alvo.

A linha de peixe-zebra usada para este estudo foi a linha transgénica *TgBAC(cftr-GFP)pd1041*[14] uma vez que, devido à fusão da proteína CFTR com GFP, esta dá-nos a possibilidade observar diretamente a influência dos baixos níveis de PKD2 na CFTR. A expressão de CFTR-GFP foi seguida por esteromicroscopia de fluorescência desde o estadio de 70% de epibolia até aos 12 dias após a fertilização. Na janela temporal usada para a execução das experiências, de 8 a 10 sómitos, a expressão de CFTR-GFP foi apenas detetada na região da KV, como anteriormente descrito[14] e manteve-se assim

até ao desaparecimento da KV. Após esse período a expressão só foi novamente detetada a partir dos 5 dias, nos ductos pancreáticos e na vesicula biliar. Por microscopia confocal em embriões vivos, foi varrida toda a KV de embriões *TgBAC(cftr-GFP)pd1041* não injetados e embriões *morphants* para a PKD2 (pertencentes à mesma postura). De seguida, com recurso a um software, os volumes das KVs foram medidos e a fluorescência avaliada. Os volumes dos *morphants* para a PKD2 revelaram-se superiores aos volumes dos embriões não injetados, tal como descrito pelo nosso grupo[13]. A fluorescência avaliada por este método também se verificou mais elevada nos *morphants* para a PKD2, tanto na medição efetuada em toda a KV como nas medições feitas apenas na membrana apical da mesma. Estes dados foram posteriormente corroborados por citometria de fluxo.

Os resultados obtidos são sugestivos de uma maior expressão de CFTR-GFP quando a PKD2 se encontra em níveis residuais. Contudo, uma análise comparativa de *microarray* efetuada pelo nosso grupo entre células da KV de embriões normais, de *morphants* para a PKD2 e de *morphants* para a CFTR (dados ainda não publicados[15]), não revelou a existência de alterações dos níveis transcricionais de CFTR quando a PKD2 se encontrava em níveis reduzidos. Assim, os resultados obtidos levam-nos a sugerir que uma maior estabilidade da proteína. Esta hipótese é apoiada pelos resultados obtidos na análise de fluorescência na membrana apical, que nos sugerem uma maior quantidade de CFTR-GFP na membrana de embriões *morphants* para a PKD2.

Na mesma análise comparativa de *microarray* foi também possível a identificação de alvos comuns para a PKD2 e para a CFTR, nomeadamente genes que codificavam diversos enzimas do metabolismo dos esfingolípidos (dados ainda não publicados[15]). Este resultado sugere que a diminuição dos níveis de PKD2 afeta a homeostase celular dos esfingolípidos, uma hipótese apoiada por estudos referentes à acumulação de dois tipos de esfingolípidos em pacientes de ADPKD [16,17]. Existem também referências na literatura que associam a CFTR a este metabolismo[18,19], pelo que se tornou relevante para nós aprofundar esta matéria. O outro grande objetivo deste trabalho foi então apurar em que medida as alterações no metabolismo dos esfingolípidos podem afetar a CFTR. Por citometria de fluxo e usando a mesma linha transgénica de peixe-zebra a influência de alterações do metabolismo dos esfingolípidos na CFTR-GFP foi avaliada. Para tal, foram comparados embriões incubados com 50 µM de Miriocina (um inibidor do primeiro passo do metabolismo dos esfingolípidos), embriões incubados com 0,5% de DMSO (usados como controlo) e embriões sem qualquer tratamento. Após 4 repetições da experiência e a análise dos resultados, não foi obtida qualquer diferença nos níveis de fluorescência de CFTR-GFP destes três grupos. Considerámos, no entanto, que estes resultados requerem uma confirmação futura a alguns problemas técnicos no decorrer da experiência.

Contudo, como a CFTR também é extensamente estudada em células de mamífero, decidimos investigar a influência da Miriocina na CFTR, em células HEK293-CFTR. Estas células estavam estavelmente transduzidas com wtCFTR[20] e segundo a nossa análise de *western-blot* expressam também endogenamente a PKD2. Por imunofluorescência foi avaliada a influência da Miriocina na localização subcelular da CFTR. Comparando as diferentes amostras (controlo, incubação durante uma noite com 100 nM de Miriocina e a incubação com 20 µM de Miriocina durante 2 e 4 horas) verificámos algumas diferenças na localização da CFTR. Sendo estas: vesículas que aparentavam estar a sair das células, a acumulação de CFTR na membrana de algumas células e a acumulação intracelular de CFTR em pequenos aglomerados. O rácio desta distribuição foi calculado para todas as amostras e as diferenças entre os controlos e as diferentes incubações com Miriocina foram avaliadas. O número de vesículas revelou-se mais elevado quando as células eram incubadas com Miriocina, tendo a incubação de 100 nM durante uma noite apresentado as maiores diferenças. A acumulação de CFTR na membrana das células também se mostrou igualmente superior quando estas eram incubadas com Miriocina, sendo que

mais uma vez, a incubação noturna de 100 nM foi a mais relevante. Juntos estes resultados parecem sugerir que quando o metabolismo dos esfingolípidos é afetado, o tráfego da CFTR também o é.

Em conclusão, os reduzidos níveis de PKD2 podem afetar a CFTR não só ao nível da sua atividade, mas possivelmente também ao nível da sua expressão e estabilidade membranar. Adicionalmente o metabolismo dos esfingolípidos pode ter um papel associado a esta influência, pelo que esta hipótese deve ser cuidadosamente avaliada no contexto da ADPKD.

Palavras-chave: Doença Poliquística Renal Autossómica Dominante (ADPKD); Policistina-2 (PKD2); Cystic Fibrosis Transmembrane conductance Regulator (CFTR); peixe-zebra; metabolismo dos esfingolípidos

ABSTRACT

The Autosomal Dominant Polycystic Kidney disease is the most common genetic disorder and the fourth leading cause of renal failure. The cause for this condition are mutations in *PKD1* or *PKD2* genes, which encode the proteins Polycystin-1 and 2, respectively. These, when disrupted, trigger cystogenesis. The main clinical manifestation of ADPKD is, therefore, the development of massive fluid filled kidney cysts, whose inflation is mediated by CFTR (Cystic Fibrosis Transmembrane conductance Regulator). Abnormal activation of CFTR has been reported to occur in cyst-lining cells in response to their increased intracellular cAMP levels. But, is this exclusively dependent on enhanced activity or does it also involve higher expression levels of CFTR? The main objective of this study was to contribute to the knowledge of the underlying mechanisms of this process. We used as working model the zebrafish Kupffer's Vesicle (KV), an organ that was previously showed by our group as suitable to study the inflation of ADPKD cysts. Mimicking them, the knockdown of PKD2 causes a CFTR-mediated enlargement of the KV. The zebrafish line used in this study was the transgenic *TgBAC(cftr-GFP)pd1041* which provides a KV specific GFP-reporter, since at these early stages of development CFTR-GFP was only detected in KV-lining cells. To perform the PKD2 knockdown, *TgBAC(cftr-GFP)pd1041* embryos were injected at their one-cell stage with an antisense MO against *pkd2* mRNA. Using confocal live-microscopy and flow cytometry, the mean fluorescence intensity of both PKD2 knocked down and non-injected embryos was determined. The obtained results were indicative of a higher expression of CFTR-GFP in the KV, namely at its apical membrane, when PKD2 is downregulated. However, we knew from a previous microarray analysis of the lab (unpublished data) that lower levels of PKD2 did not change CFTR transcriptional levels. Thus, our data point to an enhanced stability of CFTR at the cell membrane.

Results from the mentioned microarray analysis also revealed PKD2 and CFTR common gene targets. Among these were enzymes from the sphingolipid metabolism. Although in a different context, the association between CFTR and the sphingolipid metabolism has been already reported. To better understand this, the impact of the sphingolipid metabolism impairment by Myriocin on CFTR was evaluated. Flow cytometry results performed with *TgBAC(cftr-GFP)pd1041* embryos indicated no impact in the CFTR-GFP amounts. Yet, preliminary results of *in vitro* assays using HEK293 stably transduced with wild type CFTR, suggest changes of the intracellular trafficking of CFTR. In a near future, we aim to evaluate both parameters in the knockdown of PKD2.

Together our results suggest that the absence of PKD2 is indeed, directly or through changes in the sphingolipid metabolism, enhancing the stability of CFTR.

Keywords: Autosomal Dominant Polycystic Kidney (ADPKD); Polycystin-2 (PKD2); Cystic Fibrosis Transmembrane conductance Regulator (CFTR); sphingolipid metabolism; Kupffer's Vesicle (KV).

TABLE OF CONTENTS

INDEX OF FIGURES

LIST OF ABBREVIATIONS

AC	Adenyl Cyclase
ACE	Angiotensin-Converting Enzyme
ADPKD	Autosomal Dominant Polycystic Kidney Disease
AVP	Arginine Vasopressin
cAMP	3',5'-cyclic Adenosine Monophosphate
Cas9	CRISPR associated protein 9
CF	Cystic Fibrosis
cftr	Cystic Fibrosis Transmembrane conductance Regulator gene
CFTR	Cystic Fibrosis Transmembrane conductance Regulator
COPII	Coat Protein complex II
CKD	Chronic Kidney Disease
CRISPR	Clustered Regularly Interspaced Short Palindromic Repeats
CTT	C-Terminal Tail
DNA	Deoxyribonucleic acid
dpf	Days post fertilization
ER	Endoplasmic Reticulum
ERES	Endoplasmic Reticulum Exit Sites
ERK	Extracellular signal–Regulated Kinases
ESRD	End-Stage Renal Disease
GFR	Glomerular Filtration Rate
GPS	G protein–coupled receptor Proteolytic Site
HEK	Human Embryonic Kidney cells
hpf	Hours post fertilization
KV	Kupffer's Vesicle
MAPK	Mitogen-Activated Protein Kinase
MDCK	Madin-Darby Canine Kidney cells
MO	Morpholino Oligonucleotide
MSD1	Membrane-Spanning Domain-1
MSD2	Membrane-Spanning Domain-2
mTOR	mechanistic Target Of Rapamycin
NBD	Nucleotide-binding domain
NBD1	Nucleotide-binding domain-1

NBD2	Nucleotide-binding domain-2
NHERF	Na+/H+ Exchanger Regulatory Factor
PDE	Phosphodiesterase
PDZ	Resulting name from: wPSD-95 (P), Dlg (D), ZO1 (Z)
PEST	peptide sequence rich in proline (P), glutamic acid (E), serine (S), and threonine (T) residues
PKA	Protein Kinase A
PKD	Polycystic Kidney Disease
pkd1a/b	Polycystic kidney disease 1 a and b zebrafish genes, orthologous for human *PKD1*
Pkd1	Polycystic kidney disease 1 mouse and rat gene
pkd2	Polycystic kidney disease 2 zebrafish and mouse gene
Pkd2	Polycystic kidney disease 2 mouse and rat gene
PKD1	Polycystin-1 human gene
PKD1	Polycystin-1 protein
PKD2	Polycystin-2 human gene
PKD2	Polycystin-2 protein
PM	Plasma Membrane
R-Domain	Regulatory Domain of CFTR
REJ	Receptor Egg Jelly
RNA	Ribonucleic Acid
ss	Somite stage
TKV	Total Kidney Volume
TRP	Transient Receptor Potential channels super-family
TRPP	Transient Receptor Potential Polycystic family, a sub-family of the TRP superfamily
V2R	Vasopressin Receptor-2
Wnt	resulting name of fusion of: the name of the segment polarity gene *wingless* (W) in Drosophila and the vertebrate homolog *integrated (nt)*

1.INTRODUCTION

1.1 – Autosomal Dominant Polycystic Kidney Disease (ADPKD): causes, main clinical manifestations and disease progression

ADPKD is the most common genetic cause of kidney disorder and the fourth leading cause of kidney failure. Occurring worldwide in every race it has a prevalence of 1 in 400 to 1 in 1000[1,21]. It is caused by mutations in *PKD1* (85% of the cases) or *PKD2* (15% of the cases) genes, encoding polycystin-1 (PKD1) and polycystin-2 (PKD2) proteins, respectively[22]. Both genes have a high level of allelic heterogeneity with several mutations reported, varying from hypomorphic to amorphic mutations.(http://pkdb.mayo.edu/index.html)

About 20 years ago, some authors have postulated the existence of a third PKD gene, because of an apparent lack of linkage to either *PKD1* or *PKD2 loci* in a few number of families with ADPKD [23–27]. However, a recent re-analysis of those data, with new sampling, when possible, and mutation screening for PKD1 and PKD2 did not support the existence of such third ADPKD *locus*. Sample contamination and errors in the linkage analysis were indicated as a possible justifications for that misinterpretation[28].

The main clinical manifestation of ADPKD is the development of massive fluid-filled kidney cysts that grow in number and size over time, throughout patients' life (Figure 1.1). These, progressively destroy and replace the healthy renal parenchyma impairing the kidney function[7]. The progress of this disease is mostly settled in 2 key processes, cell proliferation and fluid secretion (towards the cysts lumen)[11]. Extra-renal manifestations include the development of cysts in other organs, namely in liver, pancreas and seminal vesicles[29] and an increased risk of cardiovascular dysfunction[30], hypertension[31], intracranial aneurysms, dolichoectasias, aortic root dilatation and aneurysms, mitral valve prolapse and abdominal wall hernias[32].

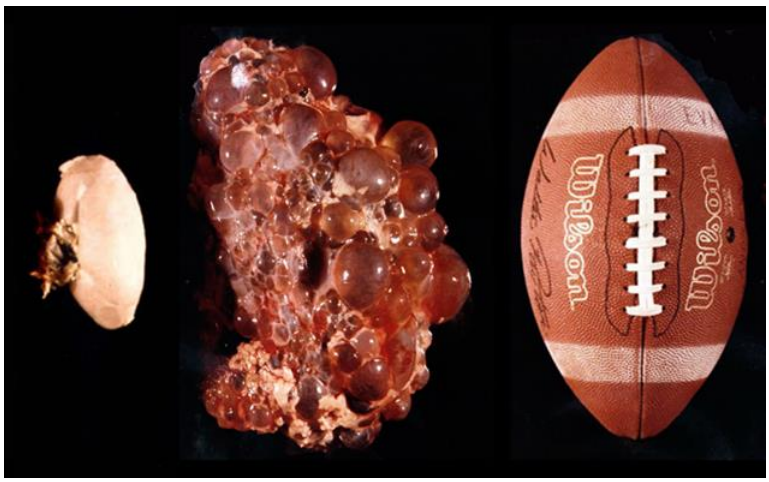

Figure 1.1 – A normal kidney (on the left), an ADPKD kidney (on the middle) and an American football ball (on the right). This image represents the comparison between a normal kidney and an ADPKD kidney, in size and structure. The size that ADPKD kidneys can reach is so exaggerated that can even be compared to the size of an American football ball. Adapted from *http://www.pkdinternational.org/what-is-pkd/adpkd/* and *https://pkdcure.org/31days/*.

Many of the symptoms that the adult ADPKD patients have are consequences of the cysts formation and inflation, which also cause kidney enlargement in about 4 to 6 times the normal size[2]. An important complication of the disease is the cysts rupture with the consequent haemorrhage and

infection. This leads the patients to recurrent antibiotics intake, drainage of the involved cysts and, ultimately, surgical resection[33,34].

The PKD Foundation (https://pkdcure.org/) describes 5 stages for ADPKD, which are assigned according to the progressive kidney damage and decrease of the kidney function, *i.e.*, according to the stage of the Chronic Kidney Disease. This is evaluated based on the glomerular filtration rate (GFR) and some other associated physical symptoms. GFR estimates how much blood passes through the glomeruli on each minute, thus, functioning as a readout of the kidney function. GFR is calculated based on creatinine blood levels, being therefore dependent on patient height, weight and gender, and declining with age. GFRs above 90% are considered to be indicative of normal kidney function. In the first stage of ADPKD, patients have normal GFR but present already signs of milder disease, namely hypertension, urinary infections, haematuria and slightly elevated levels of creatinine. During the second stage, patients have the same mild symptoms but present lower GFR levels, from 60 to 89%. The third stage corresponds to a GFR of 30-59% and moderate symptoms, including fatigue, back pain, loss of appetite, hypertension and abdominal swelling. In the fourth stage, GFR lowers to values between 15-29% and the symptoms turn to be more severe. The patient reaches the fifth stage of the disease when his/her GFR drops to values below 15%, meaning kidney failure. This stage corresponds to the End Stage Renal Disease (ESRD), a time at which patients require dialysis and renal replacement therapy. At this point, patients suffer from severe symptoms as anaemia, headaches, difficulty in concentrating, nausea, vomiting, itching, muscle cramps, change in skin colour and changes in women menstrual cycle (https://pkdcure.org/what-is-pkd/adpkd/what-are-the-stages-of-adpkd/). ADPKD patients represent 9.8% in Europe and 5% in USA of the total ESRD cases[35].

The severity of the kidney disease and extra-renal complications is dependent on the affected gene and on the type of mutation. Overall, *PKD1* mutations are associated to the severest phenotypes, whereas *PKD2* mutations have the best outcomes[9,10]. PKD1-associated patients usually have a higher incidence of extra-renal complications, as hypertension (4 times more prevalent then in PKD2-associated patients) and also a higher risk of kidney failure progression[36,37]. Indeed, it has been estimated that ESRD, in PKD1-associated patients, in average occurs approximately 20 years earlier than in patients with mutations in *PKD2*. About 50% of the PKD1-associated patients reach ESRD by age 54[38]. In contrast, the PKD2-patients median age at onset of ESRD is 69.1 years[36,37]. In 2006, Dicks *et al.* reported the results of a prospective study performed over 22 years on ADPKD patients attending nephrology/urology clinics in Newfoundland (Canada). According to them, on average *PKD1* patients reach ESRD at age 53 and death at age 67, but in *PKD2* patients ESRD was infrequent and their median age to death was 71 years[39].

1.2 – ADPKD Proteins

1.2.1 – PKD1

The *PKD1* gene spans a region of 50 kb in the 16p13.3 region at the chromosome 16[40]. With a mRNA of 14,9 kb, it is composed by 46 exons and 45 introns[41]. Also described are its six pseudogenes (PKD1P1 to PKD1P6)[40]. *PKD1* encodes PKD1, a transmembrane protein of 4302 amino acids (aa) with approximately 462 kDa[42]. It is constituted by a large extracellular N-terminal domain with 3074 aa , 11 transmembrane domains with 1032 aa and a short cytoplasmic C-terminal domain (CTT) with 197 aa[8,40]. So far, more than 2300 mutations were found to be associated with the *PKD1* gene. From these, 2323 are germline mutations and 9 are somatic. Among these, 856 were reported as being clinically neutral. However, which of these types are more frequent is not known (http://pkdb.mayo.edu).

PKD1 is expressed in epithelial cells of renal tubules[43], liver, heart, bone and exocrine glands[43]. More precisely, it is localized along the primary cilia membrane and at thigh and adherent junctions, desmosomes and focal adhesions of the cell membrane[32]. Higher PKD1 protein levels have been described for immature kidney tissues during fetal development, when compared to that of adult tissues[44]. PKD1 acts as a mechanosensor for the extracellular stimuli, sensing the signals through the primary cilia. It transduces them, thus regulating the cellular proliferation, adhesion, differentiation and morphology[3].

The N-terminal domain has several important motifs involved in protein-protein interactions or protein-carbohydrate interactions. These are: cysteine-flanked leucine-rich repeats; the cell-Wall integrity and Stress response Component domain; the C-type lectin domain; the low-density lipoprotein-A; 16 immunoglobulin-like PKD domains; the receptor for egg jelly module; and the G protein–coupled receptor Proteolytic Site (GPS)[45,46]. PKD1 CTT has several potential phosphorylation sites. It is thought to mediate protein interactions both through its G protein–binding activation site and its coiled-coil domain. The latter one is required for PKD1 interaction with the C-terminal of PKD2 (Figure 1.2). It also contains a sequence rich in proline (P), glutamic acid (E), serine (S), and threonine (T) residues, the PEST sequence, that might facilitate its ubiquitin-mediated degradation[45].

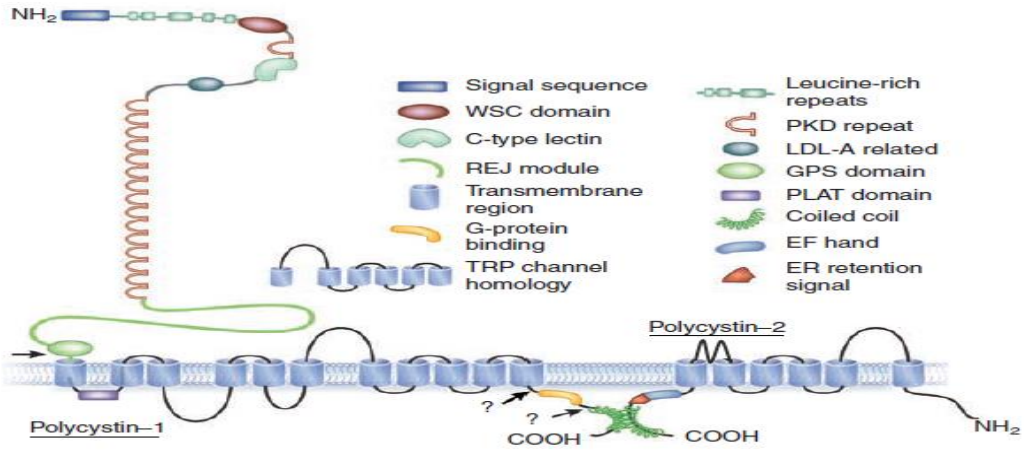

Figure 1.2 - Polycystin-1 and Polycystin-2 interaction via their C-terminal tails. Representation of their domains. The black arrows indicate PKD1 cleavage sites. cell-Wall integrity and Stress response Component (WSC); Receptor Egg Jelly (REJ); Transient Receptor Potential (TRP); Polycystic Kidney Disease domain (PKD); Low Density Lipoprotein A (LDL-A); G protein–coupled receptor Proteolytic Site (GPS); Polycystin-1, Lipoxygenase, Alpha-Toxin (PLAT); Endoplasmic Reticulum (ER). Adapted from Torres & Harris, 2009 [8].

To be fully functional PKD1 must undergo N-terminal cleavage, which is dependent on the Receptor for Egg Jelly and occurs at the GPS. The originated fragments are an N-terminal fragment that has ~325 kDa and remains tethered to the cell surface, and a C-terminal fragment with ~150 kDa[47]. A study in mammalian cells (Madin Darby Canine Kidney cells, line MDCK^{PKD1Zeo}) showed that GPS seems to play a crucial role in PKD1 biological function. Indeed, *PKD1*-missense mutations at this domain or at the Receptor for Egg Jelly prevent the PKD1 cleavage and result in loss of the tubulogenic properties of PKD1. The cells with this mutations tend to form cyst-like structures instead of tubules as occur in cells with the WT form of PKD[47].

Despite of its relevance for the function of the protein, not all PKD1 molecules undergo cleavage, generating a heterogeneous population of full-length and GPS-cleaved PKD1 proteins. The GPS cleavage occurs immediately after the PKD1 synthesis and the resulting fragments remain not-covalently bound[48]. An additional proteolytic cleavage may, however, occur releasing the CTT of about

34 kDa. *In vivo* studies using mouse models showed that this fragment accumulates in the nucleus of epithelial cells from nephron distal tubules, in response to decreased fluid flow, which may be important for the activation of the activator protein 1 pathway[49]. Activator protein 1 is a transcription factor that controls a number of cellular processes including differentiation, proliferation and apoptosis[50]. It was demonstrated that this CTT cleavage and its translocation to the nucleus is dependent and stimulated by the presence of functional PKD2[51].

A third cleavage may also occur releasing the C-terminal half of the CTT, a fragment with about 14 kDa, which interacts with the transcription factor STAT6 and the coactivator P100, stimulating STAT6-dependent gene expression. This was observed under no-flow conditions. Moreover, human ADPKD cyst-lining cells showed increased levels of this 14 kDa CTT fragment in the nucleus[45].

1.2.2 – PKD2

PKD2 is situated in the region 4q21 at chromosome 4 where it spans a 70 kb region[8]. This gene has 16 exons and 15 introns and a mRNA with 5,08 kb (https://www.ncbi.nlm.nih.gov/gene/5311). Until now 248 germline mutations and 27 somatic mutations were found to be associated with this gene. Among which 59 have been reported as clinically neutral (http://pkdb.mayo.edu/). The gene product PKD2 is a protein with 968 aa and with approximately 110 kDa[8]. PKD2 acts non-selective Ca^{2+} permeable cation channel belonging to the Transient Receptor Potential Polycystic (TRPP) subfamily of the superfamily of Transient Receptor Potential (TRP) cation channels. It has a short intracellular N-terminal cytoplasmic region, six transmembrane domains, that are homologous to the PKD1 transmembrane domain, and a short C-terminal intracellular tail[40]. PKD2 has been classified as the most distant member of the TRP channels because of its larger extracellular sequence between transmembrane domains 1 and 2 (Figure 1.2). Suggesting an important structural or functional role for this sequence, 15 ADPKD causing missense mutations were described for this sequence[52]. The PKD2 C-terminal has a coiled-coil domain through which it interacts with PKD1; an Endoplasmic Reticulum (ER) retention signal; and E and F helices loop structure (EF-hand) motif which binds to Ca^{2+}, mediates responses to perturbations in Ca^{2+} levels and also has an important role in channel gating modulation[53];

During development, PKD2 is expressed in epithelial cells of pancreas, liver, lung, bowel, brain, reproductive organs, placenta, and thymus[54]. In zebrafish and mouse embryos, it was also detected in the organs responsible for the establishment of the Left-Right asymmetry of the internal organs distribution[55,56]. In adults, PKD2 is mainly expressed in epithelial tissues from the medullary and cortical collecting ducts and in the distal convoluted tubules of kidneys[54]. Additionally, it was also described to be expressed in ovary, testis, small and large intestine tissues[57]. Moreover, PKD2 is also known to be present, in mammalian models, in endothelial cells of mesenteric arteries (in Sprague-Dawley rats injected with lenti-$TRPP2^{D511V}$)[58] and in smooth muscle cells of cerebral arteries ($TRP2^{+/-}$ C57BL/6J mice)[59] and aorta (Vascular smooth muscle cells from pig aorta)[60], suggesting an important role in the cardiovascular system [30]. At the cellular level, PKD2 is localized in the cilia membrane, basal bodies, plasma membrane (PM), cell-cell junctions, mitotic spindles and ER[4,30].

PKD2 functions as a Ca^{2+}-regulated cation channel[4]. It is regulated by a variety of stimuli including internal or external Ca^{2+} levels, voltage (since it is a TRP), pH, membrane stretching and phosphorylation[61]. It is thought that, depending on its subcellular localization, PKD2 function can be different and adapted. In the PM, it is a receptor-operated non-selective cation channel. In the ER, PKD2 functions as a Ca^{2+}-channel, releasing Ca^{2+} to the cytoplasm in response to fluctuations on it. And in primary cilia, PKD2 together with PKD1 act as a mechanosensitive channel[62]. This complex is essential

for the regulation of Ca^{2+} homeostasis. By sensing the urine flow in the renal tubular lumen, PKD1 is thought to trigger a Ca^{2+} influx through PKD2, raising the intraciliary Ca^{2+} levels. This Ca^{2+} wave stimulates the release of more Ca^{2+} from the ER storages in a PKD2-dependent manner[5]. Nevertheless, this hypothesis has been recently under discussion. Delling *et al.* claim that, if the mechanosensation has origin in the primary cilia, it does not occur via Ca^{2+} signalling. Using various cells types from a transgenic mouse (*Arl13b–mCherry–GECO1.2*), among which were kidney epithelial cells, the Ca^{2+} influx through the primary cilia was not observed under physiological and supraphysiological levels of fluid flow. They reported that the Ca^{2+} wave detected had its start in the cytoplasm and only then was propagated into the primary cilium[63], the opposite path of the classical hypothesis .

PKD2 is also thought to interact with other channels and cytoskeletal proteins, for example: pericentrin (required for assembly of primary cilia), collectrin (involved in intracellular and ciliary movement of vesicles and membrane proteins), kinesin family member 3A (Bind and regulate the activity of PKD2 in primary cilia) and kinesin family member 3B (links PKD2 and fibrocystin, mediating the regulation of PKD2 by fibrocystin), fibrocystin (prevents PKD2 downregulation), tropomyosin-1 (possibly stabilizes PKD2 at the membrane), α1 and α2-actinins (stimulate PKD2 channel activity), Epidermal Growth Factor Receptor (activates PKD2), among many others[8,64].

1.2.2.1 – PKD2 influence in left-right organ asymmetry

During vertebrates' embryonic development there is a transient organ that is important to the correct establishment of the organs asymmetry, the left-right organizer. This organ, the Node in mouse and the Kupffers' Vesicle in zebrafish, is lined by both motile and immotile cilia[65,66]. It has been suggested that immotile cilia sense the directional fluid flow generated by motile cilia. This directional fluid-flow is crucial for the activation of the *Nodal* signalling, a gene expression cascade that occurs in embryonic tissues determining the correct positioning of the internal organs. This is conserved among vertebrates. Therefore, by perturbing the normal physiology of the left-right organizer, the positioning of the thoracic and abdominal organs becomes altered[65,67]. Thus, instead of having the correct arrangement (*situs solitus*), the internal organs end up in a mirror position (*situs inversus*) or in all other abnormal combinations (heterotaxia). Left-right defects also occur in humans with several complications associated which vary in severity depending on the organ position alterations. These include cardiovascular[68], respiratory and infertility problems[69].

Showing the relevance of PKD2 in this process, *pkd2* zebrafish mutants (cup^{tc321})[56] and *pkd2*-null mouse embryos ($Pkd2^{+/-LacZ+/-}$)[55] showed left-right defects. The link between PKD2 and left-right patterning is, however, weak. Indeed, as far as we know only 4 ADPKD patients belonging to different families were reported to have PKD2 mutations and Left-Right defects[70,71].

1.2.2.2 – Cilia

Cilia are slim micro-tubular-based organelles, present in eukaryotic cells from the simplest unicellular organisms to the more complex ones, including humans[72]. Indeed, the machinery of the intraflagellar transport required for cilia assembly and maintenance is highly conserved among species[73]. Cilia are formed from a centriolar anchor, the basal body, and extend from the surface of the cell. It functions as a sensor to extracellular signals such as light, chemicals, proteins or even mechanic stimuli[74] and transduces these signals into the cell[72]. There are two types of cilia, motile and immotile (or primary cilia) which differ in their internal structure. The axoneme of a typical motile cilium has a ring of nine

outer microtubule doublets and a central pair of microtubules, the so called 9+2 configuration (Figure 1.3). This type of cilia has additional proteins that are important for the generation of movement. Among the best studied are the radial spokes, nexins and outer and inner dynein arms (Figure 1.3)[75]. Cilia motility is ensured by the activation of inner and outer dynein arms, through ATP hydrolysis in their ATPase domains. In this way, cilia beat in a rhythmic mode generating fluid flow across an epithelial surface or propelling cell movement[75,76]. Immotile or primary cilia lack the central pair, being thus described as 9+0 configuration (Figure 1.3). Furthermore, these cilia do not have none of the mentioned proteins associated to the movement generation. Although they do not move, primary cilia bend in response to flow or mechanical stress. There are however exceptions to the classical 9+0 configuration of primary cilia and the 9+2 configuration of motile cilia[75]. An example of that is 9+0 configuration of motile cilia (Figure 1.3) of the mouse node that beat in a circular motion generating a directional flow[77].

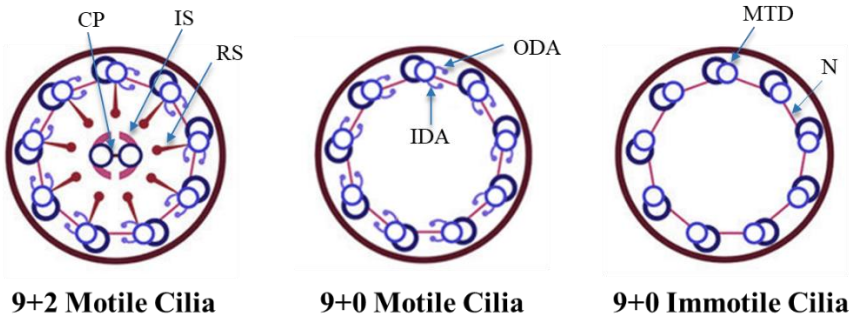

Figure 1.3 - Schematic representation of the Internal structure of motile (9+2 and 9+0) and immotile (9+0) cilia. Central pair of microtubules (CP), inner sheath (IS), radial spokes (RS), inner dynein arms (IDA), outer dynein arms (ODA), microtubules doublets (MTD), nexin(N). Adapted from Sedykh *et al*. 2016 [78].

The importance of these organelles has been highlighted by the number of genetic diseases caused by mutations that affect the cilia structure and function, the so called ciliopathies. ADPKD has been included in this group of diseases[74,76].

PKD1 and PKD2 are thought to be part of the cilia signalling proteins, a subset that is required to the homeostasis of the renal epithelia. The steady state of the physiological roles of PKD1 and PKD2 regulates the cilium-dependent signalling pathways, triggering responses of nephron tubules adaptation to either chemical or mechanical signals[79]. So, in the absence or malfunction of any of these two proteins, such signalling pathways are affected leading to the kidney cyst formation[76].

1.3- ADPKD Pathophysiology and Cystogenesis

ADPKD cysts may arise in distinct nephron segments including the glomerulus, loop of Henle and Bowman's capsule (Figure 1.4). However it is accepted that the majority of them derive from the collecting ducts[2]. Indeed, a study in human ADPKD kidney tissues showed bigger and more cysts in collecting ducts[80]. Also, ADPKD mouse models ($Pkd1^{nl/nl}$, $Pkd2^{WS25/-}$, $Pkd2^{WS25/WS25}$) showed a predominant presence of cysts in collecting ducts, loops of Henle and distal tubules in postnatal to young animals[81–83].

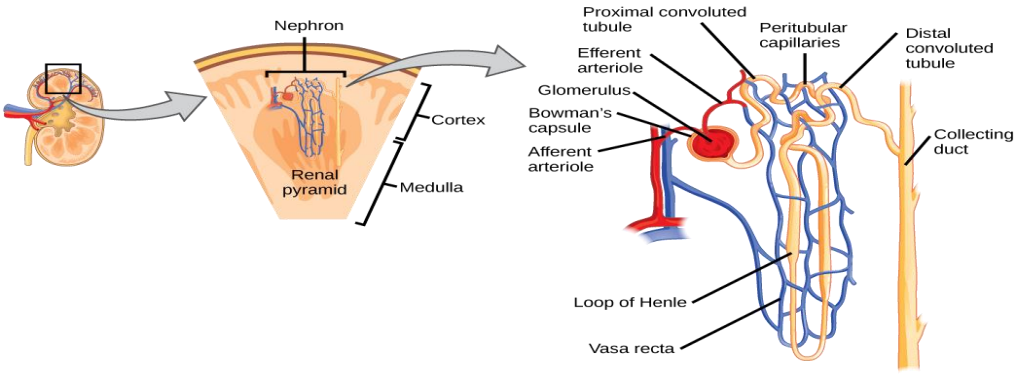

Figure 1.4 - Kidney internal anatomy with highlight on nephron segments (www.bio.libretexts.org).

1.3.1 – Dysregulated signalling pathways

Many signalling pathways appear to be involved in ADPKD (Figure 1.5), namely mitogen-activated protein kinase (MAPK), serine/threonine-protein kinase B-Raf / Extracellular signal–Regulated Kinases (B-Raf/ERK), mammalian Target Of Rapamycin (mTOR), *wingless* + *integrated* or *int-1* (Wnt)/β catenin signalling, as well as those dependent on the second messengers Ca^{2+} and cyclic adenosine monophosphate (cAMP)[84].

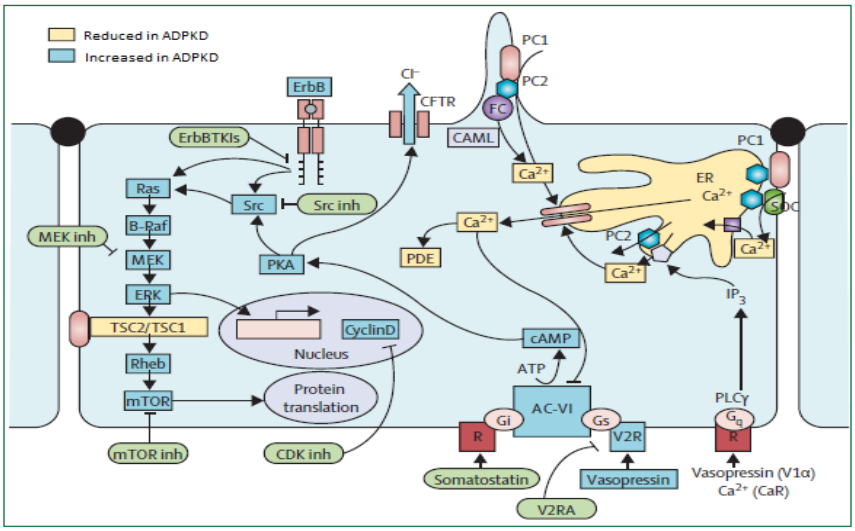

Figure 1.5 - Signaling pathways involved in ADPKD. With highlight of which are reduced and increased in ADPKD. In green, there are a few potential therapeutic agents for ADPKD. Polycystin-1 (PC1 or PKD1); Polycystin-2 (PC2 or PKD2); CFTR - Cystic Fibrosis Transmembrane conductance Regulator); Calcium Modulating Ligand (CAML); Fibrocystin (FC); Store-Operated Channels (SOC); Inositol trisphosphate (IP3); Endoplasmic Reticulum (ER); Phosphodiesterase (PDE); Cyclic Adeninosine Monophosphate (cAMP); Adenylyl Cyclase 6 (AC-VI or AC6); Vasopressin V2 Receptor (V2R); Vasopressin V2 Receptor Antagonist (V2RA); Receptor (R); Phospholipase C (PLC); heterotrimeric G protein i subunit (Gi); heterotrimeric G protein s subunit (Gs); heterotrimeric G protein q subunit (Gq); Cyclin-Dependent Kinase (CDK); Protein Kinase A (PKA); Proto-oncogene tyrosine-protein kinase Src (Src); Erythroblastic leukemia viral oncogene protein (ErbB); Tyrosine Kinase Inhibitor (TKI); Mitogen-activated protein Kinase kinase (MEK); Extracellular signal–Regulated Kinase (ERK); Tuberous Sclerosis proteins tuberin TSC1; Tuberous Sclerosis proteins hamartin (TSC2); Ras homolog enriched in brain (Rheb); mammalian Target Of Rapamycin (mtOR); Inhibitor (Inh). Adapted from Torres *et al.* 2007[22].

1.3.1.1 – MAPK

MAPKs are a conserved family of serine/threonine protein kinases that coordinately regulate cell proliferation, differentiation, motility, and survival. ERK belongs to the MAPKs family[85] being the last of three serine/threonine kinases that are serially activated in response to extracellular growth-factor stimulation of the small GTPase protein, Ras[86]. In ADPKD kidney tissues, due to the abnormally increased levels of cAMP , ERK is activated, through a sequential phosphorylation of Protein Kinase A (PKA), B-Raf and MAPK, stimulating the abnormal cell proliferation[79,86].

1.3.1.2 – mTOR

Also acting as a serine/threonine protein kinase, mTOR regulates cell metabolism, growth and proliferation, protein synthesis and gene transcription[84]. Under physiological conditions PKD1 represses mTOR signalling. Consequently ADPKD tissues showed enhanced activity of mTOR[87]. Indeed, studies using mTOR inhibitors, as sirolimus (also known as rapamycin) and everolimus, showed a deceleration in both cyst enlargement and kidney function decline[88] in ADPKD mouse ($Pkd1^{cond/cond}$)[87,89] and rat (Han:SPRD)[90] models. Everolimus was also tested in ADPKD patients, in which it delayed cyst enlargement but did not slow down the kidney impairment and the disease progression. Also there were associated side effects as leukopenia, thrombocytopenia, and hyperlipidaemia, among others[91].

1.3.1.3 – Wnt signalling

Wnt signalling is a group of signal transduction pathways in which extracellular Wnt glycoproteins (ligand) pass signals into the cell by activating the cell surface frizzled receptors. Wnt pathway is essential for cell migration, proliferation and apoptosis and, thus, for organ development, including the kidneys. It has two major branches, β-catenin-dependent canonical and noncanonical pathways. Noncanonical Wnt signaling regulates planar cell polarity which is altered in ADPKD, contributing to cyst formation[84]. These are both influenced by polycystins and involved in kidney cystogenesis. It is thought that the polycystins modulate Wnt signalling and stabilize β-catenin, increasing its amount[92]. According to a study with metanephric mesenchyme from rat embryos, when the Wnt/β-catenin signalling is sustained it blocks a post-epithelialization morphogenetic step that will end up in disorganized epithelial clusters and large dilations[93]. Also it has been showed that in ADPKD mouse and cultured cell models, this signalling is altered[94].

1.3.1.4 – Ca^{2+} homeostasis

As mentioned before, both polycystins are expressed in the primary cilia of the tubular epithelial kidney cells that are projected into the lumen of the tubule. In fact, the PKD1-PKD2 complex is essential for the maintenance of the differentiated phenotype of the tubular epithelium, which is corrupted upon the malfunction or absence of any of these two proteins. Although still controversial and in debate[63], it has been suggested that PKD1 translates mechanical or chemical stimuli into a ciliary Ca^{2+} influx through PKD2[8], which, in turn, induces the Ca^{2+} release from ER, increasing its intracellular concentration. It is known that ADPKD cyst-lining cells lack this flow sensitive Ca^{2+} signalling, exhibiting lower levels of intracellular Ca^{2+} compared to the healthy cells[8].

1.3.1.5 – cAMP signalling

Alterations in Ca^{2+} homeostasis lead to higher intracellular levels of cAMP. This second messenger has a key role in the regulation of many pathways and is involved in plenty biological processes including cell proliferation, differentiation and also in fluid transport[2,8]. The intracellular levels of cAMP are regulated by adenyl cyclases (ACs), which catalyse the production of cAMP from ATP, and phosphodiesterases (PDEs) that convert cAMP into AMP. When certain extracellular ligands bind to heterotrimeric G protein-coupled receptors in the PM, it is triggered the release of a subunit from the G-protein complex. This subunit activates ACs and, thus, the cAMP production[95,96]. In physiological conditions, most of the cell types have a higher capacity to hydrolyse cAMP instead of synthetize it, indicating that cAMP levels are, usually, regulated by PDEs activity[97].

There are nine membrane-associated ACs whose mRNA was found in ADPKD cells. Each one with specific target tissues and biochemical properties. Three of those isoforms, AC1, AC3 and AC8 are stimulated by Ca^{2+} and another two, AC5 and AC6, are inhibited by it. The latter two are the predominant isoforms expressed in kidneys[96]. In ADPKD tissues, in response to the decreased Ca^{2+} levels, the isoforms AC6 and AC5 are expected to be in their active state. In fact, studies using an ADPKD knockout mouse model specific for cells of the kidney collecting duct (CD) (the CD PKD/AC6 knockout mouse model for PKD1, that have the exons 1 to 4 floxed ($Pkd1^{cond}$) and for ADCY6 that had floxed the exons 3-12) have suggested the involvement of AC6 in the abnormal production of cAMP[8,98]. Supporting the imbalanced cAMP levels in ADPKD, $Pkd2^{WS25/-}$ (WS25 allele undergoes rapid rates of recombination/true knockout of one of the *pkd2* alleles) and $Pkd2^{WS25/WS25}$ mice and PCK rat showed a downregulation of PDE1[99]. AC5 and AC6 are also thought to be the primary ACs that mediate the effect of the antidiuretic hormone arginine vasopressin (AVP) in cAMP levels, particularly in the collecting ducts and distal nephron[100]. The AVP binds to the vasopressin receptor-2 (V2R), which become hyperactivated and potentiate the raising of the cAMP intracellular levels. Consequently, a higher resting cAMP level could make PKD cells more sensitive to V2R stimulation and/or amplify the cAMP signal. Indeed V2R are mostly expressed in collecting ducts, from where most of the cysts derive[2].

In the ADPKD context, PKA is the major downstream target of cAMP. This heterotetrameric holoenzyme (composed by two regulatory and two catalytic subunits) respond to intracellular alterations in cAMP, regulating several cellular processes[101]. Under physiological conditions, cAMP levels are not sufficient to activate PKA but when its levels are increased, as in ADPKD condition, PKA activation is achieved[101]. The combination of increased production and decreased degradation of cAMP could raise its basal concentrations to levels closer to the threshold for PKA activation. When the PKA is activated it phosphorylates the aquaporin-2 channels in cystic cells. These also become activated and move to the cell membrane where they allow the water absorption in order to regulate urine osmolarity[2].

It is known that cAMP increased levels and PKA signalling activation disrupt renal tubulogenesis[6,8]. Two studies refer that in normal human kidney cortex cells, cAMP did not induced cell proliferation whereas it did in epithelial cells from human ADPKD cysts[102,103]. Which are characterized as having lost their differentiation and become persistently proliferative[45]. cAMP increase and PKA activation also stimulate chloride and fluid secretion and activate signalling couple cell surface receptors and pro-proliferative pathways (that were previously described)[6,8]. Indeed it was found that in ADPKD, the abnormal activation of PKA contributes to the mentioned enhanced Wnt/β-catenin signalling[6] and for the abnormal activation of the chloride channel CFTR (Cystic Fibrosis Transmembrane conductance Regulator).

1.3.2 – Cystogenesis

Although being considered as a dominant inherited disease, ADPKD cystogenesis seems to be a recessive process at the cellular level. It is thought that it follows one of two genetic mechanisms: the "two-hit" model (Figure 1.6); or the hypothesis that haploinsufficiency might be sufficient to cause cyst formation[104] .

The "two-hit" model postulates that despite the presence of a germline mutation in one allele of the polycystins genes (inherited from the affected parent), a "second hit" by a somatic mutation is needed to trigger cystogenesis. That occurs in an individual cell of the nephron, inactivating the second allele of *PKD1* or *PKD2* genes. The accumulation of the two mutations allows the clonal and abnormal proliferation from this individual epithelial cell and lead to cyst formation[43,104,105]. Supporting this model, the cystic disease severity is synergistically higher in the trans-heterozygous $Pkd1^{+/-}$:$Pkd2^{+/-}$ mice than that expected by a simple additive effect of the one observed in singly heterozygous ADPKD mice ($Pkd1^{+/-}$ or $Pkd2^{+/-}$)[106]. Also, in ADPKD cyst epithelial cells was found that in cells from different cysts, but from the same patient, there were common somatic mutations, alterations of the normal copy of the *PKD1* gene and clonal chromosomal abnormalities[107–110].

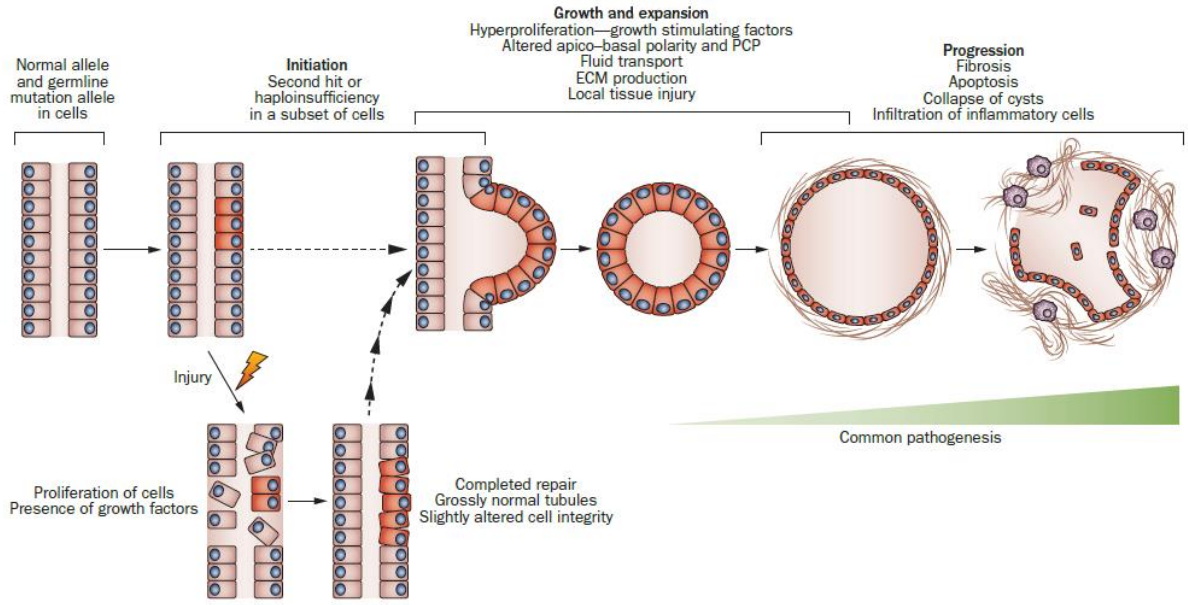

Figure 1.6 - Cystogenesis mechanisms at renal epithelial cells with representation of the two-hit hypothesis[104].

The other hypothesis of haploinsuffiency or dose effect postulates that a single allele mutated may be enough for cysts formation. This hypothesis postulate that a few loci can be sensitive to polycystins' expression levels, in which a sufficient reduction of it (about 50%) can trigger cystogenesis [111]. This is supported by evidence in a mouse model, $Pkd1^{nl/n1}$ (that produce mutant forms of the protein) where it was shown that a reduction in PKD1 expression may lead to ADPKD clinical features [81]. Also, some authors even suggest that this hypothesis can explain the vascular complications associated with ADPKD[111,112].

The abnormal cell proliferation appears to be the main cause for the tubule to start to expand, accumulating fluid from the glomerular filtrate. A dysfunction in centrosomes, as well as the activation of the canonical and inhibition of the non-canonical β-catenin-dependent Wnt signaling have been reported as the possible cause for the loss of planar cell polarity and consequently the transformation of the tubular structure into a cystic one[113]. When the cyst reaches approximately 2 mm of diameter, it

detaches from the tubule and become a round shape individualized structure, lined by an epithelial cell layer. Then the cyst enlargement is ensured by both continuous cell proliferation and trans-epithelial fluid secretion into the cyst lumen[114].

The key responsible for trans-epithelial secretion, that is also stimulated by the increased levels of cAMP, is CFTR who promotes chloride secretion and drives water towards the cyst lumen[11,12].

1.3.4 - CFTR

CFTR is a membrane protein of 1480 amino acid residues that belongs to the ATP-binding cassette (ABC) transporter superfamily. ABC-transporters are membrane transporters that bind to and hydrolyse ATP, using that energy to translocate a wide variety of substrates across cellular membranes[115]. Usually, they transport against a gradient and can either function as importers (almost exclusively in prokaryotes) or exporters[116]. But there are a few members of this family that perform different roles. One of these is CFTR which acts as a chloride channel[117] whose gating is regulated by nucleotide content of the nucleotide binding domains (NBDs)[118]. CFTR also have unique features among the other family members, namely an additional regulatory domain (R-domain) and some particular features of its NBDs. The latter include a ~35 residue insertion in NBD1 N-terminal and a ~80 residue extension at the end of the C-terminal of NBD2. These are thought to regulate CFTR function or its interaction with other proteins[116].

Malfunctioning or absence of CFTR causes the most common lethal autosomal recessive disease Cystic Fibrosis (CF). Up to now, there are 2023 mutations reported to cause CF (http://www.genet.sickkids.on.ca). The most common is the F508del mutation, a deletion of the phenylalanine 508, occurring in one allele of 85% of CF patients. The frequency of the disease varies among ethnic groups, with Caucasians having a higher prevalence[119].

It is mainly characterized by the obstruction of the airways and respiratory tract with viscous and sticky mucus that causes inflammation and leaves the tissue vulnerable to opportunistic bacterial infections [120,121]. *Staphylococcus aureus* and *Haemophilus influenzae* are usually the first to colonize the CF airways, both causing epithelial damage. Thus, it leaves an open way to *Pseudomonas aeruginosa* and to other pathogens as *Burkholderia cepacia*, *Stenotrophomonas maltophilia* and *Mycobacterium sp* later in childhood[122].

Structurally, CFTR is predicted to fold into 5 domains: 2 membrane-spanning domains (MSD1 and MSD2), each one with 6 transmembrane segments that form the channel pore; 2 cytosolic nucleotide binding domains (NBD1 and NBD2); and a R-domain, rich in phosphorylation sites by PKA that, as explained above, works in a cAMP-dependent manner. CFTR final structure is very compact and rich in intramolecular interactions. Given its complex structure, the folding of CFTR is tightly regulated to allow its correct insertion in the ER membrane and its proper maturation[119].

Biogenesis of CFTR begins in cytosolic ribosomes which are targeted to the ER membrane through the signal recognition particle to the ER membrane Sec61 complex translocon. CFTR suffers a cotranslational folding of the nascent polypeptide while it is being inserted into the ER membrane[123]. After its insertion in ER, CFTR is core-glycosilated, what consists on the addition of 14 oligosaccharide units. Such glycan moiety is the key element in quality control to the correct folding, trafficking and sorting of CFTR. The core-glycosilated CFTR is an immature form of the protein, classically known as band B, of ~150 kDa. The CFTR folding status at the ER is assessed by calnexin/calreticulin system.

After that, CFTR follows the secretory pathway exiting the ER through the ER exit sites where it assembles in COPII vesicles to be transported to the Golgi apparatus. From the early *cis*-Golgi towards the *trans*-Golgi, the glycan moiety of CFTR is processed and matured by multiple Golgi glycosyltransferases, with the removal and addition of new glycan units. All these modifications transform CFTR into a mature and functional form with a high molecular weight, the so-called band C of ~180 kDa, that is translocated to the cell membrane[118].

While being processed, CFTR needs to overcome 4 checkpoints from ER quality control that ensures the protein arriving the membrane to be fully functional. The first one occurs when its nascent polypeptide emerges from the ribosome, being regulated by a complex network of interactions with chaperones and cochaperones which are involved in the early steps of CFTR biogenesis, folding and stabilization[124,125]. The second checkpoint also takes place in the ER during protein folding and N-glycosylation, when the immature protein contacts with the calnexin/calreticulin system. Unglycosylated CFTR cannot bind to calnexin and cannot further progress. So, if the protein remains retained in this cycle for too long it is translocated to degradation in the proteasome. The third checkpoint occurs at the ER exit sites when the third glucose residue is removed from the folded CFTR, leading to protein dissociation from calnexin/calreticulin system and progression towards the Golgi[119,126]. At this level, the retention of unfolded CFTR is also assured by the exposure of arginine-framed tripeptides retention signals[127]. The last and fourth checkpoint occurs when CFTR is incorporated in COPII vesicles at ER exit sites to be transported to Golgi apparatus[119], a process that is dependent on trafficking proteins such as Sar1 GTPase and the heterodimeric Sec23–24 and Sec13–31[128].

Once at the membrane, CFTR stability is controlled by multiple protein interactors as Rab proteins, Rho small GTPases, and PDZ protein domains. So, CFTR levels at the PM are dependent on the balance between delivery from the Golgi (anterograde trafficking), endocytosis and recycling[119,123].

PDZ domains are structural motifs that potentiate protein-protein interactions. Proteins having a PDZ domain, anchor their membrane protein targets to cytoskeleton components. CFTR C-terminal have a PDZ binding motif that is complementary for several PDZ proteins, as Na^+/H^+-exchanger regulatory factor isoform (NHERF-1,2,3 and 4) and CFTR-associated ligand. NHERF1 anchors CFTR to actin cytoskeleton of PM by interacting with its PDZ domain. They form a complex that then interacts with ezrin via NHERF1 involving CFTR in an actin-tethered complex that prevents its endocytosis. NHERF also stabilize CFTR at the membrane through its interaction with small GTPases of the Rho family. These are key regulators of actin cytoskeleton dynamics, cell polarity and membrane trafficking through F-actin remodelling[119].

CFTR endocytosis is made via clatherin-coated vesicles [129] that accumulate in early endosomes. From here, it may recycle back to the PM[130] or it may go for degradation in lysosomes[123,131]. These trafficking processes are controlled by several proteins including Rab GTPases, Rme-1, myosins and kinases[132]. Trafficking of CFTR from the PM to early endosomes is controlled by Rab5. The recycling from early endosomes to the PM is done by Rab11/Myo5b-driven recycling endosomes. Rab7 regulates CFTR transport into late endosomes and from these to lysosomes. Rab 4 and Rab27a are also involved in processes that limit the CFTR expression at the PM[123]. Recycled CFTR that goes directly to the membrane without re-entering the trans-Golgi, has been considered to be the main mechanism supporting the a functional pool of CFTR at the PM[119].

Beside these conventional pathways of CFTR there are non-physiological alternative routes that have been described in CF mice ($Cftr^{F508\ del}$, $Cftr^{-/-}$ and TgGRASP55) and in human cultured cell lines (HEK293, CFPAC-1 and HeLa)[133,134]. A relevant number of transmembrane proteins reach the PM

unconventionally, either by exiting the ER in non-COPII vesicles or by bypassing the Golgi[135]. For CFTR, the alternative trafficking involves Golgi bypass in a GRASP-dependent manner through PDZ domain interaction, or the exit of ER by COPII-independent mechanisms. Both pathways lead to the arrival of immature core-glycosylated CFTR form to the membrane[133,134].

As already mentioned CFTR is known to be a cAMP/ATP-dependent Cl^- channel in epithelial cells of several tissues. So, once at the PM, CFTR must be activated and its gating must be controlled. Once activated by cAMP, PKA phosphorylates the CFTR R-domain, which is a prerequisite for channel gating by ATP[136]. It is thought that the phosphorylation of several R-domain sites has an additive effect in CFTR activity. On the other hand, an unphosphorylated R-domain has an inhibitory effect on channel opening[137]. Along with the R-domain phosphorylation, ATP binding and hydrolysis in the NBDs determines the shifting of the channel between the open and closed states[138]. When ATP binds the ATP-binding-site of each NBD the channel opens. During the gating cycle ATP is consumed, mediating the channel closing which is a unique feature of CFTR compared to other ligand-gated ion channels. NBD2 is capable of ATP hydrolysis, but NBD1 does not have ATPase activity. NBD1 is therefore a degenerated NBD[118].

1.3.4.1 – CFTR involvement in ADPKD

Unlike ADPKD patients, no renal phenotype has been reported in CF patients[117,139]. This might be explained by the fact that under physiologic conditions the levels of expression of CFTR in kidney epithelial cells are apparently already low (https://www.ncbi.nlm.nih.gov/gene/1080). Supporting this observation, the ectopic expression of PKD1 in mammalian kidney cells ($MDCK^{PKD1Zeo}$ and $MDCK^{Zeo}$) reduces the apical expression of CFTR[140].

In ADPKD cyst-lining cells the scenario is the opposite. There are few studies that relate CFTR with ADPKD. The first report dates back to 1996 when Hanaoka *et al.* referred the presence of CFTR in the apical membrane of cyst-lining cells from ADPKD patients' primary cultures and kidney extracts. They also found that the fluid accumulation within ADPKD cysts involves CFTR-like Cl^- currents[141]. Also, the Cl^- selective currents found in cultured ADPKD cyst cells were effectively blocked by diphenylamine 2-carboxylate, a Cl^- channels' blocker, and stimulated with forskolin that, acting as an agonist of adenylate cyclase, raises the cAMP levels[142].

Moreover, the use of CFTR inhibitors (steviol and $CFTR_{inh}$-172) or the impairment of the CFTR stability at the PM prevents the *in vitro* cyst expansion in both mammalian cells (type I MDCK, MDCK-wt-CFTR, MDCK-F508del-CFTR cells)[143,144] and ADPKD cultured cells[142]. *In vivo* studies that were also performed using ADPKD mice models ($Pkd1^{flox/flox}$:Pkhd1-Cre, $Pkd1^{flox/-}$; Ksp-Cre mice)[145,146] had similar results.

Altogether, these studies gave strong evidence that supports a key role of CFTR in promoting ADPKD cyst inflation. Additionally, there are 3 clinical studies referring the coexistence of ADPKD with CF. Importantly, the family members suffering from the two diseases showed a milder ADPKD kidney disease when compared to those having ADPKD alone within the same family and at comparable ages[147–149].

This led us to a question that remains unanswered in the literature: What is the real impact of the lack of polycystins on CFTR? Does it change the channel activity alone or does it also change the expression levels or membrane stability of CFTR?

1.4 – Extra-renal manifestations

Hypertension is a common feature to the majority of ADPKD adult patients, being detected long before the loss of kidney function[31]. Actually, it is already present in about 20-35% of children with ADPKD[150,151]. In ADPKD, hypertension is related with the progression of the disease and kidney enlargement, being an important risk factor for ESRD[152]. Usually it is associated with thickness of the left ventricular wall, which is a known risk factor for cardiovascular complications, that in turn have been already reported as the most common cause of death in these patients[8,153]. Activation of the renin–angiotensin–aldosterone system has been described as the apparent centre of the pathophysiology of hypertension in ADPKD. In these patients the activation of renin–angiotensin–aldosterone system is caused by decreased levels of nitric oxide, bilateral cyst expansion and intra-renal ischemia[31]. Other alterations associated with vasculature may give rise to intracranial or artery aneurisms[154] and dissections of main blood vessels. Intracranial aneurisms (often asymptomatic, *i.e.*, with low rate of rupture) and valvular heart disease are indeed common in ADPKD patients[22].

Polycystic liver disease is another common extrarenal manifestation. The formation of fluid-filled cysts in liver occur due to an excessive proliferation and enlargement of biliary ductules and peribiliary glands[8]. But, unlike in kidney cysts, primary cilia in these cysts are shorted or even absent depending on the cyst size[155]. Their growth and cell proliferation are promoted by insulin-like growth factor 1, oestrogens, growth factors and cytokines. Polycystic liver disease was usually asymptomatic, but with the extend of ADPKD patients lifespan with dialysis and transplantations, symptoms due to cysts and liver enlargement have become more common[8,32].

In a minority of patients, other organs may also develop cysts as is the case of pancreas and arachnoid membrane, which are often asymptomatic. Pancreatic cysts are however associated with recurrent pancreatitis and cancer[8]. Arachnoid membrane cysts increase the risk of subdural haematoma[22]. Seminal vesicles can also develop cysts, being a condition that affects about 50% of the male ADPKD patients, who also usually exhibit sperm abnormalities that rarely affect fertility[156].

Colonic and extracolonic diverticulosis have been also reported, having a higher prevalence in ESRD patients with ADPKD than with other renal diseases[157].

1.5 – ADPKD Diagnosis

There are no biomarkers for ADPKD, limiting its early diagnosis and preventing the accurate prediction of renal function decline. Currently, the determination of the Total Kidney Volume (TKV) is the unique available tool to monitor disease progression, severity or even treatment efficacy[158,159]. So, ADPKD diagnosis is usually confined to imaging techniques, namely Ultrasound, Computerized Tomography and Nuclear Magnetic Resonance scans. Considering their resolution, renal cysts become clinically detectable using these techniques only in adult patients, when the disease is already fully established. For example, Ultrasonography is reliable for cysts bigger than 1 cm of diameter[40]. The family history and phenotypes associated with, as the number and size of kidney cysts, are also very important for diagnosis. In ADPKD patients affected by PKD2 mutations, the diagnosis is not straightforward because of the late onset of the disease, many times making the family history hard to trace[160].

Diagnosis criteria have changed over the years[161] to minimize false-positives and false-negatives, especially in younger patients. Currently, ADPKD is diagnosed in at-risk individuals, *i.e.*,

those with ADPKD family history, if detected by ultrasound scan: at least, three unilateral or bilateral cysts in individuals aged 15 to 39 years; two or more cysts in each kidney, for the age group of 40-59; and at least four bilateral cysts in individuals over 60 years. The absence of renal cysts lowers dramatically the risk of ADPKD in individuals aged 30–39 years and excludes the disease in individuals over 40 years[160]. Nevertheless, a Nuclear Magnetic Resonance or a Computed Tomography should be done to confirm it[8].

Patients with a milder renal disease or those having a *de novo* mutation, ADPKD may be miss-diagnosed[162]. In these cases, gene-based molecular diagnosis should be the best option. However, this is always challenging because *PKD1* and *PKD2* are large multi-exon genes with considerable allelic heterogeneity for which there are already a large number of unclassified variants[163]. Additionally, *PKD1* share a high DNA sequence identity with 6 pseudogenes (PKD1P1-PKD1P6), increasing dramatically the difficulty to screen mutations[164]. Relatives of ADPKD patients who are potential kidney donors but are still young for a secure imaging-based diagnosis are also good candidates for a molecular screen[163].

The used methods include: 1 - DNA linkage analysis to detect high rates of co-segregation of putative mutated alleles underlying a familiar phenotype with the alleles at a marker *locus*. This has the disadvantage of being applicable only to families with 4 or more relatives affected. Moreover although giving information about the affected *loci*, it does not give information about the mutation itself[165]; 2 - Denaturing High-Performance Liquid Chromatography (DHPLC) using the Wave Fragment Analysis System, which allows the detection of base substitutions, small insertions or deletions based on temperature-dependent separation of DNA containing mismatched base pairs from PCR-amplified DNA fragments[166,167]; and 3 - Next Generation DNA Sequencing (NGS) which are a subset of sequencing technologies that allow the much faster and less expensive DNA or RNA sequencing than the previously used Sanger sequencing[168–170].

1.6 – Treatments

Currently there is no cure, nor specific effective treatments for ADPKD. In fact, there is only one drug medically accepted to treat ADPKD patients, Tolvaptan, which attenuates cyst growth. Unfortunately, not all patients are eligible for this treatment and it brings considerable secondary effects[6]. Therefore, for the majority of the patients, only supportive measures are used in order to minimize the ADPKD-associated morbidity. These include blood pressure control, avoidance of caffeine and oestrogens and the intake of analgesics for pain and antibiotics for the recurrent cysts bacterial infections[7]. In this scenario, the majority of the patients end up requiring life-long haemodialysis and, ultimately, renal transplantation[2].

1.6.1 – Hypertension related treatments

Early management of hypertension delays the progression of kidney disease and onset of cardiovascular events. Diet and lifestyle changes should be applied for hypertensive ADPKD patients, with a salt restriction of < 6 g per day, avoidance of caffeine intake, smoking cessation and maintenance of adequate fluid intake (3L per day)[171]. Along with these, some pharmacological treatments may be also used. Inhibition of the Angiotensin-converting–enzyme (ACE) is used as the first-line treatment for ADPKD hypertension and several studies have found that it adequately achieves blood pressure control in most patients[172,173]. Nevertheless, its renal protective effect may be limited by a compensatory-

feedback increase in renin release and in generation of angiotensin[173]. A challenge that might be overcome by the use of a combinatory treatment of ACE inhibitors with Angiotensin Receptor Blockers, direct renin inhibitors or aldosterone antagonists[174,175].

Beta blockers and calcium channel blockers also reduce blood pressure in ADPKD patients and are effective in those with cardiac disease. These are also effective as a second line treatment for those patients who still have uncontrolled blood pressure under ACE inhibitors or angiotensin receptor blockers treatment[170].

Some ADPKD patients suffer from sodium retention caused by the high levels of aldosterone. For these the use of diuretics together with the treatments above described may reduce the blood pressure, especially in the cases of reduced sodium excretion capacity[171].

1.6.2 – Cysts-related treatments

Several efforts have been made in order to overcome the main complication of the disease, the kidney cysts. The most promising drugs have as target the cAMP signalling. These include V2R antagonists and somatostatin analogues. As previously referred, vasopressin stimulates the cAMP production via AC5 or AC6 by binding to its receptors (V2Rs) in the renal collecting ducts and distal convoluted tubules of nephrons. So, inhibition of V2R suppresses the AVP-induced production of cAMP, resulting in decreased kidney cyst cell proliferation and cyst CFTR-dependent continuous inflation[176]. There are many studies using V2R antagonists, that indeed show a successful delay of disease progression in animal models[177–180]. One of those is Tolvaptan[181].

1.6.2.1 – V2R antagonist Tolvaptan

Tolvaptan is a selective and clinically effective antagonist of V2R that decreases the cAMP production and consequently the CFTR-mediated Cl^- secretion towards the cyst lumen. It has already been used in cultured ADPKD cells studies[176] and in preclinical and clinical trials, as the Tolvaptan Efficacy and safety in Management of autosomal dominant Polycystic kidney disease and its Outcomes 3:4 trial (TEMPO 3:4)[181–183] The last consisted on a 3-years trial with ADPKD patients with the first 3 CKD stages (CKD1, CKD2 and CKD3) that showed beneficial effects of the drug. It was observed an incremental reduction of 22.7% per year on the TKV rate and also an amelioration of the GFR rate decline of 0.98 ml/min per 1.73 m2 per year[183]. Although not preventing the cysts formation, tolvaptan is effective in slowing down the cyst growth[181,183]. It was initially used in clinical trials of patients with worsening heart failure, as a substitute for diuretics[184,185]. But nowadays, it has been already approved and accepted in some countries as a therapy for ADPKD slowdown. As Japan, in 2014[186], Canada in 2015 and Europe in 2015[183], where it can be currently applied in patients with evidence of a fast progression of the disease and still in the middle stage of renal impairment[187]. In USA it is not used yet since the Food and Drug Administration (FDA) requested additional data about the efficacy and safety of the drug in ADPKD patients[183].

However not all ADPKD patients are eligible to Tolvaptan treatment. According to the European Medicines Agency (EMA) Tolvaptan is indicated for ADPKD patients that are in 1-3 stages of CKD (with normal to moderately reduced kidney function) and that have evidence of rapidly progressive disease[187,188]. Also, according to the performed trials, the best results were obtained in patients with 35 years or older, with hypertension and with a bigger TKV[181,189]. Tolvaptan have important side effects. These include severe aquaretic effects (thirst and polyuria), hypertension and, the

most serious one, the raise of alanine and aspartate aminotransferases. The latter may lead to acute liver failure. Some patients had, indeed, to abandoned the trial due to aquaresis-related symptoms and liver complications[181,190]. Chest pain and headache were also described among the trial participants but in a low prevalence (0-0.9%). These side effects affect patients' daily live and should be considered before the Tolvaptan administration [189].

1.6.2.2 – CFTR inhibitors

In ADPKD, cyst expansion due to fluid secretion towards the lumen, as previous referred, is dependent on CFTR activity. So, a few CFTR inhibitors have been tested in ADPKD models. Yang *et al.* tested two type of inhibitors: thiazolidinones, which reversibly inhibit CFTR Cl^- secretion; and glycine hydrazides that bind directly to the CFTR pore at its extracellular entrance[145]. They used 3 different models: MDCK Type I cyst model in three-dimensional collagen gels, Pkd1*flox*/+; Ksp-Cre and $Pkd1^{flox/+}$ mice models. Their data suggested that in both *in vitro* and *in vivo* models, thiazolidinone- and glycine hydrazides-CFTR inhibitors at concentrations that are neither toxic or inhibitory of cell proliferation, delayed cyst growth[145].

Other investigators have tested other molecules[143,146], as steviol (from plant origin) whose interaction with renal anion transporters[191,192] and CFTR inhibition in human colonic epithelial cells was previously reported[193]. In MDCK cells, steviol retard both cyst formation and enlargement by direct inhibition of CFTR chloride channel activity and by reduction of CFTR expression via proteasome-mediated degradation[143]. $Pkd1^{flox/flox}$:Pkhd1-Cre mouse, an orthologous model of human ADPKD, steviol retarded renal cyst progression, by inhibiting CFTR expression in renal collecting duct, and cell proliferation via mTOR pathway[146]. Recently, the same group also found that in mouse mutant renal epithelial cells ($Prkcsh^{-/-}$ and $Pkd1^{-/-}$) steviol increased and stabilized PKD1 levels and promoted CFTR and β-catenin lysosomal degradation[194].

1.7 – ADPKD Models

1.7.1 – Mice and Rats

Several genetically engineered *Pkd1*- or *Pkd2*-mutant rodent models and others with spontaneous mutations have been used to gain insight into the pathogenesis of ADPKD. Indeed, they have been useful to get valuable insight into the disease initial steps and its progression[195,196,197], the role of primary cilia[196,198], the involved signalling pathways[87,198–200], the loss of planar cell polarity[198,201,202], but also to perform preclinical tests in the search of effective therapies[143,145,146,177,178]. Still, fulfilling the need for models that mimic closely the human disease remains a challenge[104].

There are different rodent models to study ADPKD, from knockout ($Pkd1^{del2–11}$ [196], $Pkd2^{d3}$ [203], conditional knockout ($Pkd1^{flox/–}$:Ksp-Cre and $Pkd2^{f3}$:γGT.Cre [204]) and inducible conditional knockout mice (Cre;$Pkd1^{del2–11,lox}$ or Cre;$Pkd1^{lox,lox}$ [196]) or even those expressing hipomorphic mutations ($Pkd1^{L3}$ [205] and $Pkd2^{WS25/-}$ [206]) to models with the overexpression of PKD1 or PKD2 proteins ($PKD1_{TAG}$ [207] and hPKD2 TG [208]). The knockout mice have in general at least one exons deleted[81,209,210] or disrupted[55,83] leading to the ablation of PKD1 or PKD2 protein expression. Mice that are heterozygous for a mutant *Pkd1* and *Pkd2* allele develop cysts in the kidneys and, later in life, in the liver[197,209]. Homozygoty of mutant alelles, for both *pkd1* and *pkd2* genes, has been sown to be lethal during embryonic development or right after birth due to severe kidney disease and cardiovascular anomalies and/or abnormalities of the placental labyrinth[83,211]. In order to overcome this and move with the research in homozygotes,

conditional knockouts have been generated. For this the Cre-loxP system was used, leading to the *pkd1* disruption in specific tissues, as renal epithelia and in some nephron segments, as proximal tubules, collecting ducts, loops of Henle and distal tubules[196,212].

The progression rate of cystogenesis and the disease itself, in general varies with the age of the animal at the onset of the disruption (decreasing with it), gender and the disrupted gene[195–198]. A limitation of these animal models is that the mechanisms that are occurring within cyst cells cannot be tracked in live but only after the animal death.

1.7.2 – Mammalian Cells

An adequate *in vitro* cellular model for ADPKD should have the ability to form cyst-like structures once grown in 3D cultures and should express the molecular machinery involved in the disease. An example of that is the MDCK cell line which have the ability of polarize and to form cyst-like structures when grown in 3D collagen gels in the presence of forskolin. MDCK cells in cysts undergo proliferation, fluid transport and matrix remodeling, as seen in tubular epithelial cells cultured from ADPKD kidneys. Also, the formation of cysts and their growth are dependent on cAMP, again as in ADPKD tissues[213]. Some studies using MDCK cells were important to disclose the role played by CFTR in cyst enlargement by testing its inhibitors, which slowed cyst enlargement[143,145]. These were also helpful on the finding that the mutant form of the CFTR, F508del-CFTR, reduced the cysts size by preventing their inflation (Li et al. 2012). This cell line was used as well to test the potential of cAMP modulators in impairing cysts growth (Tradtrantip et al. 2009). These include cAMP supressors, as the 2-(acylamino)-3-thiophenecarboxylates class[215] and stimulators, as the arginine vasopressin that promotes cyst expansion[216].

Human renal cells have also been used to further studies. For example, the Renal epithelial Tubular Cells (RTC) were used to access the role of prostaglandin E2 receptor subtype in cyst expansion. The results suggested that the binding of prostaglandin E2 to its adjacent receptors, through a mechanism that involves the blockade of apoptosis in cystic epithelial cells, stimulate cAMP signaling and cystogenesis[217].

Human Embryonic Kidney cells (HEK293) were used to study planar cell polarity in ADPKD through the role of the pathway Fz-CDC42. This protein is involved in the cell cycle being regulated by PKD1. Therefore, the lack of PKD1 might be then involved in the aberrant regulation of planar cell polarity[202]. PKD1-depleted HEK293 cells were also used in a study that evaluated the increased levels of an adenosine receptor (A3 adenosine receptor) in ADPKD kidneys and cAMP modulation by its activation. From this study came out the possible usefulness of synthetic agonists of the A3 adenosine receptor, that are known to inhibit renal injury and the growth in several tumor cell types, for ADPKD treatment[218].

1.7.3 – Zebrafish

Zebrafish (*Danio rerio*) (Figure 1.7) is a small freshwater vertebrate that belongs to *Cyprinidae* family and whose natural habitat are the shallow streams or pools in India. It was kept in aquariums even before its recognition as a good animal model for research in the 1930s[219,220]. Since then, zebrafish have been characterized as a powerful model system to study developmental and cell biology and human diseases[221].

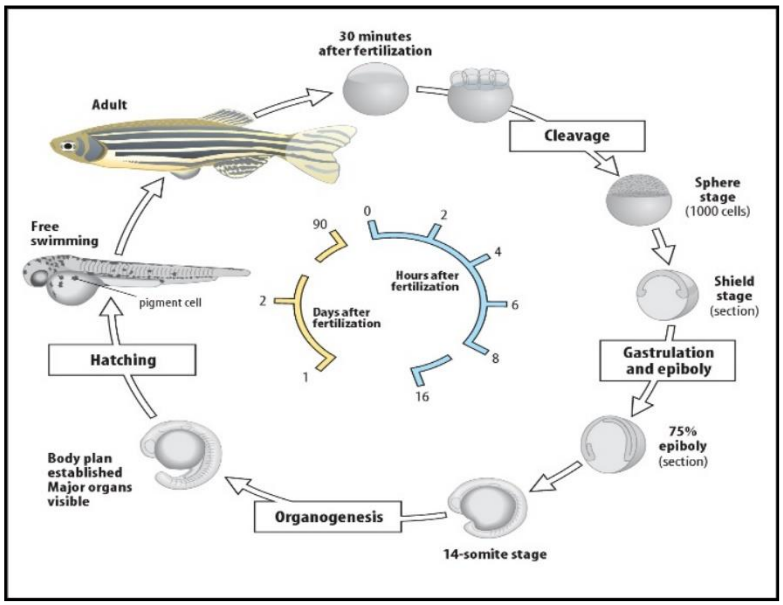

Figure 1.7 - Zebrafish lifecycle. The first cell is formed about 30 minutes after fertilization. The gastrulation starts 5-6 hours post fertilization (hpf), being followed by organogenesis from 16 hpf onwards. The hatching occurs at day 2-3 and a free larva emerge. Sexual maturity is reached 3 months of age. Adapted from http://www.mun.ca/biology/desmid/brian/BIOL3530/DEVO_03/ch03f09.jpg

This animal model presents great advantages. Unlike other vertebrate models, adult zebrafish are small (reaching a maximum of 4-5 cm in length), they reach sexual maturity at 3 months of age, and have an easy and low cost maintenance[220]. They have high fecundity with a reproductively active couple laying about 300 eggs per week[222]. Like other fish species, zebrafish have an external fertilization. Together with embryos' transparency, it allows the study of developmental stages in live[219]. Additionally, it allows the identification of phenotypic traits with dyes or antibodies with no need of tissue collection[222].

Pigmentation can be easily avoided by incubating zebrafish larvae in 0.2 mM 1-phenyl 2-thiourea solution. So, larvae are useful to study internal organs and their positioning (Figure 1.8). Given its current significance as an animal model, we have now available a considerable genomic data and several molecular tools that allow an easy genetic manipulation. These includes zinc-finger nucleases[223], Transcription Activator-Like Effector Nucleases[224], and CRISPR/Cas9 (Clustered Regularly Interspaced Short Palindromic Repeats/ CRISPR associated protein 9) system[225] to mutate target genes and generate transgenic lines.

Belonging to the teleost lineage, zebrafish suffered a whole genome duplication that occurred after their separation from the tetrapods lineage. Therefore, zebrafish usually have duplicated genes that are co-orthologous of a single mammalian gene. The study of the conserved regions that remained in fish and are present in mammalians and specially in humans, can be very useful to understand human genes roles in physiological or patological conditions[226].

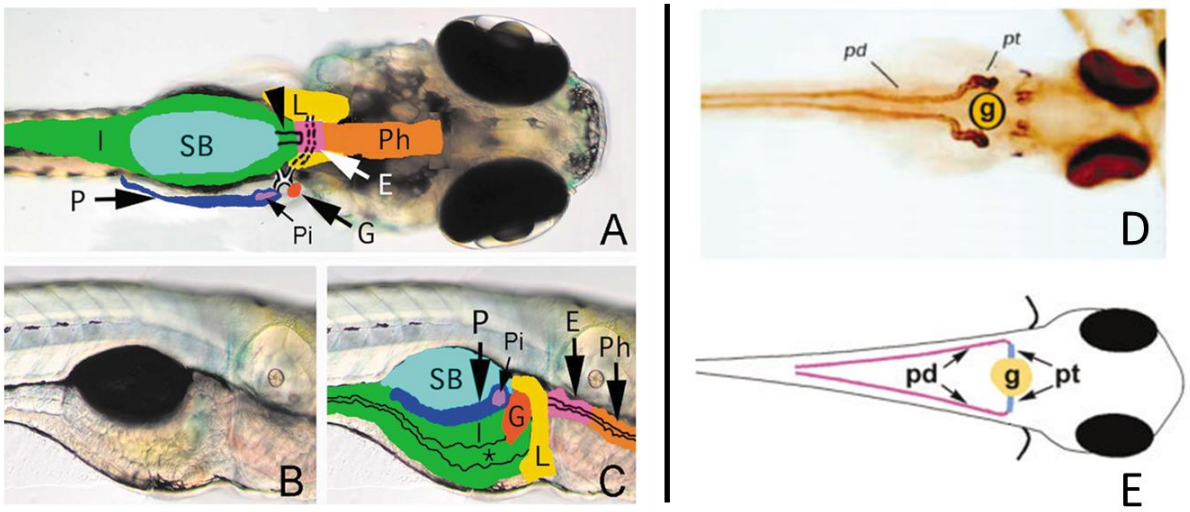

Figure 1.8 - Zebrafish larvae anatomy representation. A) dorsal view of a 5 days post fertilization (dpf) larvae. B) and C) Lateral view of a larvae with 5dpf. Organs and structures represented in colors and abbreviations are: Intestine (I), Swim bladder (SB), Pancreas (P), Solitary islet (Pi), Liver (L), Gall bladder (G), Liver (L), Esophagus (E), Pharynges (Ph). D) dorsal view of a 3.5 dpf larvae. E) Shematic representation of the pronephros elements in a 3.5 dpf larvae (dorsal view). Structures represented are: pronephric ducts (pd), pronephric tubules (pt), glomerulus (g). Adapted from Wallace & Pack 2003[227] and Hostetter *et al*. 2003[228].

In zebrafish, the knockdown of a target protein is usually done by injecting the embryo, at its one cell stage, with a specific Morpholino Oligonucleotide[229]. Antisense morpholinos oligomers (MO) are synthetic oligonucleotides of modified nucleotides (usually 25) produced by GeneTools (http://www.gene-tools.com/morpholino_antisense_oligos) that bind to specific target mRNAs. They have a neutrally charged phosphodiamidate backbone that confers to them a high binding affinity for RNA, decreases nonselective interactions with proteins and prevents their degradation by nucleases[230,231]. There are two types of MOs: the ATG MOs that block the initiation of translation at the ribosomes, impairing the protein synthesis; and the splicing MOs that interfere with the mRNA splicing process. More recently, a new class of MOs was developed: the target protector MOs that interfere with the function of endogenous microRNAs (miRNA) at their target localization (http://www.gene-tools.com/morpholino_antisense_oligos). However, the use of MOs is highly controversial among the scientific community, being the alternative the generation of mutant lines, by CRISPR/Cas9 for example, or the use of dominant negative mRNAs.

Some researchers do not trust MOs due to their toxicity. Indeed, some studies found differences in the phenotype of morphants compared to the respective mutants, with some of the morphants' traits being completely absent in the mutants with the same gene affected. Such difference were justified with possible MO's off-targets[232,233]. However, and despite the need of confirmation of the MO specificity, it is important to have in mind that MOs always induce a knockdown effect, which is not comparable to the knockout mutation. This, on the top of the lack of important controls may justify the differences observed in Kok *et al.* study[233]. A genetic compensation may also be induced by knockout mutations, justifying the differences between morphants and respective mutants[234]. Nevertheless, the validation of a MO should be done by different strategies. These include: the use of a second MO which ideally does not overlap with the first one; the use of a mismatch control MO which usually differs in 4 - 6 nucleotides from the tested MO; and, importantly, the use of a capped mRNA to rescue the MO effect, by co-injecting them[235,236].

1.7.3.1 – Zebrafish as model animal for ADPKD

Zebrafish is a useful model to study kidney development and function in general. Its pronephric kidneys are constituted by cells types that are common to all vertebrates and their organogenesis is regulated by conserved transcription factors[237]. The zebrafish mutant for the orthologous human *PKD2* gene, the curly-up (cup $^{-/-}$) mutant has been useful to study ADPKD extra-renal problems, namely cardiovascular problems[238], midline axis defects[239] or left-right organs' asymmetry[56]. But this mutant does not develop true cysts in its pronephoros, excluding it as a model for the renal ADPKD cystogenesis. Indeed, only pronepheric dilations that never get to bud off from the tubules were observed which are not representative of the vesicular architecture of ADPKD cysts[240].

However, the injection of specific MOs at one cell-stage to knockdown PKD2 in wild-type zebrafish embryos was shown to induce the development of pronephric cysts in larvae with 2.5 days, however it was not clear if those were fully individual structures[241]. Also left-right asymmetry problems, hydrocephalus and a strong dorsal axis curvature were reported[56,240,242,243]. This curly up tail phenotype results from the accumulation of type II collagen in the notochord[243]. All these defects were partially rescued by injecting human *PKD2* mRNA. A similar phenotype was observed by injecting a MO against *Pkd1a/b*, the orthologous to human *PKD1*. In this case, the developed cysts were again dilatations of the pronephros that do not form individual structures[241]. Nevertheless, a deregulation of fluid homeostasis was described for these.

Our group proposed, however, the zebrafish Kupffer's Vesicle (KV) (Figure 1.9), as a model organ to study the molecular mechanisms by which the lack of PKD2 leads to CFTR abnormal activation and, therefore, KV overgrowth. Such mechanisms should mimic those involved in the kidney cysts inflation[13]. The KV is originated from a cluster of cells located in the bud of the embryo's tail, the dorsal forerunner cells (DFCs). It is the left-right organizer in zebrafish, an organ that is transiently present in the early embryogenic stages of the fish and that is responsible for the establishment of the asymmetry of the internal organs of the fish[244].

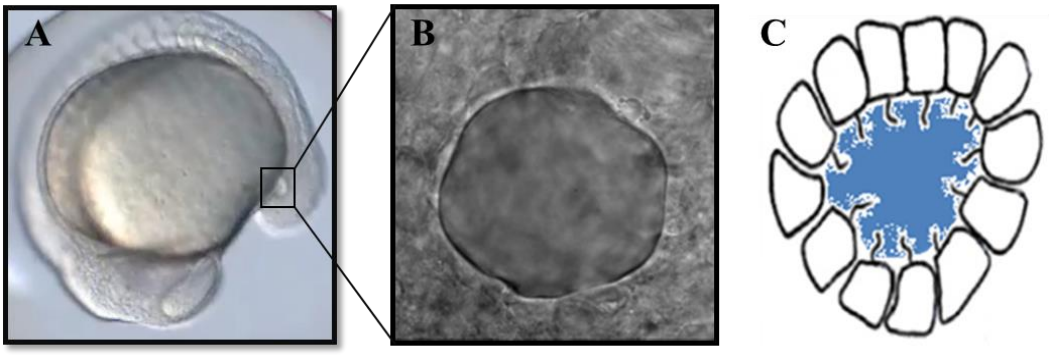

Figure 1.9 - Kupffer's Vesicle of a zebrafish embryo at 10 ss. A) and B) are snapshot images of a live embryo filmed from the dorsal side, with more detail of KV in B). C) is a schematic representation of a KV where some important features are seen: it is an enclosed fluid- filled cavity lined by one layer of monociliated cells. Adapted from Sampaio *et al*. 2014 [67]; Panel C by M Roxo-Rosa, included with permission.

Although it is not a renal-related organ, the KV has some similarities with a cyst. Indeed, it is a fluid filled vesicle lined by a monolayer of monociliated epithelial cells[67] and whose inflation depends on CFTR activity[14]. These cells, 60 on average, express both CFTR and PKD2 and their knockdown is easily ensured by the injection of specific ATG MOs. Mimicking a kidney cyst, the lack of PKD2 leads to an enlargement of the volume of the KV due to CFTR abnormal stimulation[13].

Having this in mind, our group made a comparative microarray analysis of KV sorted cells from *pkd2*-morphant, *cftr*-morphant and wild-type embryos that allowed the finding of common targets for PKD2 and CFTR. Among those, we found genes encoding several enzymes of the sphingolipid metabolism. Suggesting that the lack of PKD2 alters the cellular sphingolipid homeostasis (unpublish data)[15]. Supporting this hypothesis, the literature refers that ADPKD patients accumulate glucosylceramide and lactosylceramide[16,17]. Also there are some reports that connect CFTR with ceramide, which is the central molecule of the sphingolipid metabolism[18,19,245–247].

Our group is now working to disclose the role of the Sphingolipids in ADPKD.

1.8 – Sphingolipid Metabolism

Sphingolipids are a class of lipids that are essential constituents of eukaryotic cells that have a structural role in cell membranes. Despite that some of their metabolites, namely ceramide, sphingosine, and sphingosine-1-phosphate, are also bioactive signaling molecules involved in the regulation of cell growth, differentiation, senescence, and apoptosis[248]. All sphingolipids are synthetized in the ER and comprised of a 18-carbon amino-alcohol sphingoid base[249] that can be sphingosine, phytosphingosine, and dihydrosphingosine. In mammals sphingosine is the major sphingoid base[250].

The N-acylated form of sphingosine is called ceramide which is the central hub of this metabolism (Figure 1.10). Ceramide ends up being a key precursor for both biosynthesis and catabolism of the most important and complex sphingolipids[251,252]. Ceramide can be produced from the *de novo* synthesis (Figure 1.10) or from the breakdown of complex sphingolipids, by the hydrolytic pathway[250] (Figure 1.10).

Sphingolipids contribute to a small part of the total cellular lipid pool. Therefore, their accumulation in certain cellular compartments of some cell types underlay a group of human diseases, the sphingolipidoses[251]. These belong to the group of lysosomal storage diseases (LSDs) and include the: Gaucher disease, the most common sphingolipidose that is caused by a deficiency of glucosylceramide-β-glucosidase; GM1 and GM2-gangliosidosis variants caused by the accumulation of these glycolipids-; Fabry disease, an inborn deficiency of lysosomal α-galactosidase A which catalyzes the lysosomal hydrolysis of globotriaosylceramide; Metachromatic leukodystrophy caused by the inherited deficiency of arylsulfatase A and the consequent accumulation of sulfatide in several tissues; Krabbe disease due to inherited deficiency of galactosylceramide-β-galactosidase; Niemann–Pick disease, inherited deficiency of acid sphingomyelinase (ASM) and accumulation of sphingomyelin; Farber disease, inherited deficiency of lysosomal acid ceramidase and storage of ceramide in the lysosomes; and prosaposins, a Sap-precursor deficiency, which are activator proteins in late endosomes and lysosomes[253]. Sphingolipid metabolism has also been related to other pathologies, namely type 2 diabetes, Alzheimer's disease and hepatocellular carcinoma[251].

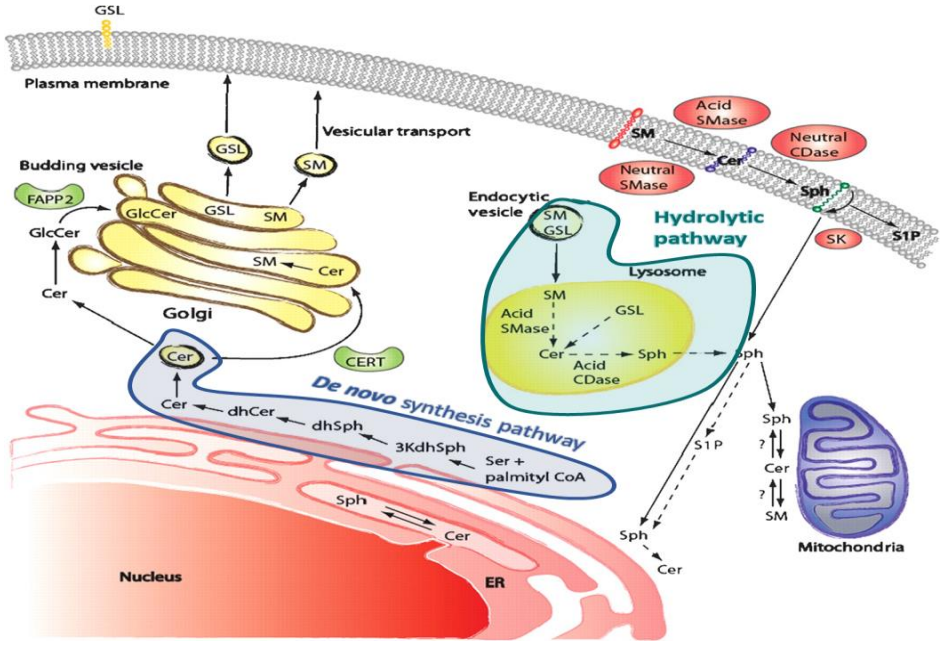

Figure 1.10 - The sphingolipid metabolism. Both pathways of ceramide synthesis, *de novo* synthesis and hydrolytic pathway, are highlighted. Ceramide (Cer); sphingosine (Sph); Serine(Ser); 3-keto-dihydrosphingosine (3KdhSph); dihydrosphingosine (dhSph); dihydroceramide (dhCer); sphingolipids transport protein Four-Phosphate-Adaptor Protein 2 (FAPP2); glucosylceramide (GlcCer); glycosphingolipids (GSL); sphingomyelin (SM); ceramide transfer protein (CERT); sphingomyelinase (SMase); ceramidase (CDase); Sphingosine Kinase (SK); sphingosine-1-phosphate (S1P). Adapted from Bartke & Hannun 2009 [248].

1.8.1 – *De novo* sphingolipid synthesis

The *de novo* biosynthesis of sphingolipids occurs in the ER, where a coordinated group of enzymes generate ceramides with different acyl chains and lengths. It starts in the cytoplasmic side of the ER with the conversion of L-Serine plus palmitoyl CoA into dihydroceramide. This occur by the sequential action of the enzymes serine palmitoyltransferase, which is the rate-limiting enzyme, the 3-keto-dihydrosphingosine reductase and the (dihydro) ceramide synthase[250,251].

Then, the dihydroceramide is desaturated to form ceramide, through the action of the dihydroceramide desaturase[249,251]. Ceramide can still be used in ER, to form for example α-galactosylceramide or it can be transported to Golgi. At the Golgi, different fatty acyl chains are added to the C1-hydroxyl position of ceramide in order to form the different classes of complex sphingolipids. These head groups include: phosphate, for ceramide-1-phosphate; phosphocholine, for sphingomyelin; and carbohydrates, for glycosphingolipids[250].

Then, Golgi transportation can be done by vesicular-mediated and non-vesicular mechanisms. The latter involves the ceramide transfer protein[249,251] and is utilized to generate sphingomyelins and Glycosphingolipids. Sphingomyelins production is catalyzed by sphingomyelin synthase in Golgi lumen and glucosylceramide synthesis occurs at the cytoplasmic side of the Golgi membrane[249–251]. The glucosylceramide is then translocated into Golgi's lumen via membrane-bound transporter and further transformed to complex Glycosphingolipids[250]. Those are then transported, mainly in vesicles, to the membrane[249–251].

1.8.2 – Hydrolytic pathway of sphingolipid synthesis

In addition to the previous mechanism, ceramide can also be synthetized by the hydrolysis of complex sphingolipids, by lysosomal degradation pathway. Which has the function to regulate the number of complex sphingolipids in the cell. The complex sphingolipids are divided into 3 major groups: 1) galactosphingolipids, 2) derivatives of glucosylceramide that vary according to the sugar attached and 3) derivatives of sphingomyelin[249,250]. Different groups of sphingolipids follow different hydrolysis routes. For example, the regeneration of ceramide from sphingomyelin is done by acidic, neutral and alkaline sphingomyelinases which act in different cell compartments according to their optimal pH activity[249,254]. From glycosphingolipids, ceramide can be generated by the disruption of sugar residues forming glucosyl ceramide and galactoceramide. These are then hydrolyzed by specific enzymes and transformed into ceramide. If needed, ceramide can be then re-acylated with a different fatty acid in the ER and originate sphingosine (Sph) by the action of the acid ceramidase[249,250].

1.8.3 – CFTR and the Sphingolipid Metabolism

Some studies suggest that CFTR colocalizes with membrane regions that are rich in cholesterol and sphingomyelin, the lipid rafts[255,256]. Moreover, the expression of F508del-CFTR and the total absence of CFTR were associated with alterations in the sphingolipid metabolism. It was postulated that CFTR-deficient cells suffer a disruption of the balance between acid sphingomyelinase and ceramidase activities, which should result in an increase of the ceramide *de novo* or hydrolytic synthesis. These could explain the increased levels of ceramide observed in CFTR-deficient cells[18,257,258].

However, other studies refer that the absence or dysfunction of CFTR, in both human tissues and CF mice model (C57BL/6-Cftr-KO), leads to a deficiency in several ceramide species. A deficiency rescued by the administration of fenretinide, a drug that corrupts lysosomal activity and sends ceramidase and sphingomyelinase for proteolytic degradation, restoring the normal ceramide levels[259]. These opposing results may be related to differences in the animals' diet followed in each study. Guilbault *et al*. used a mice diet (Peptamen) that was chosen in order to minimize intestinal obstruction problems, but that itself causes a reduction in ceramide levels and activity of acid sphingomyelinase[258]. Differences in the used mice strains, animals' age or even of the sphingolipid quantification method could also account for those controversial results[258,259].

It was also reported that sphingomyelinases of pathogens, namely *Bacillus anthracis and Staphylococcus aureus*, that infect the human airways, inhibit the CFTR function. More precisely, the enzymatic hydrolysis of the host sphingomyelin by bacterial sphingomyelinases into ceramide, ceramide 1-phosphate, phosphocholine or choline, disturbs the phosphorylation of CFTR R-domain, impairing its activation. The same authors have suggested that such bacterial-host interaction could aggravate the pulmonary infection in CF patients or, even, elicit a CF-analogous condition in non-CF patients suffering from *S.aureus* lung infection[245]. This inhibition of CFTR currents goes accordingly to the finding that accumulation of ceramide and ceramide-1-phosphate mediates inflammation, cell death and also susceptibility to infections, a hallmark of CF[258,260].

Taking these data in account, even if observed in a CF context, considering the key role of CFTR in ADPKD cyst inflation[141,143–146] and the changes of the sphingolipid metabolism that seem to occur in a ADPKD context[16,17] (not published[15]), we must deepen in what is the role of the sphingolipids in the ADPKD disease.

2. OBJECTIVES

The current available ADPKD models are limited to study the molecular mechanisms by which the lack of PKD2 influences and activate CFTR. However, recently our group have suggested a new model that enables it, the Kupffer's Vesicle from zebrafish. In zebrafish, this is a transient organ responsible for the correct left-right asymmetry in the internal organs. Although it is not a kidney related structure, it has specific characteristics that reassemble it to an ADPKD cyst. Among which the fact that PKD2 and CFTR are both expressed in it, that its inflation if dependent on CFTR activity and that the absence of PKD2 causes it enlargement through CFTR overstimulation[13]. However, is the lack of PKD2 only affecting CFTR activity or something else?

So, one of the aims of this project was to find if the lack of PKD2 only alters CFTR activity or also its expression levels and subcellular localization. In order to do that we have used embryos from a zebrafish transgenic line, *TgBAC(cftr-GFP)pd1041*. This line not only provides us with the KV as an organ model for ADPKD as also allow us to have a live readout of the influence of the absence of PKD2 on CFTR.

Currently, the available therapeutic measures for ADPKD patients are very restrict. Despite the existent studies in the subject, there is only one medicine authorized by the responsible authorities. Which is Tolvaptan and whose target is the cAMP signalling. Tolvaptan acts by slowing the cyst enlargement and the progression of the disease, however also not every ADPKD patients are eligible for this treatment. To contribute to the development of new and successful therapies, eventually other mechanisms or metabolisms involved in this disease that are not so studied and unveiled in the field should be taken in account. Indeed, a microarray experiment previously performed by our group, using zebrafish embryos, revealed that when the PKD2 is absent, there are enzymes from the sphingolipid metabolism that appear to be altered. And these were also common targets for CFTR (data not published) [15].

In order to deepen the knowledge on this apparent association, another objective that we had was to see if and how is CFTR influenced when the sphingolipid metabolism is altered. To do that, embryos from the transgenic zebrafish line *TgBAC(cftr-GFP)pd1041,* were used again. The results that could arise from these experiments would be very interesting and valid. So, to try to answer to that question, HEK-293 stably transduced with WT-CFTR were used.

Other objective that we had on the beginning of this project was to evaluate the relevance of the findings that we had with the previous model used, in ADPKD tissue samples. However, the samples that we received until today were from a tissue type that is unlikely to have CFTR expression. Hence, and also by time restriction we did not proceed with the experiments in these samples.

3. MATERIALS AND METHODS

3.1 – Zebrafish strains and maintenance

Adult zebrafish lines were maintained in appropriate tanks with fresh water at 28 ºC, with a photoperiod of 13.5 h light and 10 h dark and were fed 3 times a day. The strains used were WT and *TgBAC(cftr-GFP)pd1041*[14], all of AB background. The latter was gently given by Bagnat's laboratory (Department of Cell Biology, Duke University Medical Center, Durham, USA). All the experiments were done using embryos obtained from incrosses of those lines. The zebrafish embryos used in this study are not considered animals and so, they do not require the approval of the Portuguese Direcção Geral de Veterinária. Nevertheless, their use was approved by the ethics committee of the Nova Medical School/Faculdade de Ciências Médicas, Universidade Nova de Lisboa.

The incrosses were done with 10 to 14 zebrafish couples. For that, on the afternoon before the eggs collection, each couple was placed in a breeding chamber with a partition separating the male from the female. On the next day, the eggs were collected 20 minutes after the partition removal, guaranteeing a batch of synchronized eggs at their one cell stage of development[261]. Eggs were then incubated in embryonic medium E3 (5 mM NaCl; 0.17 mM KCl; 0.33 mM $CaCl_2$; 0.33 mM $MgSO_4$ and methylene blue (all the products were purchase from Sigma (Sigma-Aldrich, USA) with exception of NaCl which was purchase from VWR Chemicals (VWR International,LLC , USA)) at 28 ºC until the desired developmental stage. Whenever necessary, the eggs were incubated at 25 ºC for a slower development.

To preserve the line in the lab and to raise the number of adult fish to work with, both incrosses of the line and outcrosses with ABs were done. The screening of GFP positive zebrafish was performed in the larval stage at 7 days post fertilization (dpf) with the help of a fluorescent stereoscope (Lumar V12, Zeiss, Germany). This stereoscope was also used to the characterization of the line, *TgBAC(cftr-GFP)pd1041*.

3.2 –Microinjections

Injection of the MO was done following the directions of "Microinjection Techniques: Injecting through the chorion" [262]. It was done using a glass needle engender from a 1 mm capillary tube where the MO of interest was inserted. With the help of a stereoscope (SMZ745, Nikon Corporation, Japan), an injector (Pneumatic Pico Pump PV820, from WPI (World Precision Instruments, USA) and a graticule (S1 Stage Micrometer, 10 mm/0.1 mm, from Pyser-SGI (Pyser Optics, United Kingdom) for the needle calibration.

The knockdown of *pkd2* was ensured by the injection of a *pkd2*-augMO (Gene Tools LLC, Philomath, USA) at one cell stage embryos. This MO (5'-AGGACGAACGCGACTGGAGCTCATC-3') begins at the start AUG and extends through the first exon of the *pkd2* gene[13,56]. The injected amount varied according to the used batch, 1.8 ng for the first and 2.5 ng for the second.

3.3 – Mammalian Cells

Two different cell lines were use. These were the Madin-Darby canine kidney type II-CFTR (MDCK-wtCFTR)[263] and Human Embryonic Kidney 293Flp-In CFTR (HEK293-wtCFTR)[20] cells, both stably expressing the human WT-CFTR. These were gently given by Margarida Amaral's Laboratory

(BioISI – Biosystems & Integrative Sciences Institute, Department of Chemistry and Biochemistry, Faculty of Sciences, University of Lisboa, Portugal).

Cells were cultured in Dulbecco's Modified Eagle Medium (DMEM, Gibco®, Life Tecnologies,USA) supplemented with 10 % (v/v) of heat-inactivated Fetal Bovine Serum (FBS, Gibco®), 1 % (v/v) of Penicillin and Streptomycin (PenStrep, Gibco®) and 2 mg/mL of Blasticidin S Hydrochloride Biochemica (PanReac Applichem, ITW Reagents, USA) for MDCK-wtCFTR cells or 1mg/mL of Hygromycin B (VWR Chemicals) for HEK293-wtCFTR cells. They were maintained in a humidified incubator at 37 ºC, with 5 % of CO_2.

3.5 – Zebrafish KV Confocal Live Microscopy

Live *TgBAC(cftr-GFP)pd1041* embryos at their 8 - 10 somite stage (ss) were dechorionated with clamps and mounted in 2 % (w/v) agarose (Lanza, USA) moulds, with the help of a stereoscope (SMZ745, Nikon Corporation). Embryos were then covered with a layer of 2 % (w/v) low melting agarose (Sigma-Aldrich). Whole KVs were scanned by confocal microscopy (confocal microscope - LSM710, Zeiss; software – Zen 2010 B SP1), using a 40× water objective. Z-sections of 0.5 μm and acquisition rate lower than 1 frame per second were used for better imaging.

3.5.1 – KV volumes

KV volumes were evaluated analysing the confocal KV stacks with the ImageJ software (version 1.50i) (http://imagej.nih.gov/ij). More precisely, using the plugin Measure Stack, the KV was delineated and its luminal area was determined in all z-sections. Then, areas of all KV focal planes were summed to calculate the KV volume. From this point onward, KV volumes refer the average volume of the mentioned group of embryos.

3.5.2 – Mean fluorescence intensity

CFTR-GFP mean fluorescence intensity was evaluated in the KV stacks obtained by live confocal microscopy. To accomplished that we started by making an image that was composed by the sum of all the slices from each KV, which represented the whole KV in a 2D image.

CFTR-GFP mean fluorescence intensity was measured in: 1) whole KVs; anterior and posterior parts of the KV, separately; and at the apical membrane of KV-lining cells. For the first, the full area of the image (2.0×10^4 μm^2) was considered and this was equal for all the analyzed samples. For the second, the full area of the image was divided in 2 equal-sized parts, one referring to the anterior part and the other to the posterior part of the KV. The mean fluorescence intensity of both parts was measured individually for each KV and then compared. The third measurement was performed by defining a ring-shaped involving the KV apical membrane.

For all these measurements, the following parameters were considered: selected area (2.0×10^4 μm^2); mean gray value, *i.e.*, the sum of the gray values of all pixels in the selected area divided by the total number of pixels; and integrated density, *i.e.*, the product of the selected area and the mean gray value. The integrated density was normalized with the background mean fluorescence intensity, by determining the normalized Mean Fluorescence Intensity (normalized MFI) using the following equation (https://sciencetechblog.com/2011/05/24/measuring-cell-fluorescence-using-imagej/):

(3.1) normalized MFI = Integrated Density of selected Area – (selected Area × background Mean Gray value)

After all those measurements, the respective normalized MFIs were compared between non-injected embryos and *pkd2*-morphants. A statistical analysis was performed to evaluate the significance of the differences obtained.

3.6 – Flow Cytometry Analysis of zebrafish embryos

GFP mean fluorescence intensity of *TgBAC(cftr-GFP)pd1041* embryos was also measured by flow cytometry analysis. This allowed a comparative evaluation of the CFTR-GFP levels among 3 different conditions: *pkd2*-morphants; non-injected embryos; and non-injected embryos treated with 50 μM Myriocin (Cayman Chemical, USA). WT AB embryos were always used to exclude the natural auto fluorescence that zebrafish embryos have and to calibrate the parameters required to do this analysis.

For each experiment replicate, approximately 200 embryos per condition were dechorionated at their 10 ss stage, by incubation with Pronase (2 mg/mL) (EMD Millipore, MERK, Germany) for 3 minutes at room temperature (RT). For those under Myriocin (Cayman Chemical, USA) treatment, embryos were dechorionated at their 6 ss and Myriocin was added to their E3 medium at a final concentration of 50 μM (stock solution: 10 mM in DMSO). These were grown at 28 ºC until their 10 ss. Chorion-free embryos were transferred to 2 mL tubes with clean E3 medium and centrifuged at 700 *g* for 3 min, at RT. The pellet of embryos was then re-suspended in 1 mL of DMEM-F12 (11320074, Gibco®, Life Technologies) supplemented with 5 mM EDTA (Sigma). This procedure ensures the mechanical rupture of the yolk membrane, allowing the suspension of the yolk lipidic content in the medium. On the other hand, functioning as a Ca^{2+} chelator, EDTA allows cell dissociation by acting in Ca^{2+}-dependent adhesion molecules and weakening their interactions. After an additional centrifugation at 700 *g*, for 3 min at RT, the supernatant was discarded and the pellet of the yolk-free embryo cells was again re-suspended in 1 mL of DMEM-F12 supplemented with 5 mM EDTA. These steps were repeated 3 times. The final pellet of cells was re-suspended in 300 μL of DPBS (Gibco®, Life Technologies).

All samples were kept on ice until their analysis by flow cytometry (flow cytometer BD FACSCanto II, BD Biosciences, USA). The established gates for these analyses were established based on WT embryos samples and they were: 1) exclusion of the debris and medium components, 2) exclusion of cell agglomerates; 3) exclusion of auto-fluorescent cells; and 4) selection of GFP-positive cells. All the gates were defined following the order from 1 to 4.

In order to have the same number of GFP-positive cells analysed in each sample, we run $4x10^5$ events per sample, which translates in $4x10^5$ counts of cells. We also established that the minimum number of GFP-positive cells that should be obtained per sample were 300 and these should represent at least 0.1 % of the total number of cells. We considered only the experiments that reached at least two of the three parameters, *i.e.*, $4x10^5$ events, 300 GFP-positive cells or 0.1 % of the cell population. Nevertheless, for the majority of the experiments we reached the 3 parameters simultaneously. Both mean and median of the fluorescence intensity, the number of GFP-positive cells and the percentage of those in the entire population of cells (after excluding debris) were calculated by the software of acquisition BD FACSDIVA™ (version 8.0.1) (BD Biosciences). The presented flow cytometry plots were generated with the FlowJo® software (version 10.3) (FlowJo LLC, USA).

3.7 – Protein extraction and Western-blot analysis

3.7.1 – Zebrafish embryos protein extracts

For the protein extraction of zebrafish embryos at 8 - 10ss, the pellet of cells was prepared exactly as in the flow cytometry experiments (see section 3.7 of Materials and Methods). This pellet was then resuspended in 100 µL of Lysis Buffer 1× (1.5 % (w/v) SDS (ThermoFisher Scientific, USA), 5 % (v/v) Glycerol (VWR International), and 0.5 mM DTT (Sigma Aldrich), 31 mM Tris-HCL at pH 6.8)) supplemented with 1 µL of proteases inhibitors cocktail (from Molecular Probes, Life Technologies, ThermoFisher). Samples were stored at -20ºC.

3.7.2 – Mammalian cells protein extracts

Once at the desired confluence (about 80% of confluency), cells were lysed with 100 µL or 200 µL of Lysis Buffer 1×, supplemented with 1µL of proteases inhibitors. To facilitate the process, the flask or wells containing the cells were scrapped. Samples were stored at -20ºC.

3.7.3 – Western-blot analysis

For both zebrafish and mammalian cells protein extracts, DNA was sheared by passing the samples first through a 20G and then a 26G needle, until the viscosity of the sample has dropped.

Proteins were then quantified using the RC DC Protein Assay (BioRad) according to the manufacture instructions, which is based on the Lowry assay. After quantification Bromophenol Blue was added to each sample to a final concentration of 0.001 % (w/v).

Proteins were separated by SDS-PAGE (SDS-polyacrylamide gel electrophoresis) (Mini Protean electrophoresis system, BioRad), at 20 mA per gel, with constant voltage. Polyacrylamide mini-gels composition: stacking gel of 4 % (Tris-HCl 129 mM pH 6.8, 4 % (v/v) acrylamide (BioRad), 0.1% (v/v) glycerol , 0.1 % SDS (v/v), 0.11 % (v/v) PSA (BioRad) and 0.17 % (v/v) TEMED (BioRad)); separating gel of 7.5 % (Tris-HCl 373 mM pH 8.8, 7.5 % (v/v) acrylamide, 0.1% (v/v) glycerol, 0.1 % (v/v) SDS, 0.11 % (v/v) PSA and 0.08 % (v/v) TEMED). The run was at RT for 2.5 hours.

Proteins were then transferred onto Polyvinylidene Difluoride (PVDF) membranes (BioRad, USA), using the same apparatus, at 100 V with a constant current, for 1 hour and with the system cooled. Ponceau S (which binds to the positively charged amine groups of proteins) was used to confirm the efficiency of the protein transfer.

To eliminate non-specific binding sites, the membranes were blocked with a 5 % (w/v) skimmed milk solution in PBST (PBS 1× + 0.1% (v/v) Tween 20 (Calbiochem, Merck, Germany)) for two hours at RT. Membranes were incubated with the primary antibodies diluted in the same solution (5 % (w/v) skimmed milk in PBST), overnight at 4 ºC, with gentle shaking. For zebrafish samples, it was used a 1:100 diluted anti-PKD2 polyclonal antibody, raised against zebrafish PKD2 (this antibody was gently given by Drummond's Laboratory, Massachusetts General Hospital and Harvard Medical School, Charlestown, Massachusetts, USA). For mammalian cells, we used a 1:1000 diluted anti-PKD2 polyclonal antibody, raised against human PKD2 (GTX113802 from GeneTex, USA) and a 1:750 diluted anti-CFTR monoclonal antibody, raised for human CFTR (A4-596, gently sent by Cystic Fibrosis Foundation, USA). In both cases, α-Tubulin was detected with a 1:1000 diluted anti-α-tubulin monoclonal antibody (DM1A clone, Sigma).

On the next day, the membranes were washed 3 times for 5 minutes, with PBST. Then, they were incubated with the proper secondary antibodies diluted in the 5 % (w/v) skimmed milk-PBST

solution, for 1 hour, at RT, with gentle shaking. For the primary polyclonal antibodies, the secondary antibody that was used was the 1:1000 diluted anti-rabbit IgG (H+L) horseradish-peroxidase conjugated antibody (#1706515, BioRad). For the primary monoclonal antibody, the secondary antibody was the 1:1000 anti-mouse IgG (H + L)-HRP Conjugated (#1706516, BioRad). After that the membranes were washed again with PBST for 3 times for 5 minutes.

Blots were developed using the SuperSignal™ West Pico PLUS Chemiluminescent Substrate detection kit (ThermoFisher Scientific), according to the manufacturer instructions. Chemiluminescense was captured using the ChemiDoc™ Touch Imaging system (BioRad). Densitometry analysis was done using the Fiji software (https://fiji.sc/, GitHub, Inc., USA). α-Tubulin levels were used to normalize the protein levels.

3.8 – Mammalian cells Immunofluorescence

Cells were grown in 8 well chamber slide (Nunc™ Lab-Tek™ II Chamber Slide™ System, ThermoFisher) in an antibiotic-free medium. When at about 80% of confluency, cells were incubated with Myriocin at 37 ºC with humidity and CO_2 at 5 %, in the following conditions: overnight with 100 nM Myriocin; 2 hours and 4 hours with 20 µM Myriocin.

Cells were then washed twice with cold DPBS supplemented with 1 mM $CaCl_2$ and 1 mM $MgCl_2$, fixed for 30 minutes with 4 % (v/v) paraformaldehyde and washed twice again with PBST. Cells permeabilization was ensured by a 15 minutes incubation at RT with PBS + 0.2 % (v/v) Triton X-100. Then cells were washed 3 times with PBST and were blocked with 1 % (w/v) BSA in PBST, for 30 minutes at RT. After that, cells were incubated at RT for 30 minutes with the primary anti-CFTR monoclonal antibody (#A2-570, Cystic Fibrosis Foundation), 1:250 diluted in 0.5 % (w/v) BSA PBST solution. After 3 washing steps in PBST, cells were incubated for 30 minutes at RT with the secondary antibody Alexa Fluor 488 anti-mouse (#SAB 4600387, Sigma) 1:500 diluted. The Alexa Fluor 546 Phalloidin (#A22283, Molecular Probes, Life Technologies, USA) 1:40 diluted was also used for actin cytoskeleton detection. All antibodies were diluted in 0.5 % BSA (w/v) PBST solution. After that 3 washes with PBST, cells were covered with DAPI in 50 % (v/v) glycerol and were stored at 4 ºC until they were analysed.

Just before the confocal analysis, the plastic chambers were removed from the slide and a glass coverslip was mounted on top of it. The excess of DAPI-glycerol was removed.

The acquisition of the images was performed by confocal microscopy (Zeiss LSM710) with 63× oil objective. The acquired images were then analysed using the ImageJ and statistical analysis was performed.

3.9 - Statistical Analysis

The statistical analyses of the obtained results were performed using the software GraphPad Prism, version 6.01 (GraphPad Software Inc, USA). Paired or unpaired Students's *t*-test were used according to the sample. Paired analysis was used for the comparison of the normalized MFIs of KV anterior versus posterior parts and for flow cytometry zebrafish data. Unpaired analysis was used for the rest of the analyzed data.

4. RESULTS

4.1 – Characterization of the *TgBAC(cftr-GFP)pd1041* zebrafish line

The inflation of kidney cysts is one of the key processes of ADPKD. Several models including mammalian and human cell lines[143,176,214] as well as mouse models[145,146] have been used to study this process. These were useful in demonstrating the involvement of CFTR in cyst inflation and in evaluating the therapeutic potential of CFTR inhibitors. However, they are limited in the study of the *in vivo* mechanisms by which the lack of polycystins influences CFTR, stimulating it. Does it mean enhanced CFTR-activity alone or could this also mean higher levels of CFTR in the cyst-lining cells?

Our group have recently proposed the Kupffers' Vesicle as a model system to study the molecular mechanisms involved between the PKD2 downregulation and the CFTR abnormal activation. It was demonstrated that the lower levels of PKD2 lead to an enlargement of the KV by CFTR-mediated fluid secretion towards the lumen, mimicking an ADPKD cyst[13]. To answer the previous question, we decided to use the *TgBAC(cftr-GFP)pd1041* zebrafish line which gives us a live readout of CFTR expression. This is a transgenic zebrafish line that expresses a CFTR-GFP fused protein and that was gently given to us by Bagnat's group (Department of Cell Biology, Duke University Medical Center, Durham, USA). This line was generated using the zebrafish *cftr* BAC (DKEY-270I2). This contains ~50 kb of genomic DNA upstream and 100 kb downstream of the coding sequence, being, therefore, expected to include critical transcriptional regulatory elements[14]. GFP was fused with the CFTR C-terminal by replacing its stop codon with GFP, separated by a sequence encoding a 20 aa spacer to provide some insulation from GFP. According to Navis *et al.*, CFTR-GFP protein, by comparison with similar C-terminal fusion proteins of human CFTR, is expected to maintain similar localization and channel activity to untagged CFTR[14]. Nevertheless, we should keep in mind that the fused CFTR-GFP is not the WT CFTR which means that the folding, glycosylation and maturation of both protein may not be exactly the same.

To our work, it was important to have a clear notion of the embryonic tissues that do express CFTR, namely at the early developmental stages of the KV.

In a previous study, our group showed by whole mount *in situ* hybridization that, at the transcription level, *cftr* is expressed in the KV region and additionally in the brain, neural floorplate and, although with less intensity, in the primordia of pronephric ducts of zebrafish embryos at their 10 - 11 ss [13]. At that time, these data corroborated the findings of Navis *et al.* showing that at the 3 ss, *cftr* mRNAs were highly concentrated at the KV and at the 10 ss they were additionally detected in the chordamesoderm[14]. By confocal-live imaging analysis of 10 to 15 ss *TgBAC(cftr-GFP)pd1041* embryos, however, they have detected CFTR-GFP signal highly restricted to the KV-lining cells, mainly at their apical membrane[14].

In the present work, the CFTR-GFP expression was followed by a whole embryo live-fluorescence stereomicroscopy along the embryo and larva development in a larger time window, from the 70% of epiboly to 12 dpf.

No CFTR-GFP expression was detected before the 2 ss. At this developmental stage, which corresponds to the stage where the KV starts to inflate, a weak GFP signal was exclusively detected at the KV boundaries (Figure 11, panels A and B). This became stronger with time and it was clearly detected in this region until the KV disassembling at about the 15 ss. This is in agreement to what was previously reported [14]. But, this restricted CFTR-GFP expression does not match the findings from the *in situ* hybridization experiments performed by our group[13] and Navis *et al.* [14]. That discrepancy on the

regions of CFTR expression may result from: (1) CFTR-GFP levels bellow our detection threshold in all the other tissues apart from the KV; or (2) notwithstanding the regulatory region included in the *cftr* BAC used for transgenesis, it may not include the elements required for the expression of *cftr* in other tissues apart form the KV.

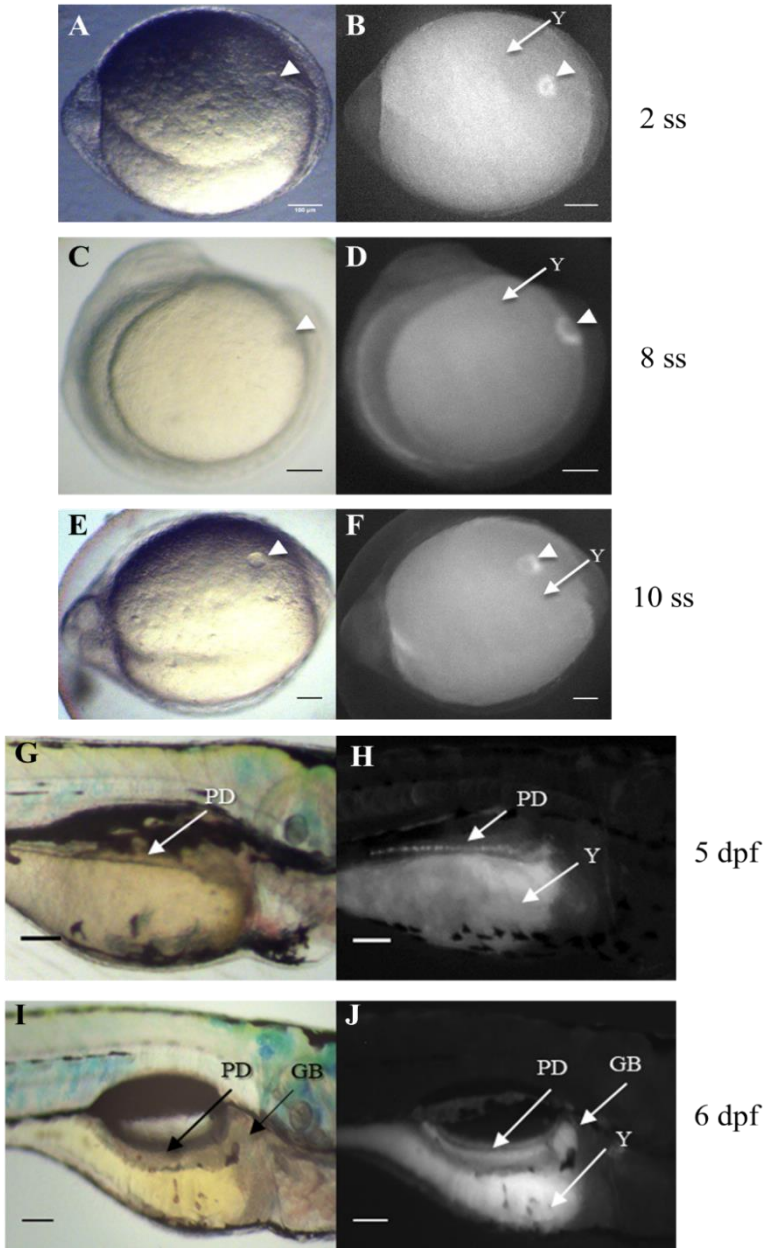

Figure 11 - *TgBAC(cftr-GFP)pd1041* zebrafish line characterization. A), C), E), G) and I) are bright field captured images. B), D), F), H) and J) were acquired by fluorescence stereomicroscopy. A)-F), white arrow heads indicate the KV. A) and B), ventral view of an embryo at 2 ss. C) and D), lateral view of an embryo at 8 ss. B), D) and F), fluorescent yolk (Y). E) and F), ventral view of an embryo at 10 ss. G) and H), right lateral view of larva with 5 dpf with CFTR-GFP signal in pancreatic ducts (PD). I) and J), right lateral view of a 7 dpf larva with CFTR-GFP signal whose location is suggestive of being the gall bladder (GB). H) and J), yolk auto fluorescence (Y). Scale bars: 10 μm.

It is important to mention that at this developmental time window the intensity of the CFTR-GFP signal was highly variable among embryos, being many times undetectable. This fact turned the work with these embryos harder than expected. At the beginning, we were screening the embryos by fluorescence stereoscopy before any further experiment. After several attempts, we thought we were photobleaching them, so, we continued the experiments without a prior screening of the CFTR-GFP

positive embryos. Instead, we started to use a significantly higher number of them, to increase the probability of having embryos with detectable GFP-fluorescence. A possible explanation for this variation could be an attempt of the animal tissues to bring to normal values the levels of CFTR expression. Indeed, it is plausible to think that the transgenesis may result in a CFTR overexpression. Therefore, by regulating both the transcription and translation of either the endogenous *cftr* or the transgene, the CFTR-GFP positive cells could maintain the levels of this protein under their physiological levels.

After the KV disassembling no CFTR-GFP signal was detected until 5 dpf. At this developmental time, the localization and the punctate pattern of CFTR-GFP expression was suggestive of being localized in pancreatic ducts. The signal became stronger and diffused along the pancreas of the animal in the following days. This observations are in total agreement with the confocal microscopy analysis of histologic sections of 6 dpf larvae and adult tissues previously reported by Navis and Bagnat [264].

At 6 dpf however, we have additionally detected the CFTR-GFP signal in the right side of the fish, in a structure that is likely to be the gall bladder (Figure 11, panels I and J). Indeed, this structure is compatible to what was described by Wallace and Pack (Figure 1.7) as being the gall bladder[227]. This was not reported by Navis *et al.*[14,264].

On the following days and at least until 12 dpf, this expression pattern remained the same. These results are supported by data obtained from human tissues analyses, according to which there is a strong expression of CFTR in the pancreas and gall bladder (https://www.ncbi.nlm.nih.gov/gene/1080).

Yet, to confirm the exact location and to identify the exact organ that have CFTR expression, specific markers or transgenic lines specific for these organs would be necessary. Navis *et al.* already confirmed the CFTR expression in pancreatic ducts. For that they have used transgenic zebrafish lines that labelled different parts of the pancreas. These were: the *Tg(ins:dsRed)* line in which pancreatic β-cells were labelled with dsRed; the *Tg(ela:GFP, lfabp:dsRed)* line which has GFP expression in the pancreatic acinar cells and dsRed expression in the liver; and a zebrafish line generated by the cross of three other lines, *TgBAC(cftr-RFP),TgBAC(cftr:Gal4*) and *Tg(UAS:GFP),* which allowed the finding that CFTR is expressed on the apical membrane of duct epithelial cells[264].

To confirm the expression of CFTR-GFP in the region suggestive of being the gall bladder, it will be also necessary to use transgenic lines or specific markers for the gall bladder. However, as far as we know, currently there are none of those for zebrafish. It was reported that the knockdown of specific genes and mutant lines (there are 10 of each reported) have the gall bladder structure and function affected. Therefore, these might be useful in the future (https://zfin.org/action/ontology/show-all-clean-fish/ZDB-TERM-100331-195?page=1).

The pancreatic and gall bladder-like CFTR-GFP expression was used to screen CFTR-GFP positive larvae required for the maintenance of the line at the CEDOC's zebrafish facility.

During the characterization of this line, we could not forget the auto-fluorescence that is naturally associated with zebrafish embryos and larvae. This auto-fluorescence was mainly seen at the yolk of both embryos and larvae (Figure 11, panels B, D, F, H and J).

4.2 – The impact of PKD2 knockdown over CFTR

With the use of the *TgBAC(cftr-GFP)pd1041* transgenic zebrafish line, we aimed to find how the knockdown of PKD2 influences the expression of CFTR-GFP, having a live readout of it.

4.2.1 – Evaluation of the PKD2 knockdown efficiency

First, we confirmed how efficient the knockdown of PKD2 was. By western-blot analysis of whole embryo protein extracts, the levels of PKD2 were compared between non-injected and *pkd2*-augMO injected embryos (*pkd2*-morphants) (Figure 12). Our group has previously evaluated the efficiency of this MO by immunohistochemistry which did not allow the quantification of it[13]. Indeed, all the commercially available antibodies against mammalian PKD2 that were tested at the time, failed in detecting the zebrafish protein by western blot [13]. Luckily, Drummond's group gently gave to us an aliquot of the unique antibody developed for zebrafish PKD2[241].

α-tubulin was used as an internal control since it is a protein known to be constitutively expressed in almost all tissues and cells[266]. It was clearly useful in this particular case, because as it can be seen in plate A of the Figure 12, there was a problem with the protein quantification or during the sample application on the SDS-page gel. Indeed, the levels of α-tubulin between the two tested samples are different and they should not if the same quantity of protein of each sample was applied to the gel. This problem was, nevertheless, overcome by the densitometry analysis of the blots where the bands intensity was normalized with the corresponding α-tubulin band. In Figure 12 panel B, densitometry analysis results are presented with the analysis of two heavier PKD2 detected bands. Despite the problem associated with the blot, we have no doubt of the efficient knockdown of the PKD2. Indeed, there was an almost complete ablation of the 110 kDa PKD2 band, which should correspond to the full-length protein, in *pkd2*-morphants compared to the non-injected controls. This is a much stronger phenotype than that expected from the immunohistochemistry analysis previously reported[13].

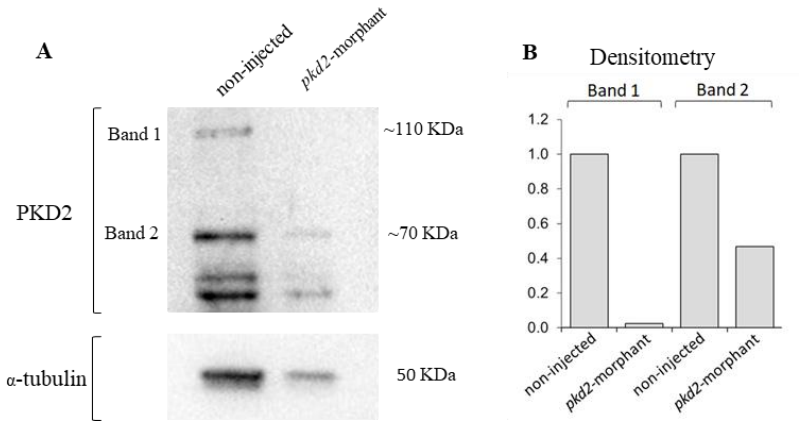

Figure 12 – Evaluation of the PKD2 knockdown with the *pkd2*-augMO. A) comparison of PKD2 expression levels between non-injected embryos and embryos injected with *pkd2*-augMO, by western-blot analysis. B) densitometry analysis required to evaluate PKD2 normalized protein levels between two bands from each batch of embryos (injected and non-injected). Total protein amount per lane = 25 μg.

4.2.2 – The impact of the knockdown of PKD2 over the KV volume

The KV volume of 23 *pkd2*-morphants was measured and compared to that of 24 non-injected sibling embryos at their 8 -10 ss (Figure 13). For that, the whole KV was scanned by confocal live-microscopy and then the volume was determined with the Measure Stack plugin of the ImageJ software.

Comparing both middle focal plans and orthogonal views from the most representing KVs, it is visible that *pkd2*-morphant KVs have larger dimensions than those from non-injected siblings (Figure 13, panels A and B). The measured volumes reflected that difference, being 1.2 times larger in the *pkd2*-morphants than in the non-injected embryos. With an average and standard deviation of $133x10^3 \pm 38x10^3$ µm^3 and $108\ x10^3 \pm 43x10^3$ µm^3, respectively. A statistical analysis was performed using the *t*-test and the difference obtained between groups was significant with a *p* value of 0.0415 (Figure 13, panel C).

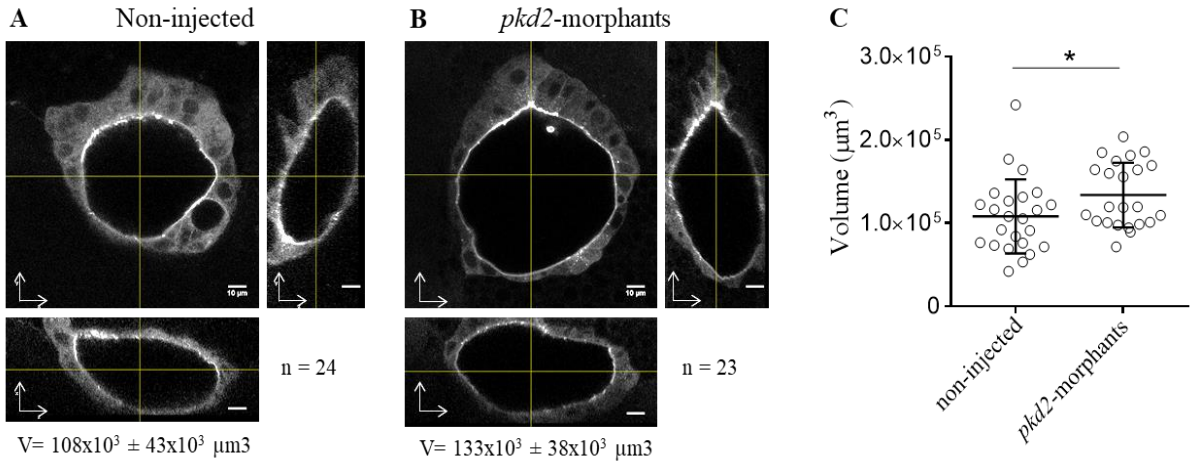

Figure 13 - Analysis of the KV volumes from injected and non-injected embryos of the *TgBAC(cftr-GFP)* line. Middle plan and respective orthogonal views of the most representative A) non-injected KV and B) *pkd2*-morphant siblings. The respective volume (V) average, standard deviation and number of embryos analyzed are indicated. C) Estimated KV volumes and statistical analysis of the 24 non-injected and 23 *pkd2*-morphant embryos. Means ± standard deviations are indicated; $*p < 0.05$. Scale bar: 10 µm.

As previously proven by our group in other zebrafish line, the knockdown of PKD2 leads to an enlargement of the KV through the CFTR stimulation and not because an increase in cell proliferation [13]. Indeed, there was no difference in the number of KV-lining cells (approximately 60), comparing non-injected and *pkd2*-morphants [13]. However, it is not completely understood if this volume enlargement was solely due to a higher CFTR activity or if it results simultaneously from higher expression levels of CFTR.

4.2.3 – The impact of the knockdown of PKD2 over CFTR expression

We know already from a previous microarray analysis made by our group that the knockdown of PKD2 does not interfere with the *cftr* transcriptional levels (unpublished data from our group[267]). What about the protein levels? We postulated that the lack of PKD2 may enhance the protein levels of CFTR.

In order to see if that was the case, we quantified the normalized Mean Fluorescence Intensity (normalized MFI) of the CFTR-GFP signal throughout the KV of *TgBAC(cftr-GFP)pd1041* embryos. For each embryo, we calculated the normalized MFI of the resulting KV image from the sum of all slices of each whole KV scan, obtained by confocal live-microscopy (panels A and B in Figure 14). As explained in the Material and Methods section, the presented normalized MFI values were normalized with the background of the respective image and determined using the ImageJ software. Interestingly, our data showed *pkd2*-morphant normalized MFI levels 1.9 times higher than non-injected normalized

MFI (non-injected normalized MFI =$1.3\times10^6 \pm 0.2\times10^6$; *pkd2*-morphant normalized MFI =$2.5\times10^6 \pm 0.3\times10^6$; p=0.0166) (Figure 14). This strongly supports our hypothesis that the knockdown of PKD2 is enhancing the levels of CFTR.

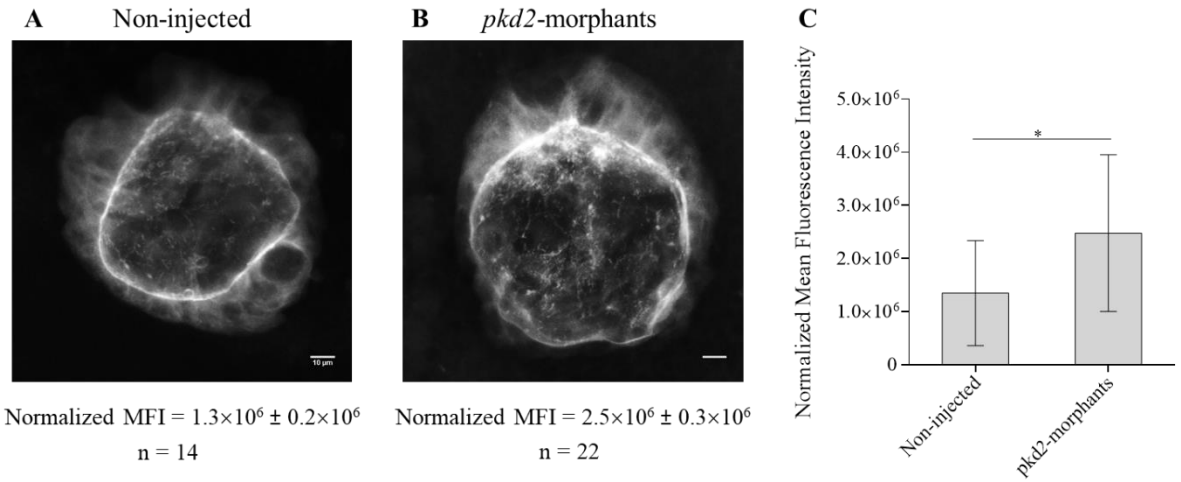

Figure 14 - Normalized MFI comparison between non-injected embryos and *pkd2*-morphants. Image resulting from the sum of all slices of a representative KV of A) non-injected embryos and B) *pkd2*-morphants. C) Estimated normalized MFI values and statistical analysis of the obtained results. Means ± standard deviation and number of embryos for each group are indicated; * p <0.05. Scale bars: 10µm.

This led us to ask: Is CFTR-GFP equally distributed throughout the KV? And does this distribution change upon the knockdown of PKD2? To assess that, a similar analysis was made but this time comparing the normalized MFI of the CFTR-GFP from the anterior part of the KV with that of the KV posterior part (panels A and B, Figure 15).

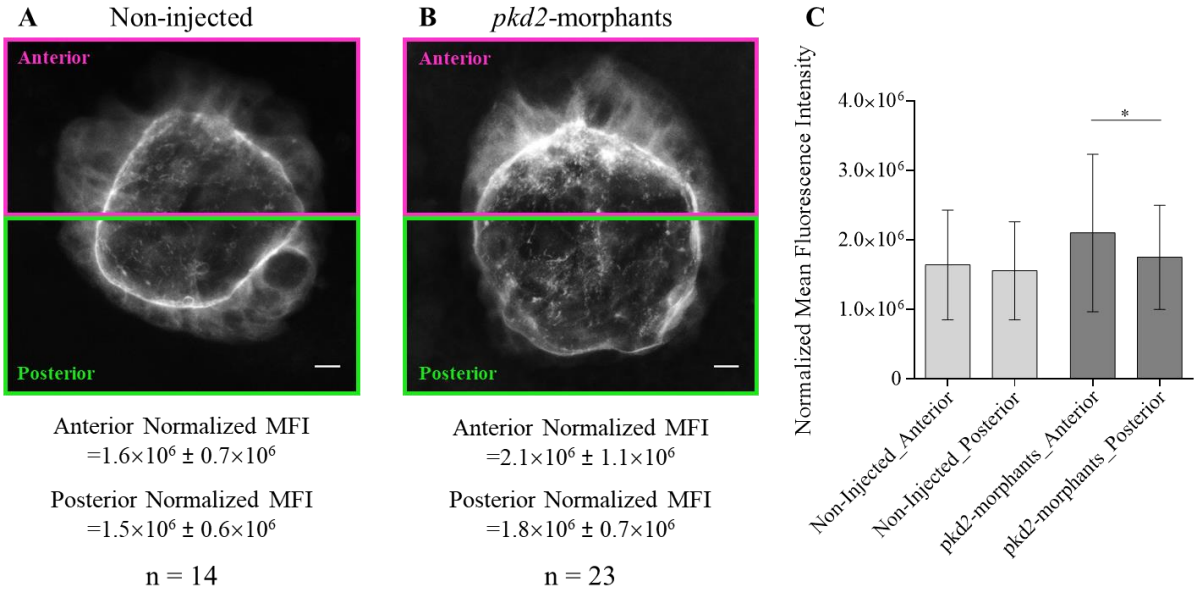

Figure 15 – Normalized MFI of the anterior (magenta area) of the KV versus its posterior (green area) part. A) and B) Images resulting from the sum of all slices in both non-injected embryos and *pkd2*-morphants with the representation of the areas that were defined as anterior and posterior parts of the KV. C) Means ± standard deviations are indicated for each measurement with each group; paired t-test * p <0.05. Scale bars: 10 µm.

No significant difference was observed in the distribution of CFTR-GFP along the anterior/posterior axis of the KV of non-injected embryos (light grey bars of panel C in Figure 15). However, this changed in *pkd2*-morphants KVs. The anterior part of the *pkd2*-morphant KVs had a normalized MFI 1.2 times higher than their posterior part (anterior normalized MFI $=2.1\times10^6 \pm 1.1\times10^6$; posterior normalized MFI $=1.8\times10^6 \pm 0.7\times10^6$; p=0.0166) (dark grey bars in the panel C of Figure 15).

Analysing the whole KV scans (Figure 13, panel A), we were able to observe that CFTR-GFP accumulates at the apical surface of the KV-lining cells, facing the lumen of this organ. This was already reported by Navis *et al.*[14]. We then asked if the higher levels of CFTR-GFP observed in *pkd2*-morphants could mean more CFTR-GFP at the apical membrane of the KV-lining cells. To answer this question, we made a similar analysis, but this time comparing the normalized MFI of the apical CFTR-GFP from non-injected embryos and *pkd2*-morphants (Figure 16). Interestingly, our results point to a normalized MFI 1.6 times higher (non-injected normalized MFI $=2.4\times10^5 \pm 0.3\times10^5$; *pkd2*-morphants normalized MFI $=3.7\times10^5 \pm 0.4\times10^5$; p=0.0272) in the apical membrane of the KV lining cells from the *pkd2*-morphants, when comparing with their non-injected siblings. Suggesting that there are higher amounts of CFTR-GFP in the apical membrane of the *pkd2*-morphants.

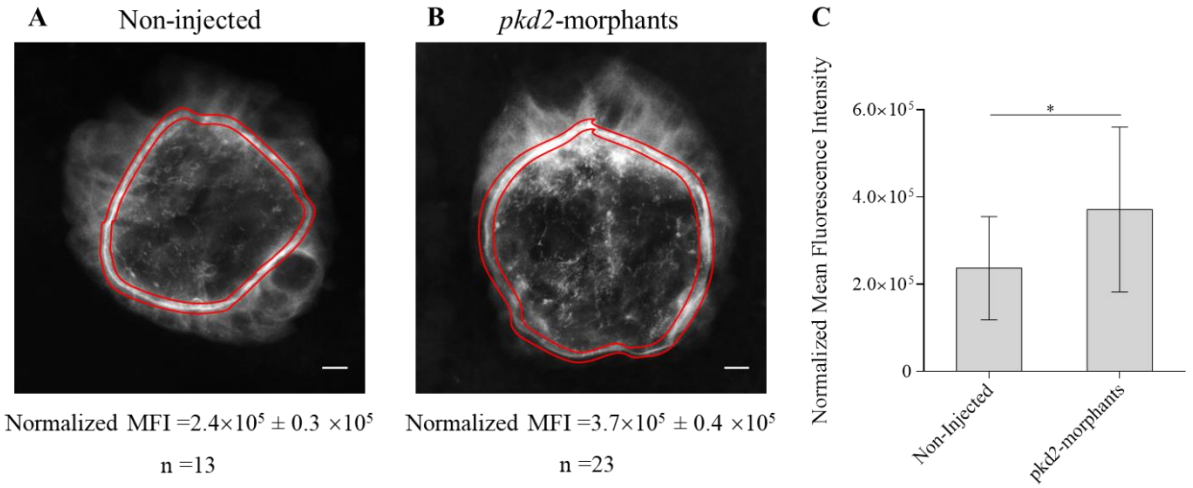

Figure 16 - Comparison of the normalized MFI of the apical CFTR-GFP from non-injected embryos and *pkd2*-morphants. A) and B) Images from the sum of KV slices from representative KVs of non-injected embryos and *pkd2*-morphants. In red is represented the area used to measure the normalized MFI of the apical CFTR-GFP. C) Statistical analysis of the normalized MFI from both groups. Means ± standard deviations and number of embryos analysed are indicated. * p <0.05. Scale bars: 10 µm.

Another observation that came out from our whole KV scans was the presence of CFTR-GFP positive intracellular vesicles within the KV-lining cells, especially at the anterior part of the organ (Figure 17). These appeared to be involved in CFTR-GFP intracellular trafficking. Interestingly, *pkd2*-morphants always seemed to have a higher number these vesicles than their non-injected siblings. However, their quantification/tracking was not possible because of the time and resources required for this analysis. Indeed, it would be necessary to acquired confocal scans of the KVs with a much higher resolution than the used in our films, which would be very time consuming, requiring several hours of confocal microscopy.

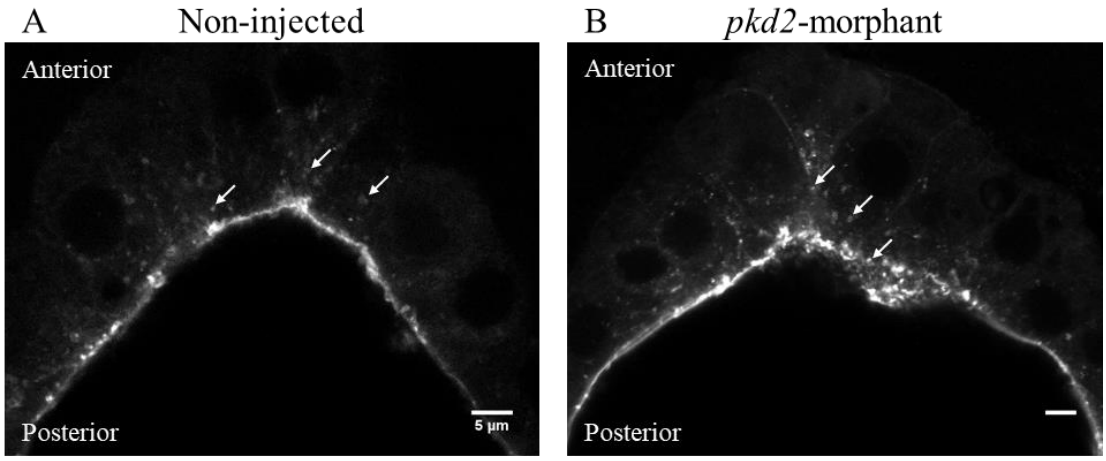

Figure 17 - Detailed snapshot of the anterior part of the middle focal plan of the KV. White arrows indicate intracellular CFTR-GFP positive vesicles. A) non-injected embryo and B) *pkd2*-morphant. Both embryos were at their 8 - 10 ss. Scale bar: 5 µm.

Despite our positive results, we decided to evaluate the *in vivo* impact of the knockdown of PKD2 in the CFTR-GFP levels using a different and perhaps more sensitive method. We decided to do so, because given the already mentioned variability of the CFTR-GFP signal, we had always to select the best embryos use for the live-confocal microscopy acquisition. Therefore, we wanted to be absolutely sure that this selection was being done in an unbiased manner.

4.2.4 – Evaluation of CFTR-GFP fluorescence intensity by flow cytometry

A more sensitive method that in theory could be used to compare the CFTR-GFP expression levels between *pkd2*-morphants and non-injected embryos would be the western-blot. However, all the attempts made using 2 different anti-CFTR monoclonal antibodies (#A4-596 and #A2-570 from Cystic Fibrosis Foundation) raised against the human CFTR, failed. A plausible explanation could be that they do not recognize de zebrafish CFTR. An additional and unsuccessful attempt was made using an antibody against GFP (A-11122, Invitrogen, Thermo Scientific). However, this was not completely surprising if we consider that, according to the data shown above, at the 8-10 ss only about 60 cells of the embryo, the KV lining cells, do express CFTR-GFP. Therefore, the CFTR-GFP pool must be highly diluted in the used whole embryo protein extracts making this analysis impossible.

Our next step was to perform this analysis by flow cytometry. Although having all the requirements, we weren't absolutely sure that it would work for the *TgBAC(cftr-GFP)pd1041* zebrafish embryos. Both *pkd2*-augMO injected and non-injected *TgBAC(cftr-GFP)pd1041* embryos at 8 - 10 ss were analyzed using the BD FACSCanto II flow cytometer. In each experiment, WT zebrafish embryos were used to trace the limiting gates (Figure 18, panel A) in order to exclude: (1) debris and medium components; (2) cell agglomerates; (3) and auto-fluorescent cells. In this way, only CFTR-GFP-positive single cells were considered for the analysis.

GFP-positive cell population was clearly distinguished in *TgBAC(cftr-GFP)pd1041* embryos, as shown in panel A of Figure 18. In this way, it was possible to determine and compare the MFI of the CFTR-GFP cells in *pkd2*-morphants with that of non-injected embryos. For that $4x10^5$ cell events per sample were required. Indeed, considering the about 60 KV-lining cells per embryo, less events would

not achieve the minimum % of GFP-positive cells accepted to perform statistical analysis, *i.e.*, 0.1 % of total cells or more than 300 GFP-positive cells.

This experiment was replicated three times with different batches of 200 embryos from different progenitors and in different days. Then a statistical analysis (Figure 18, panel B) with all the data was done, using a paired *t*-test, to evaluate the relevance of the MFI data obtained. The results showed a significant increase ($p = 0.0359$) of the MFI in the *pkd2*-morphants (average MFI =581) comparing with their non-injected siblings (average MFI =476). This means a CFTR-GFP MFI 1.2 times higher in *pkd2*-morphants than in non-injected controls.

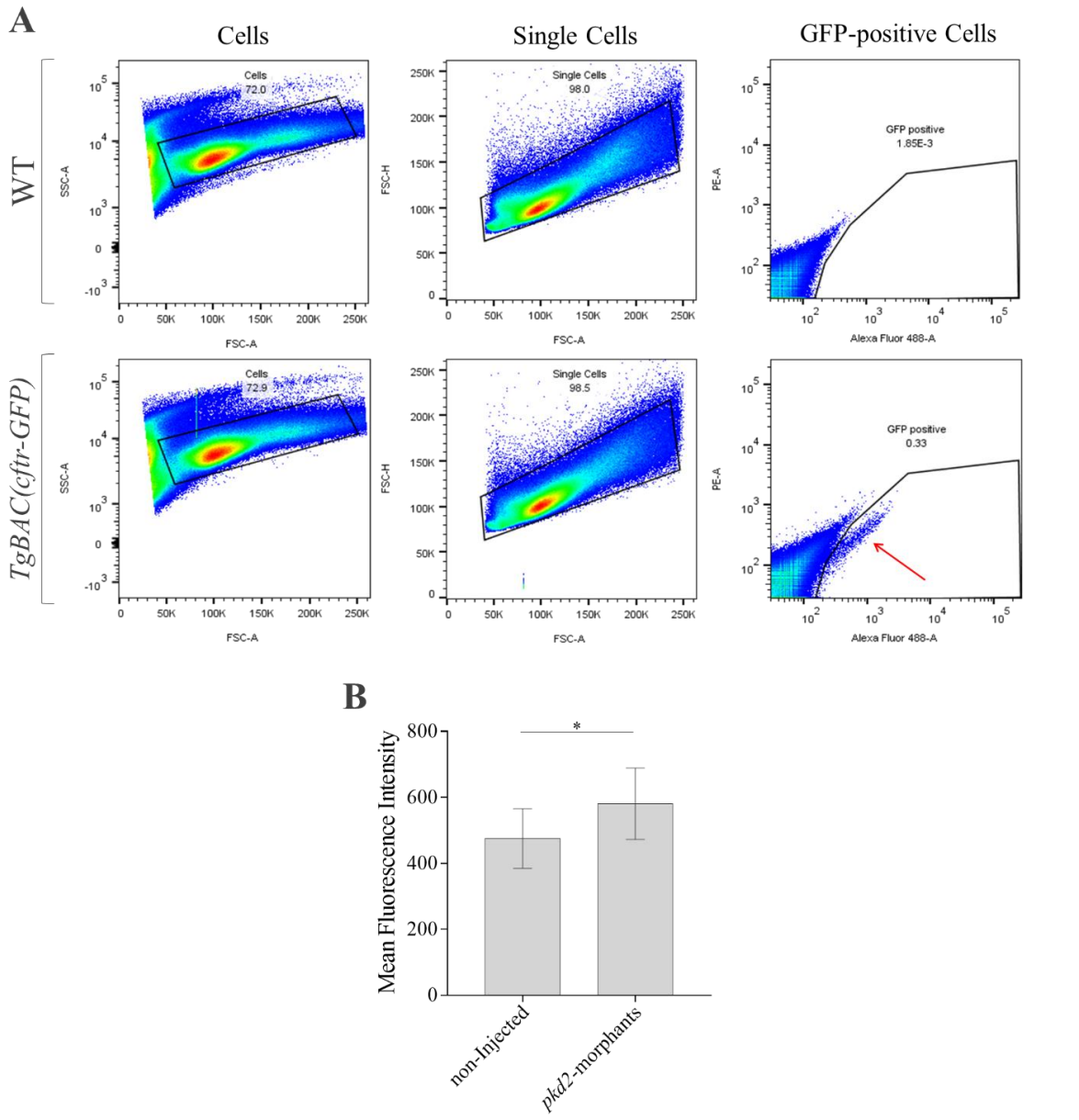

Figure 18 - Flow cytometry analysis. A) Flow cytometry plots representative of the established limiting gates for WT control embryos and for *TgBAC(cftr-GFP)pd1041* embryos, all at 8 - 10 ss. First excluding cell debris and medium components from cells, secondly excluding cell agglomerates from isolated cells, and in third place, excluding autofluorescent cells. These were established for each replicate. In this way, only GFP-positive cells (red arrow) were considered for the analysis. B) Statistical analysis of the mean fluorescence intensity from the data measured for non-injected (3 replicates) and injected embryos (3 replicates). * $p<0.05$. Forward SCatter (FSC) - cell size; Side SCatter (SSC) - granularity and internal complexity of the cell; Forward Scatter-A (FSC-A) - area of the fluorescence peak of the cell; Forward Scatter-H (FSC-H) - peak height; and Phycoerythrin (PE) fluorophore which is excited by a 488 nm tuned laser.

Altogether, the presented results were suggestive of an increase of CFTR-GFP amounts upon the knockdown of PKD2. Considering that this is not occurring at the *cftr* transcription level, since no difference was found in the *cftr* mRNA levels of *pkd2*-morphants compared to non-injected embryos (unpublished microarray data of our group), our data point to: higher translation rates or enhanced protein stability.

4.3 – The impact of Myriocin treatment over CFTR

As mentioned in the Introduction section, the comparative microarray analysis previously performed by our group revealed that the mRNA expression levels of some key enzymes of the sphingolipid metabolism were altered upon the knockdown of PKD2 (unpublish data[15]). Based on these data and on literature, we postulate that changes in this metabolism may play a role in ADPKD and, in particular, in the relationship between PKD2 and CFTR. Supporting this hypothesis are reports connecting CFTR to sphingolipid metabolism, namely ceramide levels [18,257,258]. Moreover, unpublished results from our group showed that the inhibition of the first step in ceramide *de novo* synthesis by Myriocin, reduces significantly the KV volume of non-injected embryos and rescues the KV enlargement of the PKD2 knocked down embryos[267].

4.3.1 – Using the *TgBAC(cftr-GFP)* zebrafish embryos

So, in order to deepen our knowledge of this issue, a flow cytometry experiment was done with a previous incubation of the embryos with Myriocin for 2 hours. Myriocin was chosen since it is a potent specific inhibitor of the enzyme that catalyses the first step of sphingolipid metabolism, the serine palmitoyltransferase (https://www.caymanchem.com/product/63150), affecting directly the ceramide production. It is important to mention that one subunit of this enzyme is in the list of the target gene that came out from the mentioned microarray analysis.

Again, WT zebrafish embryos were used to set the gates exactly as described above. The samples analysed were non-treated *TgBAC(cftr-GFP)pd1041* 10-11 ss embryos, *TgBAC(cftr-GFP)pd1041* 10-11 ss embryos incubated with 0.5 % (v/v) DMSO as control (since this was the solvent of myriocin solution) and *TgBAC(cftr-GFP)pd1041* 10-11 ss embryos incubated with 50 µM of Myriocin from 6 ss onwards.

There were some difficulties with this protocol optimization. Namely, we had to deal with a higher mortality rate of the embryos. These was probably related to the fact that in the procedure it was necessary to dechorionate the embryos with 12.5% (v/v) pronase, prior the incubation with Myciocin. This may have enhanced the sensibility of the embryos and potentiated the toxicity of the drug. Therefore, the $4x10^5$ cell events, 300 GFP-positive cells and the 0.1% of GFP-positive cells that are required for a good analysis were not able to be simultaneously achieved in every 4 replicates. Nevertheless, we were able to reach two of those parameters simultaneously, what allows us to present our preliminary results (Figure 19). According to these, there is no significant differences among the analysed samples, suggesting that the incubation with Myriocin does not affect the amount of CFTR-GFP in the KV-lining cells. Therefore, the reduction of the KV volume observed to occur in non-injected embryos upon Myriocin treatment (unpublished data from the group[267]) is probably caused by an impairment of the CFTR activity or of its membrane stability. In the near future, we will repeat these experiments in non-injected embryos and we will also do the same analysis on *pkd2*-morphants.

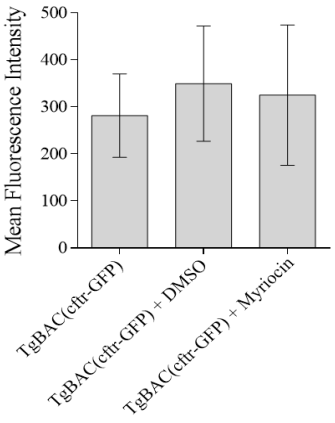

Figure 19 - Statistical analysis of the experiment performed to access the impact of Myriocin treatment over CFTR, using *TgBAC(cftr-GFP)pd1041* embryos (data from the 4 replicates). It is represented the MFI for: *TgBAC(cftr-GFP)pd1041* non-treated embryos; *TgBAC(cftr-GFP)pd1041* embryos incubated with 0.5% (v/v) of DMSO; and *TgBAC(cftr-GFP)pd1041* embryos incubated with 50 µM of Myriocin.

4.3.2 – Using Mammalian Cells

CFTR has been extensively studied in mammalian cell lines, namely in those derived from airways epithelia. So, we decided to give a step forward in our analysis and study the impact of Myriocin over CFTR in mammalian cells. However, we wanted to select a cell line that was more closely related to the ADPKD context, *i.e.*, a cell line of kidney epithelial cells. As these do not express endogenously detectable levels of CFTR, we chose to test two different cell lines ectopically expressing CFTR, which were a kind gift of Margarida Amaral's group (BioISI – Biosystems & Integrative Sciences Institute, Department of Chemistry and Biochemistry, Faculty of Sciences, University of Lisboa, Portugal). These were the MDCK-wtCFTR and HEK 293-wtCFTR cells [20,263]. First, we verified by western-blot the expression levels of both PKD2 (endogenous expression) and CFTR (ectopic expression) (Figure 20). Both cell lines express the two proteins (Figure 20).

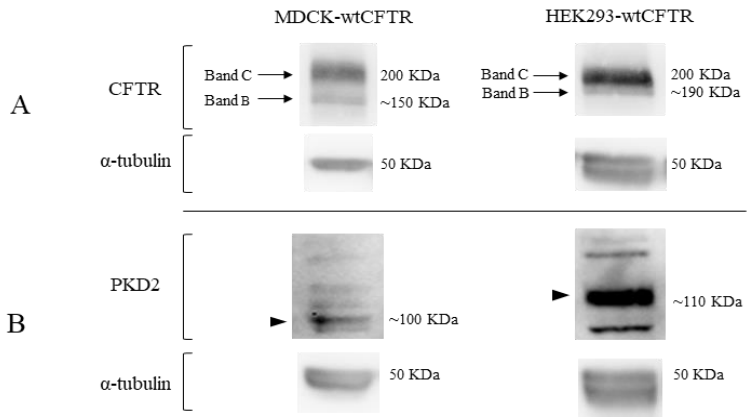

Figure 20 - Western-blot for analysis of CFTR and PKD2 expression in both MDCK-wtCFTR and HEK293-wtCFTR cell lines. A) On the western-blot for CFTR, both bands C and B of this protein were detected. B) On the western-blot for PKD2, the black arrow heads indicate the mature form of PKD2, with about 110kDa. In this blot, all the other bands may correspond to other glycosylated and/or phosphorylated status of the protein. Total protein amount per lane = 33.4 µg.

However, the HEK293-wtCFTR line seemed to be more efficient in CFTR maturation. Indeed, these cells express a more intense band C and lower levels of band B than the MDCK-wtCFTR cells. Moreover, the endogenous expression of PKD2 was much higher in HEK293-wtCFTR cells than in

MDCK-wtCFTR cells. Having these data in account and considering that HEK293-wtCFTR are human derived cells we chose this cell line to proceed with the next experiences.

Following the same line of thought applied in zebrafish embryos, the impact of Myriocin in CFTR was evaluated in HEK293-wtCFTR cell line. For that, cells were first cultured in a chamber slide (with 8 wells, 4 samples + 4 replicates). By the time they reached about 70 – 80 % of confluency, cells were incubated with 100 nM of Myriocin overnight or with 20 µM of Myriocin for 2 or 4 hours. After that an immunofluorescence was performed to detect CFTR and the slides were analysed by confocal microscopy (Figure 4.21). Myriocin concentrations used in this experiment were chosen based the literature[268–270].

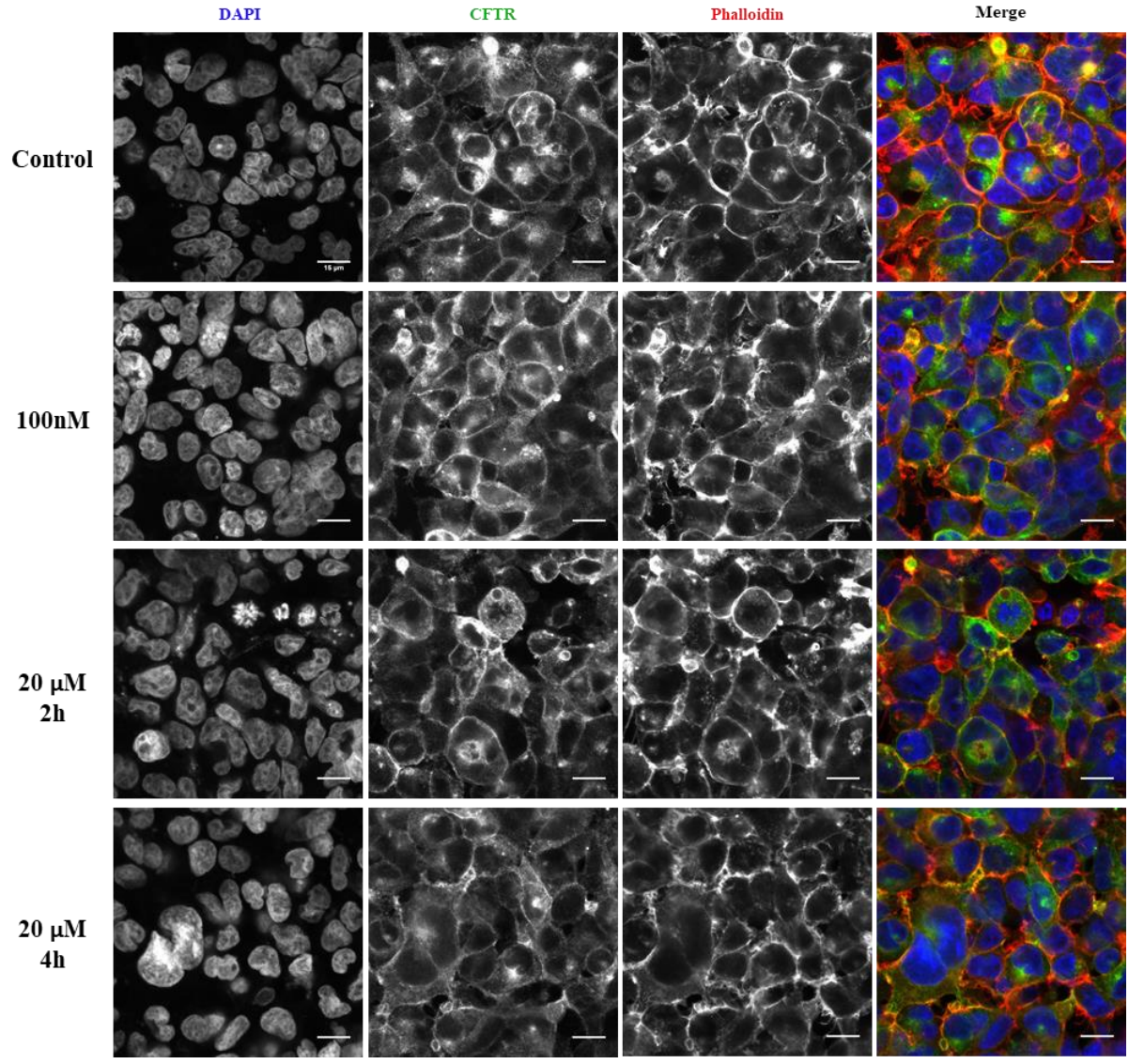

Figure 4.21 – Immunofluorescence detection (by confocal microscopy) of structural differences between HEK293-wtCFTR control cells and those incubated with different concentrations of myriocin, 100 nM overnight and 20µM for 2h and 4h. Cells were stained for CFTR (green), which can be seen at the cells membrane, in the budding vesicles, in intracellular aglomerates and dispersed by the cytoplasm; phalloidin (red), to help defining the boundaries of each cell; and DAPI (blue) to identify cell nuclei. All of the stainings are represented individually and merged. Scale bar: 15 µm.

We decided to evaluate differences in: the ratio of "budding vesicles" (V), *i.e.*, vesicles budding out of the cells that were simultaneously positive for CFTR and F-actin (phalloidin); the ratio of cells expressing CFTR at the membrane (M), *i.e.*, cells clearly showing a co-localization between CFTR and

the phalloidin staining; and the ratio of cells presenting intracellular agglomerates of CFTR (I). An example of each of these parameters are easily observed in Figure 22 .

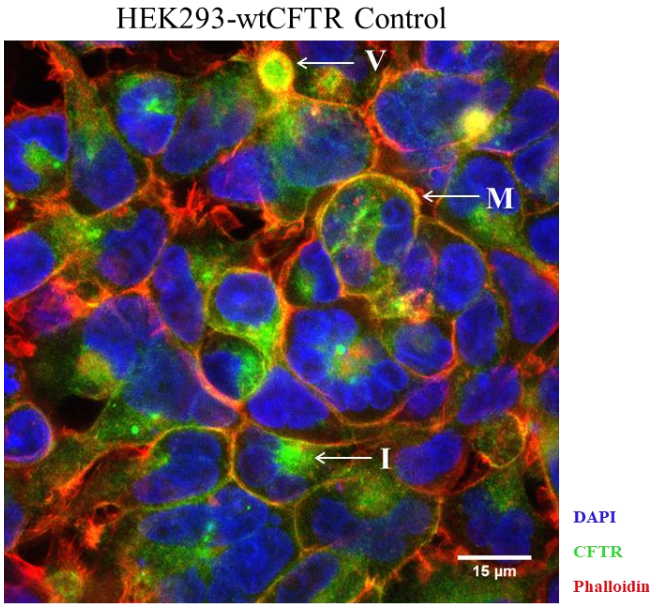

Figure 22 - Immunofluorescence image of the HEK293-wtCFTR control sample. It is represented the structural parameters that were compared among the samples. (V) "budding vesicles", (M) cells with CFTR concentrated at the membrane and (I) cells with intracellular CFTR accumulation. Scale bar: 15 µm.

Those established parameters were quantified and normalized by dividing the number of positive cells by the total number of cells present in each analysed image. For each sample 5-10 images were analysed and the whole experiment was repeated 3 times. After the quantifications of the 3 experiments, a *t*-test was done (Figure 23).

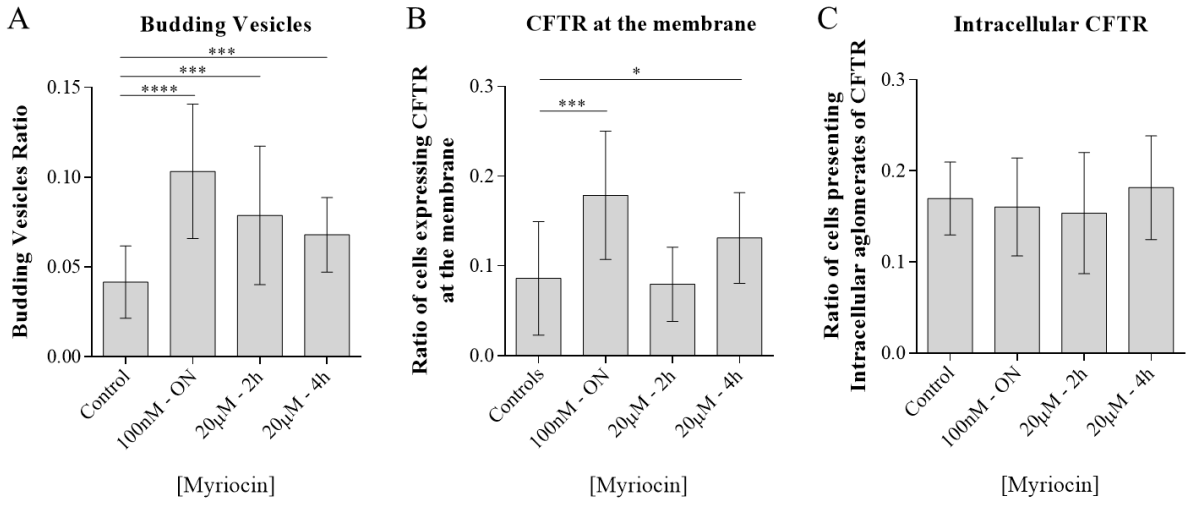

Figure 23 - Statistical analysis of the parameters analysed in HEK293-wtCFTR cell samples. A) Ratio of budding vesicles counting per cell. B) Ratio of cells with CFTR at the membrane. C) Ratio of cells with intracellular CFTR. *t*-test **** $p < 0.0001$, *** $p < 0.001$ and * $p < 0.05$.

It was interesting to observe that the treatment of HEK293-wtCFTR with Myriocin increased significantly the number of CFTR-positive budding vesicles coming out of the cells (panel A, Figure 23). The strongest effect was seen in cells incubated with the lowest dose but for a longer period of time, *i.e.*, 100 nM, overnight (V in control cells = 0.04 ± 0.005; V in 100 nM ON = 0.1 ± 0.009, $p < 0.0001$). This was concordant with the observation that Myriocin treatment led to an increase of the ration of cells expressing CFTR at their membrane, again with a strongest effect registered with 100 nM of Myriocin, overnight (V in control cells = 0.09 ± 0.01; V in 100 nM ON = 0.2 ± 0.02, $p < 0.0001$) (panel B, Figure 23). This suggests that, in this model system, the disruption of the sphingolipid metabolism enhances the trafficking of CFTR towards the membrane. On the other hand, we saw no difference in terms of the number of cells presenting intracellular agglomerates when comparing control cells and those incubated with Myriocin (Figure 23, panel C).

5. DISCUSSION AND FUTURE PERSPECTIVES

In ADPKD, renal cysts are the major clinical manifestation. Although the mechanisms of cystogenesis still remain largely unknown, there are 2 key steps involved: the abnormal cell proliferation in kidney tubule epithelia; and the inflation of the recently formed cysts that require the transepithelial fluid secretion towards the cyst lumen[2,11]. The role of CFTR in this process has been assessed using different models. In 1996, it was reported the presence of Cl^- selective currents in ADPKD cultured cells that were blocked with CFTR inhibitors and stimulated with cAMP analogues[142]. Simultaneously, it was reported that ADPKD cyst lining cells do express CFTR[141]. Later on, cell[143,144,176] and mouse[145,146] models for ADPKD have been used to demonstrate the key role of CFTR in cyst inflation and the effectiveness of CFTR inhibitory molecules in preventing this event.

These model systems are, however, limited in studying the precise *in vivo* mechanisms by which the lack of Polycystins affect CFTR, leading to its abnormal stimulation. A gap that can be partly overcome by the use of the zebrafish KV as a model-organ[13]. Indeed, the KV has important features to serve this role: it is a fluid-filled cavity architecture that reassembles an ADPKD cyst; it is lined by monociliated cells, exactly as epithelial ADPKD cyst lining cells are; these cells express endogenously both CFTR and PKD2 proteins which knockdown is relatively easy to achieve; it has a fluid-flow induced by Ca^{2+} signalling and mediated by PKD2 in normal conditions and that is altered by the absence of PKD2[271]; importantly, its inflation is dependent and mediated by CFTR and the lack of PKD2 leads to an enlargement of the KV through CFTR abnormal stimulation [13]. The biggest disadvantage of the KV as a model organ for ADPKD kidney cysts is the fact that it does not expresses PKD1 limiting our study to PKD2. We know (unpublished data from the lab) that KV cells express PKD1L1 (PKD1-like-1) protein, a close but shorter paralog of PKD1, that functions and the partner of PKD2 in the cells of the left-right organizer in other animal models[272].

5.1 – *TgBAC(cftr-GFP)pd1041* – CFTR-GFP expression in the KV, pancreas and gall bladder

The combination of the use of the zebrafish transgenic line *TgBAC(cftr-GFP)pd1041* and the KV as a model-organ for ADPKD study revealed to be very useful. The fusion of CFTR with GFP provided a live readout of the CFTR expression. This allowed the *in vivo* evaluation by live microscopy of CFTR-GFP expression over time and allowed the analysis of the impact of PKD2 knockdown over it, both by confocal live microscopy and by flow cytometry.

We observed that in the early stages of development of the zebrafish embryo, CFTR-GFP was first detected at the 2 ss, being its expression restricted to the KV. This corroborates the requirement of CFTR for the KV inflation previously described[13,14]. This expression pattern was observed all along the KV time window suggesting its requirement for the maintenance of the volume of the KV. Its expression ceased at the 16 ss, time point at which the KV is disassembled[67].

It is important to mention that the CFTR-GFP expression does not fully matched with the *cftr* mRNA expression pattern described by both our group[13] and Navis *et al.*[14]. Indeed, besides the KV, *cftr* mRNA were detected by *in situ* hybridization in the chordamesoderm[14], brain, neural plate mesoderm and primordia of the pronephric ducts[13]. This unconformity of results may be caused by CFTR-GFP levels that were lower than the detection threshold by stereomicroscopy. Additionally, it cannot be excluded the possible lack of the regulatory elements required for the *cftr* transcription in those tissues in the BAC used for the transgenesis.

After the closure and disassembling of the KV, we detected CFTR-GFP again only at 5 dpf, restricted to a structure that is suggestive of being the pancreatic ducts (Figure 11, plates G and H). This signal became stronger in the following day (Figure 11, plates I and J). This comes in agreement with a study of Navis and Bagnat, where it is shown that CFTR is expressed along the pancreatic ducts of 3, 5 and 6 dpf larvae and of adult *TgBAC(cftr-GFP)pd1041* zebrafish[264]. Under the limits of detection of the Navis and Bagnat study, the CFTR-GFP expression in this zebrafish line is restricted to the epithelial cells of the pancreatic ducts, not being detected in β-cells of the pancreatic islet. Although our images do not have resolution to evaluate at this level, the stronger and diffused signal along the fish pancreas, observed in our imagens at 6 dpf, might be explained by higher levels of CFTR-GFP expression or even by pancreatic ducts growth in size and number.

This is in agreement with what it is known for human CFTR expression. CFTR is known to be expressed in pancreatic duct epithelia where it enables the transport of anions and water to the lumen of these ducts. In fact, CF patients also have severe problems associated with maldigestion and malnutrition due to the malfunction and destruction of this organ, caused by the lack of CFTR[273].

Therefore, an interesting additional use for the *TgBAC(cftr-GFP)pd1041* zebrafish line may be the study of ADPKD pancreatic disease. Indeed, as mentioned before, pancreatic cysts are an important complication of this disease. Thus, we could use this zebrafish line to study the relevance of CFTR, if any, in the pancreatic disease upon the absence of PKD1 or PKD2.

At 6 dpf we were able to additionally detect CFTR-GFP in a gall bladder-like structure (Figure 11, plates I and J). Indeed, CFTR-GFP signal was detected in an organ similar to the gall bladder described in the images of the work of Wallace and Pack (Figure 1.8, panels A and C) [227]. The expression of CFTR-GFP in the gall bladder was not reported by Bagnat's group, however, it is highly supported by human data (https://www.ncbi.nlm.nih.gov/gene/1080). To confirm that the expression of CFTR-GFP is in fact in the gall bladder, we should follow a similar strategy used by Navis *et al.* for the pancreatic expression. However, as far as we know, currently there are no available zebrafish markers or transgenic lines for the gall bladder. So, in order solve this issue a specific marker could be created by us in the future.

This line when used together with the zebrafish CF model (*cftr*^{pd1049})[14] may also be a useful tool for the CF field. Providing a live readout of CFTR expression, it allows testing the influence of relevant therapeutic molecules in this protein. Also, as in the study of Navis and Bagnat, CFTR-GFP expression in zebrafish pancreas may be useful to study CF pancreatic disease. These include destruction of pancreatic tissue that can lead to pancreas insufficiency and CF related diabetes[264].

It is important to mention that the intensity of the CFTR-GFP signal was highly variable among embryos, being many times undetectable. This variability was seen in every batch, being much more evident in embryos within the KV time window that in the larval stages. This was not described by the authors of the line[14,264] and brought an additional difficulty for our experiments. It is reasonable to think that it could be explained by some sort of cellular mechanisms to balance the levels of CFTR. This might happen because this line could have an overexpression of CFTR, since the fused CFTR-GFP protein was added by a BAC vector and these fish still have the endogenous expression of the protein. In that case, the animal tissues could maintain the levels of CFTR under their physiological levels regulating the transcription and/or the translation of either the endogenous *cftr* or the *cftr-gfp* transgene. We thought about evaluating this by Real-Time PCR, but unfortunately, we were not able to perform this analysis by the lack of time. Nevertheless, it is still an important analysis to do in the future.

5.2 – The impact of the knockdown of PKD2 over CFTR

TgBAC(cftr-GFP)pd1041 pkd2-morphants had a significant increase of their KV volume when compared with non-injected siblings. These data is in total agreement to what was previously reported by our group[13]. One possible explanation for this KV enlargement in *pkd2*-morphants could be an increase in cell proliferation. This hypothesis was already discarded by our group since there was no difference in the number of KV-lining cells (about 60 cells) between non-injected embryos and *pkd2*-morphants[13]. Therefore, the enlargement of the KV volumes of the *pkd2*-morphants should be totally dependent on CFTR. Indeed, it was demonstrated by our group and by Navis *et al.* that the lack or the knockdown of CFTR impairs the KV inflation[13,14]. But even more important is the fact that a 30 µM solution of CFTRinh-172, a specific inhibitor of CFTR, reduced significantly the KV volume of WT embryos and rescued it in *pkd2*-morphants to normal values, as shown by our group[13]. Additionally, by studying the effect of CFTR potentiators (forskolin + IBMX) plus the PKD2 knockdown, it was observed a synergistic effect of these two conditions with the KV volume of these embryos being 3.6 times higher than the volume of their WT siblings[13]. We want to understand mechanisms behind this, because they will give us clues about the ADPKD cyst inflation.

It will be interesting to compare in the future the cAMP levels of the KV-lining cells of non-injected embryos and *pkd2*-morphants. Indeed, as already mentioned, CFTR activity depends on cAMP, with elevated levels of it being translated in enhanced CFTR activity[136]. ADPKD cyst-lining cells have higher levels of cAMP and, therefore, increased CFTR activity[6]. There are commercially available kits (for example: Cyclic AMP XP® Assay Kit #4339, Cell Signaling Techonology, USA; Direct cAMP ELISA kit, Enzo Life Sciences Inc., USA; Cyclic AMP ELISA Kit, Cayman Chemical; cAMP-Glo™ Assay, Promega, USA) that would allow us to make those measurements. Having a more accurate measurement of CFTR activity in the KV-lining cells would be highly valuable. A possible strategy would be to establish a zebrafish transgenic line with a promoter of a KV specific gene (for example *foxj1a*) driving a ratiometric genetically encoded Cl^- indicator. This would be, however, difficult to execute.

Nevertheless, we postulated that the knockdown of PKD2 is also increasing the amount of CFTR in the cell and that it should have a role in ADPKD cystogenesis. So, we decided to evaluate the *in vivo* impact of the knockdown of PKD2 in the levels of CFTR in our zebrafish transgenic line of choice.

By comparing the normalized MFI for the CFTR-GFP of *pkd2*-morphant whole KVs with that of non-injected whole KVs, using the scans acquired by live-confocal microscopy, we observed that, indeed, the former have 1.9 times higher levels of the protein. These data were corroborated by the findings with the flow cytometry analysis. Here, we observed MFI values 1.2 times higher for the *pkd2*-morphant KVs than for non-injected embryos. The difference between the two observations could be related to the specificities of each technique, being the most accurate one for this particular purpose the flow cytometry analysis. Indeed, it allowed the analysis of a pool of about 200 embryos per sample minimizing the variability of the fluorescence among embryos. Additionally, the flow cytometry allowed the measurement of fluorescence intensity at a single cell level. Although, flow cytometry does not truly distinguish the membrane pool from the intracellular pool of the protein, more protein at the membrane results in higher MFIs. Therefore, the increased MFI observed for *pkd2*-morphants may not only mean higher amount of CFTR-GFP in general, but it may also reflect the higher amount of CFTR-GFP detected at the apical membrane of the KV lining cells in the whole KV confocal stacks. Indeed, using the confocal live-microscopy KV scans we observed that the apical membrane normalized MFI is higher in the *pkd2*-morphants. Together these results suggest that the absence of PKD2 leads to a stabilization of CFTR-GFP, in particular at the apical membrane of these epithelial cells.

Additionally, we evaluated the distribution of CFTR-GFP throughout the KV. According to our results, there is no significant difference of the amount of CFTR-GFP in the anterior versus the posterior parts of the KV of non-injected embryos. However, it appears to be different in the *pkd2*-morphants, with higher amounts on the anterior part (Figure 15). This conclusion is *per se* quite important for those that study the functioning of the organ as is the case of our group. Indeed, this may influence the flow generated inside the KV and deserves to be explored in the future. But, we cannot forget the results that our group has previously obtained, concerning the differences in the cells' shape from the anterior and posterior parts of the KV. In *pkd2*-morphants the KV-lining cells became shorter at the anterior region and longer at the posterior part compared to the WT KVs[13]. Therefore, this could account for the accumulation of CFTR-GFP at the anterior region of the *pkd2*-morphant KVs. During confocal live microscopy experiments, it was also observed that were also present intracellular vesicles positive for CFTR-GFP, which could possibly be involved in its trafficking. These seemed more abundant in *pkd2*-morphants than in non-injected embryos (Figure 17), especially at the anterior part of the KV. It would be interesting to have their quantification, but, with the available confocal microscope (LSM710, Zeiss), the image acquisition for this analysis would be highly time consuming in order to have the required resolution. This analysis would be even harder considering the variability in the CFTR-GFP signal among embryos.

We have also tried to evaluate the CFTR expression levels by western-blot, with the advantage that this would include both endogenous CFTR and CFTR-GFP proteins. However, as far as we know, there are no antibodies for the zebrafish CFTR and the ones against the human CFTR that we tested did not recognized the zebrafish protein. We have also tried to detect CFTR-GFP by western-blot using a GFP antibody, but it did not work. The reason for that could be to the fact that each embryo has only about 60 cells lining the KV [13] and so, expressing CFTR-GFP in the studied time point. This, associated with the fluorescence variability among embryos results in undetectable amounts of protein.

5.4 – The impact of the sphingolipid metabolism impairment over CFTR

Taking in account the results from the previously performed microarray (unpublished data from the group), that revealed changes in the mRNA levels of enzymes from the sphingolipid metabolism in *pkd2*-morphants[15], we were interested in understanding their impact over CFTR. Favouring this rational, there are in the literature papers connecting CFTR with the sphingolipid metabolism[18,257,258].

We decided to work with Myriocin because it is a specific inhibitor of the enzyme that catalysis the first step of this metabolism. Favouring its use, one subunit of this enzyme is in our list of target genes affected by the knockdown of PKD2. Our preliminary data of flow cytometry analysis of embryos treated with Myriocin showed no significant difference in terms of the MFI when compared to non-treated controls. Suggesting that Myriocin, although impairing the normal inflation of the KV, does not affect the amount of CFTR-GFP. Nevertheless, these experiments must be repeated. In some of the replicates, a reasonable number of the embryos died along the process, changing the number of embryos between samples. Therefore, this reduced the number of flow cytometry events, meaning that for some samples, we were not able to achieve simultaneously the $4x10^5$ events, the 300 GFP-positive cells and the 0.1 % of GFP-positive cells, which was required for a good analysis. We also aim to perform this experiment in *pkd2*-morphants.

5.5 – Evaluation of the relevance of the findings in mammalian cells

The mammalian cells that we could use to validate the previous findings needed to express both CFTR and PKD2. We had access to two cell lines both stably transduced with WT CFTR, MDCK-wtCFTR and HEK293-wtCFTR cells[20,263]. Since both were epithelial kidney cells they would be expected to express endogenous PKD2. Indeed, by a western-blot analysis it was confirmed that both lines expressed CFTR and endogenous PKD2. By analysing this result, we chose to continue the experiments with the HEK293-CFTR cells since they expressed more abundantly the mature form of CFTR and PKD2. Moreover, these are human cells. However, in the future, we should also analyse the MDCK-wtCFTR cells because these have the ability to form cyst-like structures.

Our initial goal was to verify the influence of the lack of PKD2 in CFTR levels and/or localization. However, we had problems with the plasmid that we had available to perform the PKD2 knockdown. This was the hPKD2-L224X pcDNA 3.1(-), which cDNA encodes the truncated form L224X of PKD2 and that was described to be a dominant negative for PKD2. It was given to us by Ong's laboratory (Academic Nephrology Unit, Sheffield Kidney Institute, University of Sheffield, Sheffield, United Kingdom)[274]. However, we were not able to reproduce the effect of dominant negative of L224X-PKD2 using this plasmid. Thus, given our lack of time, we move forward to evaluate the effect of Myriocin over the CFTR intracellular localization in HEK293-wtCFTR cells. A major drawback in our analysis may be the fact that the cells were not polarized. We should not forget that membrane polarity in epithelial cells (as in other cell types) is physiologically important for intracellular trafficking. Nevertheless, in these preliminary experiments, we were able to observe some differences in the CFTR localization caused by Myriocin treatment. These included a significant higher ratio of CFTR-containing vesicles budding out of the cells and also of cells with membrane expression of CFTR. The strongest effect was observed with the longer exposure, but with the lowest concentration, *i.e.* 100 nM of Myriocin overnight. This suggests that the Myriocin effect increases with its exposure time. This result suggests that Myriocin causes an alteration in the intracellular trafficking process, enhancing the secretory pathway and, thus, the transport of CFTR towards the membrane. To be absolutely sure about the expression of CFTR at the cell surface, biotinylation assays in polarized cells must be performed.

5.6 – ADPKD patients' samples

Initially, it was planned to evaluate all the results obtained with the zebrafish and mammalian cell using human tissue samples of ADPKD patients and non-ADPKD controls. The study was approved in the first semester of 2017 by the ethic committees of both Nova Medical School/Faculdade de Ciências Médicas, Universidade Nova de Lisboa and Centro Hospitalar de Lisboa Central.

The human samples received so far were sections of epigastric artery of 5 controls and 4 ADPKD patients. These sections are routinely collected during the surgical procedure of kidney transplantation. However, these samples may not be the most suitable for this part of the project.

Some reports claim the expression of CFTR in endothelial cells of orthologous models: mouse aorta endothelial cells [275]; in mouse pulmonary endothelial cells and in sheep bronchial artery endothelial cells [276]; in rat intrapulmonary arterial cells [277]; in bovine corneal [278] and aorta endothelial cells [279]. Additionally, some others have reported the expression of CFTR in human cultured cells: in lung microvascular endothelial cells [276]; in human endothelial cells from umbilical vein [280]; and even in human pulmonary artery endothelial cells from surgical fragments of non-CF and CF lungs [281]. However, the expression and activity of CFTR in human endothelial cells is not well established yet.

Because of this and since both time and sample quantity were reduced, the analysis of CFTR expression in these tissues were not tested yet, but it will be in the near future.

Other samples, from ADPKD kidneys, were also approved to be used in this study but we have not received any of them yet. These would be more suitable samples to study the impact of the lack of PKD2 or of PKD1 in CFTR. However, these are rare samples because usually the ADPKD kidney is not removed during the transplantation procedure. Moreover, given the high risk of bleeding because of their massive cysts, biopsy samples are not usually collected from ADPKD kidneys.

6. CONCLUSION

One of the main objectives from this work was to evaluate the molecular mechanisms by which the lack of PKD2 influences CFTR. From the literature, we already knew that CFTR was a key protein involved in ADPKD cysts inflation. We chose to use as model organ the zebrafish Kupffer's Vesicle given it mimics an ADPKD cyst[13] and we decided to use the *TgBAC(cftr-GFP)pd1041* transgenic line because it gave us a live-readout of the CFTR-GFP expression.

We knew already that the lack of PKD2 caused the KV enlargement, through CFTR activation[13] and that CFTR-GFP was expressed in the apical membrane of the KV-lining cells[14]. With the experiments performed along this year, we observed that *pkd2*-morphants have a significantly higher MFI in the KV-lining cells compared to non-injected embryos, measured both by confocal microscopy and flow cytometry analyses. These data indicated higher levels of CFTR-GFP in *pkd2*-morphants. Moreover, our data clearly showed that the amount of CFTR-GFP at the apical membrane of these cells was significantly higher in *pkd2*-morphants than in controls. Together these data point to a stabilization of CFTR-GFP protein which strongly supports the enlargement of the KV observed for the *pkd2*-morphants.

Additionally, following a major goal of the group which is to understand to role of the Sphingolipid Metabolism in ADPKD, here it was studied the effect of Myriocin over CFTR. Our preliminary results of flow cytometry analysis using *TgBAC(cftr-GFP)pd1041* embryos showed no significant differences in CFTR-GFP levels. However, as we faced several problems along these experiments, we consider that they must be repeated. Nevertheless, our preliminary results in HEK293-wtCFTR cells, suggest that Myriocin affects the intracellular transport of CFTR towards the membrane by affecting the secretory pathway.

In conclusion, CFTR is influenced by the lack of PKD2, not only at its activity level as described for ADPKD cysts, but also at the protein stability and expression levels. Moreover, there is space for changes in Sphingolipids to play a role in this crosstalk between lower levels of PKD2 and abnormal activation of CFTR. This should be carefully analysed in the context of ADPKD.

7. REFERENCES

The references in this work are written according to Nature Genetics guidelines.

1. Gall, E. C. *et al.* Type of PKD1 Mutation Influences Renal Outcome in ADPKD. *J. Am. Soc. Nephrol.* **24,** 1006–1013 (2013).
2. Wallace, D. P. Cyclic AMP-mediated cyst expansion. *BBA - Mol. Basis Dis.* **1812,** 1291–1300 (2011).
3. Dalagiorgou, G., Basdra, E. K. & Papavassiliou, A. G. Polycystin-1: Function as a mechanosensor. *Int. J. Biochem. Cell Biol.* **42,** 1610–1613 (2010).
4. Koulen, P. *et al.* Polycystin-2 is an intracellular calcium release channel. *Nat. Cell Biol.* **4,** 191–197 (2002).
5. Nauli, S. M. *et al*. Polycystins 1 and 2 mediate mechanosensation in the primary cilium of kidney cells. *Nat. Genet.* **33,** 129–137 (2003).
6. Torres, V. E. & Harris, P. C. Strategies targeting cAMP signaling in the treatment of polycystic kidney disease. *J. Am. Soc. Nephrol.* **25,** 18–32 (2014).
7. Patel, V., Chowdhury, R. & Igarashi, P. Advances in the pathogenesis and treatment of polycystic kidney disease. *Curr. Opin. Nephrol. Hyper.***18,** 99–106 (2009).
8. Torres, V. E. & Harris, P. C. Autosomal dominant polycystic kidney disease : the last 3 years. *Kidney Int.* **76,** 149–168 (2009).
9. Rossetti, S. *et al*. The Position of the Polycystic Kidney Disease 1 (PKD1) Gene Mutation Correlates with the Severity of Renal Disease. *J. Am. Soc. Nephrol.* **13,** 1230–1237 (2002).
10. Rossetti, S. *et al.* Association of mutation position in polycystic kidney disease 1 (PKD1) gene and development of a vascular phenotype. *Lancet* **361,** 2196–2201 (2003).
11. Terryn, S., Ho, A., Beauwens, R. & Devuyst, O. Fluid transport and cystogenesis in autosomal dominant polycystic kidney disease. *Biochim. Biophys. Acta* **1812,** 1314–1321 (2011).
12. Lemos Barbosa, C. M. *et al.* Regulation of CFTR Expression and Arginine Vasopressin Activity Are Dependent on Polycystin-1 in Kidney-Derived Cells. *Cell. Physiol. Biochem.* **38,** 28–39 (2016).
13. Roxo-Rosa, M., Jacinto, R., Sampaio, P. & Lopes, S. S. The zebrafish Kupffer's vesicle as a model system for the molecular mechanisms by which the lack of Polycystin-2 leads to stimulation of CFTR. *Biol. Open* **4,** 1356–1366 (2015).
14. Navis, A., Marjoram, L. & Bagnat, M. Cftr controls lumen expansion and function of Kupffer's vesicle in zebrafish. *Development* **140,** 1703–12 (2013).
15. Roxo-Rosa, M. & Lopes, S. S. The Crosstalk Between Polycystin-2 and CFTR in Autosomal Dominant Polycystic Kidney Disease. Poster Session/ Report - *Nephrol. Dial. Transplant.* **31,** 94 (2016).
16. Chatterjee, S., Shi, W. Y., Wilson, P. & Mazumdar, A. Role of lactosylceramide and MAP kinase in the proliferation of proximal tubular cells in human polycystic kidney disease. *J. Lipid Res.* **37,** 1334–1344 (1996).
17. Natoli, T. A. *et al.* Inhibition of glucosylceramide accumularion results in effective blockade of polycystic kidney disease in mouse models. *Nat. Med.* **16,** 788–792 (2010).

18. Hamai, H., Keyserman, F., Quittell, L. M. & Worgall, T. S. Defective CFTR increases synthesis and mass of sphingolipids that modulate membrane composition and lipid signaling. *J. Lipid Res. Res.* **50,** 1101–1108 (2009).

19. Bodas, M., Min, T., Mazur, S. & Vij, N. Critical modifier role of membrane-CFTR dependent ceramide signaling in lung injury and emphysema. *J. Immunol.* **186,** 602–613 (2011).

20. Igreja, S., Clarke, L. A., Botelho, H. M., Marques, L. & Amaral, M. D. Correction of a Cystic Fibrosis Splicing Mutation by Antisense Oligonucleotides. *Hum. Mutat.* **37,** 209–215 (2016).

21. Lariviere, W. B., Irazabal, M. V. & Torres, V. E. Novel therapeutic approaches to autosomal dominant polycystic kidney disease. *Transl. Res.* **165,** 488–498 (2015).

22. Torres, V. E., Harris, P. C. & Pirson, Y. Autosomal dominant polycystic kidney disease. *Lancet* **369,** 1287–1301 (2007).

23. Bogdanova, N. *et al.* Genetic heterogeneity of polycystic kidney disease in Bulgaria. *Hum. Genet.* **95,** 645–650 (1995).

24. Daoust, M. C., Reynolds, D. M., Bichet, D. G. & Somlo, S. Evidence for a third genetic locus for autosomal dominant polycystic kidney disease. *Genomics* **25,** 733–736 (1995).

25. Turco, a E., Clementi, M., Rossetti, S., Tenconi, R. & Pignatti, P. F. An Italian family with autosomal dominant polycystic kidney disease unlinked to either the PKD1 or PKD2 gene. *Am. J. Kidney Dis.* **28,** 759–761 (1996).

26. Ariza, M. *et al.* A family with a milder form of adult dominant polycystic kidney disease not linked to the PKD1 (16p) or PKD2 (4q) genes. *J. Med. Genet.* **34,** 587–589 (1997).

27. Almeida, E., Martins Prata, M. M., Almeida, S. & Lavinha, J. Long-term follow-up of a family with autosomal dominant polycystic kidney disease type 3. *Nephrol. Dial. Transplant.* **14,** 631–634 (1999).

28. Paul, B. M. *et al.* Evidence of a third ADPKD locus is not supported by re-analysis of designated PKD3 families. *Kidney Int.* **85,** 383–392 (2014).

29. Danaci, M. *et al.* The prevalence of seminal vesicle cysts in autosomal dominant polycystic kidney disease. *Nephrol. Dial. Transplant.* **13,** 2825–2828 (1998).

30. Du, J., Fu, J., Xia, X. & Shen, B. The functions of TRPP2 in the vascular system. *Nat. Publ. Gr.* **37,** 13–18 (2016).

31. Chapman, A., Stepniakowski, K. & Rahbari-Oskoui, F. Hypertension in Autosomal Dominant Polycystic Kidney Disease. *Adv. Chronic Kidney Dis.* **17,** 153–163 (2010).

32. Simms, R. Autosomal dominant polycystic kidney disease. *Br. Med. J.* **352,** 1–10 (2016).

33. Suwabe, T. et al. Infected hepatic and renal cysts: Differential impact on outcome in Autosomal Dominant Polycystic Kidney Disease. *Nephron Clin. Pract.* **112,** c157–c163 (2009).

34. Lantinga, M. A. *et al.* Management of renal cyst infection in patients with autosomal dominant polycystic kidney disease: a systematic review. *Nephrol. Dial. Transplant.* **32,** 144–150 (2016).

35. Chebib, F. T. & Torres, V. E. Autosomal Dominant Polycystic Kidney Disease: Core Curriculum 2016. *Am. J. Kidney Dis.* **67,** 792–810 (2016).

36. Rossetti, S. & Harris, P. C. Genotype-phenotype correlations in autosomal dominant and autosomal recessive polycystic kidney disease. *J. Am. Soc. Nephrol.* **18,** 1374–1380 (2007).

37. Hateboer, N. *et al.* Comparison of phenotypes of polycystic kidney disease types 1 and 2. *Lancet* **353,** 103–107 (1999).

38. Harris, P. C. & Rossetti, S. Determinants of Renal Disease Variability in ADPKD. *Adv. Chronic Kidney Dis.* **17,** 131–139 (2010).

39. Dicks, E. *et al.* Incident renal events and risk factors in autosomal dominant polycystic kidney disease: a population and family-based cohort followed for 22 years. *Clin. J. Am. Soc. Nephrol.* **1,** 710–717 (2006).

40. Tan, Y., Blumenfeld, J. & Rennert, H. Autosomal dominant polycystic kidney disease : Genetics , mutations and microRNAs. *Biochim. Biophy. Acta* **1812,** 1202–1212 (2011).

41. Hughes, J. et al. The polycystic kidney disease 1 (PKD1) gene encodes a novel protein with multiple cell recognition domains. *Nat. Genet.* **10,** 151–160 (1995).

42. Smyth, B. J., Snyder, R. W., Balkovetz, D. F. & Lipschutz, J. H. Recent advances in the cell biology of polycystic kidney disease. *Int. Rev. Cytol.* **231,** 51–89 (2003).

43. Chapin, H. C. & Caplan, M. J. The cell biology of polycystic kidney disease. *J. Cell Biol.* **191,** 701–710 (2010).

44. Chauvet, V. *et al.* Expression of PKD1 and PKD2 Transcripts and Proteins in Human Embryo and during Normal Kidney Development. *Am. J. Pathol.* **160,** 973–982 (2002).

45. Low, S. H. et al. Polycystin-1 , STAT6 , and P100 Function in a Pathway that Transduces Ciliary Mechanosensation and Is Activated in Polycystic Kidney Disease. *Dev. Cell* **10,** 57–69 (2006).

46. Geary, D. & Schaefer, F. *Compreensive Pediatric Nephrology: Ch 9.* (Mosby, Maryland Heights, 2008).

47. Qian, F. *et al.* Cleavage of polycystin-1 requires the receptor for egg jelly domain and is disrupted by human autosomal-dominant polycystic kidney disease 1-associated mutations. *PNAS* **99,** 16981–16986 (2002).

48. Wei, W., Hackmann, K., Xu, H., Germino, G. & Qian, F. Characterization of cis -Autoproteolysis of Polycystin-1 , the Product of Human Polycystic Kidney Disease 1 Gene. *J. od Biol. Chem.* **282,** 21729–21737 (2007).

49. Chauvet, V. *et al.* Mechanical stimuli induce cleavage and nuclear translocation of the polycystin-1 C terminus. *J. Clin. Invest.* **114,** 1433–1443 (2004).

50. Shaulian, E. & Karin, M. AP-1 as a regulator of cell life and death. *Nat. Cell Biol.* **4,** E131-136 (2002).

51. Bertuccio, C. A. *et al.* Polycystin-1 C-terminal Cleavage Is Modulated by Polycystin-2 Expression. *J. Biol. Chem.* **284,** 21011–21026 (2009).

52. Shen, P. S. *et al.* The Structure of the Polycystic Kidney Disease Channel PKD2 in Lipid Nanodiscs. *Cell* **167,** 763-773 (2016).

53. Allen, M. D., Qamar, S., Vadivelu, M. K., Sandford, R. N. & Bycroft, M. A high-resolution structure of the EF-hand domain of human polycystin-2. *Protein Sci.* **23,** 1301–1308 (2014).

54. Ong, A. C. *et al.* Coordinate expression of the autosomal dominant polycystic kidney disease proteins, polycystin-2 and polycystin-1, in normal and cystic tissue. *Am. J. Pathol.* **154,** 1721–1729 (1999).

55. Pennekamp, P. *et al.* The Ion Channel Polycystin-2 Is Required for Left-Right Axis Determination in Mice. *Curr. Biol.* **12,** 938–943 (2002).

56. Schottenfeld, J., Sullivan-Brown, J. & Burdine, R. D. Zebrafish curly up encodes a Pkd2 ortholog that restricts left-side-specific expression of southpaw. *Dev. Dis.* **134,** 1605–1615 (2007).

57. Mochizuki, T. *et al.* PKD2, a gene for polycystic kidney disease that encodes an integral membrane protein. *Science* **272,** (1996).

58. Du, J. et al. TRPV4, TRPC1, and TRPP2 assemble to form a flow-sensitive heteromeric channel. *FASEB J.* **28,** 4677–4685 (2014).

59. Abdi, A. *et al.* TRPP2 modulates ryanodine- and inositol-1,4,5-trisphosphate receptors-dependent Ca2+ signals in opposite ways in cerebral arteries. *Cell Calcium* **58,** 467–475 (2015).

60. Torres, V. E. *et al.* Vascular expression of polycystin-2. *J. Am. Soc. Nephrol.* **12,** 1–9 (2001).

61. Grieben, M. *et al.* Structure of the polycystic kidney disease TRP channel. *Nat. Struct. Mol. Biol.* **24,** 114–122 (2017).

62. Tsiokas, L., Kim, S. & Ong, E.-C. Cell biology of Polycystin-2. *Cell Signal* **19,** 444–453 (2007).

63. Delling, M. *et al.* Primary cilia are not calcium-responsive mechanosensors. *Nature* **531,** 656–660 (2016).

64. Chen, X. Z. *et al.* Submembraneous microtubule cytoskeleton: Interaction of TRPP2 with the cell cytoskeleton. *FEBS J.* **275,** 4675–4683 (2008).

65. McGrath, J., Somlo, S., Makova, S., Tian, X. & Brueckner, M. Two populations of node monocilia initiate left-right asymmetry in the mouse. *Cell* **114,** 61–73 (2003).

66. Tavares, B. *et al.* Notch/Her12 signalling modulates, motile/immotile cilia ratio downstream of Foxj1a in zebrafish left-right organizer. *eLIFE* **6,** e25165 (2017).

67. Sampaio, P. *et al.* Left-Right Organizer Flow Dynamics : How Much Cilia Activity Reliably Yields Laterality ? *Dev. Cell* **29,** 716–728 (2014).

68. Ramsdell, A. F. Left-right asymmetry and congenital cardiac defects: Getting to the heart of the matter in vertebrate left-right axis determination. *Dev. Biol.* **288,** 1–20 (2005).

69. Guichard, C. *et al.* Axonemal Dynein Intermediate-Chain Gene (DNAI1) Mutations Result in Situs Inversus and Primary Ciliary Dyskinesia (Kartagener Syndrome). *Am. J. Hum. Genet.* **68,** 1030–1035 (2001).

70. Bataille, S. *et al.* Association of PKD2 (Polycystin 2) mutations with left-right laterality defects. *Am. J. Kidney Dis.* **58,** 456–460 (2011).

71. Oka, M., Mochizuki, T. & Kobayashi, S. A novel mutation of the pkd2 gene in a japanese patient with autosomal dominant polycystic kidney disease and complete situs inversus. *Am. J. Kidney Dis.* **64,** 660 (2014).

72. Goetz, S. C. & Anderson, K. V. The Primary Cilium: A Signaling Center During Vertebrate Development. *Nat. Rev. Genet.* **11,** 331–344 (2010).

73. Silverman, M. A. & Leroux, M. R. Intraflagellar transport and the generation of dynamic, structurally and functionally diverse cilia. *Trends Cell Biol.* **19,** 306–316 (2009).

74. Malicki, J. J. & Johnson, C. A. The Cilium: Cellular Antenna and Central Processing Unit. *Trends Cell Biol.* **27,** 126–140 (2017).

75. Leigh, M. W. *et al.* Clinical and Genetic Aspects of Primary Ciliary Dyskinesia / Kartagener Syndrome. Genet. Mdicine Off. J. Am. Coll. Med. Genet. **11,** 473–487 (2009).

76. Dell, K. M. The Role of Cilia in the Pathogenesis of Cystic Kidney Disease. *Curr. Opin. Pediatr.* **27,** 212–218 (2015).

77. Shinohara, K. *et al.* Absence of Radial Spokes in Mouse Node Cilia Is Required for Rotational Movement but Confers Ultrastructural Instability as a Trade-Off. *Dev. Cell* **35,** 236–246 (2015).

78. Sedykh, I. *et al.* Novel roles for the radial spoke head protein 9 in neural and neurosensory cilia. *Sci. Rep.* **6,** 34437 (2016).

79. Lee, S. H. & Somlo, S. Cyst growth, polycystins, and primary cilia in autosomal dominant polycystic kidney disease. *Kidney Res. Clin. Pract.* **33,** 73–78 (2014).

80. Heggo, O. A microdissection study of cystic disease of the kidneys in adults. *J. Pathol. Bact.* **91,** 311–315 (1966).

81. Lantinga-van Leeuwen, I. S. *et al.* Lowering of Pkd1 expression is sufficient to cause polycystic kidney disease. *Hum. Mol. Genet.* **13,** 3069–3077 (2004).

82. Thomson, R. B. *et al.* Histopathological analysis of renal cystic epithelia in the Pkd2WS25/- mouse model of ADPKD. *Am.J.Physiol Ren. Physiol* **285,** 870–880 (2003).

83. Wu, G. *et al.* Somatic inactivation of Pkd2 results in polycystic kidney disease. *Cell* **93,** 177–188 (1998).

84. Saigusa, T. & Bell, P. D. Molecular Pathways and Therapies in Autosomal-Dominant Polycystic Kidney Disease. *Physiology* **30,** 195–207 (2015).

85. Cargnello, M. & Roux, P. P. Activation and Function of the MAPKs and Their Substrates, the MAPK-Activated Protein Kinases. *Microbiol. Mol. Biol. Rev.* **75,** 50–83 (2011).

86. Yamaguchi, T. *et al.* Cyclic AMP activates B-Raf and ERK in cyst epithelial cells from autosomal-dominant polycystic kidneys. *Kidney Int.* **63,** 1983–1994 (2003).

87. Shillingford, J. M. *et al.* The mTOR pathway is regulated by polycystin-1, and its inhibition reverses renal cystogenesis in polycystic kidney disease. *PNAS* **103,** 5466–5471 (2006).

88. Wüthrich, R. P., Kistler, A. D. & Serra, A. L. Impact of mammalian target of rapamycin inhibition on autosomal-dominant polycystic kidney disease. *Transplant. Proc.* **42,** S44–S46 (2010).

89. Shillingford, J. M., Piontek, K. B., Germino, G. G. & Weimbs, T. Rapamycin ameliorates PKD resulting from conditional inactivation of Pkd1. *J. Am. Soc. Nephrol.* **21,** 489–497 (2010).

90. Tao, Y., Kim, J., Schrier, R. W. & Edelstein, C. L. Rapamycin Markedly Slows Disease Progression in a Rat Model of Polycystic Kidney Disease. *J. Am. Soc. Nephrol.* **16,** 46–51 (2005).

91. Walz, G. *et al.* Everolimus in Patients with Autosomal Dominant Polycystic Kidney Disease. *N. Engl. J. Med.* **363,** 830–840 (2010).

92. Kim, E. *et al.* The Polycystic Kidney Disease 1 Gene Product Modulates Wnt Signaling. *J. Biol. Chem.* **274,** 4947–4953 (1999).

93. Gallegos, T. F. *et al.* A protein kinase A and Wnt-dependent network regulating an intermediate stage in epithelial tubulogenesis during kidney development. *Dev. Biol.* **364,** 11–21 (2012).

94. Wuebken, A. & Schmidt-Ott, K. M. WNT /beta-catenin signaling in polycystic kidney disease.

Kidney Int. **80,** 135–138 (2011).

95. Stangherlin, A. & Zaccolo, M. Phosphodiesterases and subcellular compartmentalized cAMP signaling in the cardiovascular system. *Am. J. Physiol. Heart Circ. Physiol.* **302,** H379-H390 (2012).

96. Pinto, C. S., Reif, G. a., Nivens, E., White, C. & Wallace, D. P. Calmodulin-sensitive adenylyl cyclases mediate AVP-dependent cAMP production and Cl- secretion by human autosomal dominant polycystic kidney cells. *Am. J. Physiol. Ren. Physiol.* **303,** 1412–1424 (2012).

97. Cheng, J. & Grande, J. P. Cyclic nucleotide phosphodiesterase (PDE) inhibitors: novel therapeutic agents for progressive renal disease. *Exp. Biol. Med.* **232,** 38–51 (2007).

98. Rees, S. *et* al. Adenylyl Cyclase 6 Deficiency Ameliorates Polycystic Kidney Disease. *J. Am. Soc. Nephrol.* **25,** 232–237 (2014).

99. Wang, X., Ward, C. J., Harris, P. C. & Torres, V. E. Cyclic Nucleotide Signaling in Polycystic Kidney Disease. *Kidney Int.* **77,** 129–140 (2010).

100. Chabardès, D. *et al.* Localization of mRNAs Encoding Ca 2 -inhibitable Adenylyl Cyclases along the Renal Tubule. *J. Biol. Chem.* **271,** 19264–19271 (1996).

101. Banales, J. M. *et al.* The cAMP Effectors Epac and PKA are Involved in the Hepatic Cystogenesis of an Animal Model of ARPKD. *Hepat.* **49,** 160–174 (2009).

102. Hanaoka, K. & Guggino, W. B. cAMP regulates cell proliferation and cyst formation in Autosomal Polycystic Kidney Disease Cells. *J. Am. Soc. Nephrol.* **11,** 1179–1187 (2000).

103. Yamaguchi, T. *et al.* cAMP stimulates the in vitro proliferation of renal cyst epithelial cells by activating the extracellular signal-regulated kinase pathway. *Kidney Int.* **57,** 1460–1471 (2000).

104. Happé, H. & Peters, D. J. M. Translational research in ADPKD: lessons from animal models. *Nat. Rev. Nephrol.* **10,** 587–601 (2014).

105. Pei, Y. A 'two-hit' model of cystogenesis in autosomal dominant polycystic kidney disease? *Trends Mol. Med.* **7,** 151–156 (2001).

106. Wu, G. *et al.* Trans-heterozygous Pkd1 and Pkd2 mutations modify expression of polycystic kidney disease. *Hum. Mol. Genet.* **11,** 1845–1854 (2002).

107. Qian, F., Watnick, T. J., Onuchic, L. F. & Germino, G. G. The molecular basis of focal cyst formation in human autosomal dominant polycystic kidney disease type I. *Cell* **87,** 979–987 (1996).

108. Brasier, J. L. & Henske, E. P. Loss of the polycystic kidney disease (PKD1) region of chromosome 16p13 in renal cyst cells supports a loss-of-function model for cyst pathogenesis. *J. Clin. Invest.* **99,** 194–199 (1997).

109. Watnick, T. J. *et al.* Somatic mutations in individual kidney and liver cysts support a 'two-hit' model of cystogenesis in autosomal dominant polycystic kidney disease. *Mol. Cell* **2,** 247–251 (1998).

110. Pei, Y. *et al.* Somatic PKD2 mutations in individual kidney and liver cysts support a 'two-hit' model of cystogenesis in type 2 autosomal dominant polycystic kidney disease. *J. Am. Soc. Nephrol.* **10,** 1524–1529 (1999).

111. Harris, P. C. What Is the Role of Somatic Mutation in Autosomal Dominant Polycystic Kidney Disease? *J. Am. Soc. Nephrol.* **21,** 1073–1076 (2010).

112. Qian, Q. *et al.* Pkd2 haploinsufficiency alters intracellular calcium regulation in vascular smooth muscle cells. *Hum. Mol. Genet.* **12,** 1875–1880 (2003).

113. Lal, M. *et al.* Polycystin-1 C-terminal tail associates with β-catenin and inhibits canonical Wnt signaling. *Hum. Mol. Genet.* **17,** 3105–3117 (2008).

114. Grantham, J. J., Geiser, J. L. & Evan, A. P. Cyst formation and growth in autosomal dominant polycystic kidney disease. *Kidney Int* **31,** 1145–1152 (1987).

115. Li, C. & Naren, A. P. CFTR chloride channel in the apical compartments: spatiotemporal coupling to its interacting partners. *Integr. Biol. (Camb.).* **2,** 161–77 (2010).

116. Cant, N., Pollock, N. & Ford, R. C. CFTR structure and cystic fibrosis. *Int. J. Biochem. Cell Biol*. **52,** 15–25 (2014).

117. Souza-Menezes, J., da Silva Feltran, G. & Morales, M. M. CFTR and TNR-CFTR expression and function in the kidney. *Biophys. Rev.* **6,** 227–236 (2014).

118. Wilkens, S. Structure and mechanism of ABC transporters. *F1000Prime Rep.* **7,** 1–9 (2015).

119. Farinha, C. M. & Canato, S. From the endoplasmic reticulum to the plasma membrane : mechanisms of CFTR folding and trafficking. *Cell. Mol. Life Sci*. **74,** 39–55 (2017).

120. Collins, F. S. Cystic fibrosis: molecular biology and therapeutic implications. *Science* **256,** 774–779 (1992).

121. Cutting, G. R. Cystic fibrosis genetics: from molecular understanding to clinical application. Nat. Rev. Genet. **16,** 45–56 (2015).

122. Coutinho, H., Falcão-Silva, V. S. & Gonçalves, G. Pulmonary bacterial pathogens in cystic fibrosis patients and antibiotic therapy: a tool for the health workers. *Int. Arch. Med.* **1,** 1–7 (2008).

123. Farinha, C. M., Matos, P. & Amaral, M. D. Control of cystic fibrosis transmembrane conductance regulator membrane trafficking: Not just from the endoplasmic reticulum to the Golgi. *FEBS J.* **280,** 4396–4406 (2013).

124. Farinha, C. M., Nogueira, P., Mendes, F., Penque, D. & Amaral, M. D. The human DnaJ homologue (Hdj)-1/heat-shock protein (Hsp) 40 co-chaperone is required for the in vivo stabilization of the cystic fibrosis transmembrane conductance regulator by Hsp70. *Biochem. J*. **366,** 797–806 (2002).

125. Meacham, G. C. *et al.* The Hdj-2/Hsc70 chaperone pair facilitates early steps in CFTR biogenesis. *EMBO J.* **18,** 1492–1505 (1999).

126. Farinha, C. M. & Amaral, M. D. Most F508del-CFTR is targeted to degradation at an early folding checkpoint and independently of calnexin. *Mol. Cell. Biol.* **25,** 5242–5252 (2005).

127. Roxo-Rosa, M. *et al.* Revertant mutants G550E and 4RK rescue cystic fibrosis mutants in the first nucleotide-binding domain of CFTR by different mechanisms. *PNAS* **103,** 17891–17896 (2006).

128. Yoo, J.-S. *et al.* Non-conventional trafficking of the cystic fibrosis transmembrane conductance regulator through the early secretory pathway. *J. Biol. Chem.* **277,** 11401–11409 (2002).

129. Lukacs, G. L., Segal, G., Kartner, N., Grinstein, S. & Zhang, F. Constitutive internalization of cystic fibrosis transmembrane conductance regulator occurs via clathrin-dependent endocytosis and is regulated by protein phosphorylation. *Biochem. J.* **328,** 353–361 (1997).

130. Cholon, D. M., O'Neal, W. K., Randell, S. H., Riordan, J. R. & Gentzsch, M. Modulation of endocytic trafficking and apical stability of CFTR in primary human airway epithelial cultures. *Am. J. Physiol. Lung Cell. Mol. Physiol.* **298,** L304–L314 (2010).

131. Gentzsch, M. *et al.* Endocytic Trafficking Routes of Wild Type and ΔF508 Cystic Fibrosis Transmembrane Conductance Regulator. *Mol. Biol. Cell* **15,** 2684–2696 (2005).

132. Farinha, C. M. & Matos, P. Rab GTPases regulate the trafficking of channels and transporters – a focus on cystic fibrosis. *Small GTPases* **0,** 1–9 (2017).

133. Gee, H. Y., Noh, S. H., Tang, B. L., Kim, K. H. & Lee, M. G. Rescue of Δf508-CFTR trafficking via a GRASP-dependent unconventional secretion pathway. *Cell* **146,** 746–760 (2011).

134. Piao, H. *et al.* Sec16A is critical for both conventional and unconventional secretion of CFTR. *Sci. Rep.* **7,** 1–17 (2017).

135. Grieve, A. G. & Rabouille, C. Golgi bypass: Skirting around the heart of classical secretion. *Cold Spring Harb. Perspect. Biol.* **3,** 1–15 (2011).

136. Bozoky, Z. *et al.* Synergy of cAMP and calcium signaling pathways in CFTR regulation. *PNAS* **114,** E2086–E2095 (2017).

137. Hwang, T. C. & Kirk, K. L. The CFTR Ion channel: Gating, regulation, and anion permeation. *Cold Spring Harb. Perspect. Med.* **3,** 1–15 (2013).

138. Farinha, C. M., Swiatecka-urban, A., Brautigan, D. L. & Jordan, P. Regulatory Crosstalk by Protein Kinases on CFTR Trafficking and Activity. *Front. Chem*. **4,** 1–11 (2016).

139. Morales, M. M., Falkenstein, D. & Lopes, A. G. The cystic fibrosis transmembrane regulator (CFTR) in the kidney. *An. da Acad. Bras. Ci.* **72,** 399–406 (2000).

140. Ikeda, M. *et al.* A regulatory role of polycystin-1 on cystic fibrosis transmembrane conductance regulator plasma membrane expression. *Cell. Physiol.* Biochem. **18,** 9–20 (2006).

141. Hanaoka, K., Devuyst, O., Schwiebert, E. M., Wilson, P. D. & Guggino, W. B. A role for CFTR in human autosomal dominant polycystic kidney disease. *Am. J. Physiol.* **270,** 389–399 (1996).

142. Davidow, C. J., Maser, R. L., Rome, L. A., Calvet, J. P. & Grantham, J. J. The cystic fibrosis transmembrane conductance regulator mediates transepithelial fluid secretion by human autosomal dominant polycystic kidney disease epithelium *in vitro*. *Kidney Int.* **50,** 208–218 (1996).

143. Yuajit, C. *et al.* Steviol Reduces MDCK Cyst Formation and Growth by Inhibiting CFTR Channel Activity and Promoting Proteasome-Mediated CFTR Degradation. *PLoS One* **8,** 1–11 (2013).

144. Li, H., Yang, W., Mendes, F., Amaral, M. D. & Sheppard, D. N. Impact of the cystic fibrosis mutation F508del-CFTR on renal cyst formation and growth. *Am. J. Physiol. Renal Physiol*. **303,** F1176-F1186 (2012).

145. Yang, B., Sonawane, N. D., Zhao, D., Somlo, S. & Verkman, A. S. Small-Molecule CFTR Inhibitors Slow Cyst Growth in Polycystic Kidney Disease. *J. Am. Soc. Nephrol.* **19,** 1300–1310 (2008).

146. Yuajit, C. *et al.* Steviol retards renal cyst growth through reduction of CFTR expression and inhibition of epithelial cell proliferation in a mouse model of polycystic kidney disease. *Biochem. Pharmacol.* **88,** 412–421 (2014).

147. O'Sullivan, D. A. *et al.* Cystic fibrosis and the phenotypic expression of autosomal dominant polycystic kidney disease. *Am. J. Kidney Dis.* **32,** 976–983 (1998).

148. Persu, A. *et al.* CF Gene and Cystic Fibrosis Transmembrane Conductance Regulator Expression in Autosomal Dominant Polycystic Kidney Disease. *J. Am. Soc. Nephrol.* **11,** 2285–2296 (2000).

149. Xu, N. *et al.* Autosomal dominant polycystic kidney disease coexisting with cystic fibrosis. *J.Nephrol.* **19,** 529–534 (2006).

150. Seeman, T. *et al.* Ambulatory blood pressure correlates with renal volume and number of renal cysts in children with autosomal dominant polycystic kidney disease. *Blood Press. Monit.* **8,** 107–110 (2003).

151. Marlais, M. *et al*. Hypertension in autosomal dominant polycystic kidney disease: a meta-analysis. *Arch. Dis. Child*. **101,** 1142–1147 (2016).

152. Chapman, A. B. *et al.* Renal structure in early autosomal-dominant polycystic kidney disease (ADPKD): The Consortium for Radiologic Imaging Studies of Polycystic Kidney Disease (CRISP) cohort. *Kidney Int.* **64,** 1035–1045 (2003).

153. Fick, G., Johnson, A., Hammond, W. & Gabow, P. Causes of death in autosomal dominant polycystic kidney disease. *J. Am. Soc. Nephrol.* **5,** 2048–2056 (1995).

154. Sans-Atxer, L., Torra, R. & Fernández-Llama, P. Hypertension in autosomal-dominant polycystic kidney disease (ADPKD). *Clin. Kidney J.* **6,** 457–463 (2013).

155. Alvaro, D. *et al.* Morphological and functional features of hepatic cyst epithelium in autosomal dominant polycystic kidney disease. *Am. J. Pathol.* **172,** 321–332 (2008).

156. Torra, R. *et al.* Prevalence of cysts in seminal tract and abnormal semen parameters in patients with autosomal dominant polycystic kidney disease. *Clin. J. Am. Soc. Nephrol.* **3,** 790–793 (2008).

157. Kumar, S., Adeva, M., King, B. F., Kamath, P. S. & Torres, V. E. Duodenal diverticulosis in autosomal dominant polycystic kidney disease. *Nephrol. Dial. Transplant* **21,** 3576–8 (2006).

158. Tangri, N. *et al.* Total Kidney Volume as a Biomarker of Disease Progression in Autosomal Dominant Polycystic Kidney Disease. *Can. J. Kidney Heal. Dis.* **4,** 1–6 (2017).

159. Alam, A. *et al.* Total kidney volume in autosomal dominant polycystic kidney disease: A biomarker of disease progression and therapeutic efficacy. *Am. J. Kidney Dis.* **66,** 564–576 (2015).

160. Pei, Y. *et al.* Unified Criteria for Ultrasonographic Diagnosis of ADPKD. *J. Am. Soc. Nephrol.* **20,** 205–212 (2009).

161. Ravine, D. *et al.* Evaluation of ultrasonographic diagnostic criteria for autosomal dominant polycystic kidney disease 1. *Lancet* **343,** 824–827 (1994).

162. Pei, Y. Diagnostic approach in autosomal dominant polycystic kidney disease. *Clin. J. Am. Soc. Nephrol*. **1,** 1108–1114 (2006).

163. Rossetti, S. *et al.* Comprehensive Molecular Diagnostics in Autosomal Dominant Polycystic Kidney Disease. *J. Am. Soc. Nephrol.* **18,** 2143–2160 (2007).

164. Hwang, Y.-H. *et al.* Refining Genotype-Phenotype Correlation in Autosomal Dominant Polycystic Kidney Disease. *J. Am. Soc. Nephrol.* **27,** 1861–1868 (2016).

165. Lee, K.-B. Genetic diagnosis of autosomal dominant polycystic kidney disease: linkage analysis versus direct mutation analysis. *Kidney Res. Clin. Pract.* **35,** 67–68 (2016).

166. Fenell, J. P. & Baker, A. *Methods in Molecular Medicine - Ch* 13 (Humana Press Inc., Totowa, 2005).

167. Rossetti, S. *et al.* A complete mutation screen of the ADPKD genes by DHPLC. *Kidney Int.* **61,** 1588–1599 (2002).

168. Shendure, J. & Ji, H. Next-generation DNA sequencing. *Nat. Biotechnol.* **26,** 1135–1145 (2008).

169. Rossetti, S. *et al.* Identification of Gene Mutations in Autosomal Dominant Polycystic Kidney Disease through Targeted Resequencing. *J. Am. Soc. Nephrol.* **23,** 915–933 (2012).

170. Tan, A. Y. *et al.* Molecular Diagnosis of Autosomal Dominant Polycystic Kidney Disease Using Next-Generation Sequencing. *J. Mol. Diagno.***16,** 216–228 (2014).

171. Helal, I., Al-Rowaie, F., Abderrahim, E. & Kheder, A. Update on pathogenesis, management, and treatment of hypertension in autosomal dominant polycystic kidney disease. *Saudi J. Kidney Dis. Transplant.* **28,** 253-260 (2017).

172. Schrier, R. W. *et al.* Blood pressure in early autosomal dominant polycystic kidney disease. *N. Engl. J. Med.* **371,** 2255–2266 (2014).

173. Torres, V. E. *et al.* Angiotensin Blockade in Late Autosomal Dominant Polycystic Kidney Disease. *N. Engl. J. Med.* **371,** 2267–2276 (2014).

174. Susantitaphong, P. *et al.* Efficacy and safety of combined vs. Single renin-angiotensin-aldosterone system blockade in chronic kidney disease: A meta-analysis. *Am. J. Hypertens.* **26,** 424–441 (2013).

175. Hian, C. K., Lee, C. L. & Thomas, W. Renin-Angiotensin-Aldosterone System Antagonism and Polycystic Kidney Disease Progression. *Nephron* **134,** 59–63 (2016).

176. Reif, G. a. *et al.* Tolvaptan inhibits ERK-dependent cell proliferation, Cl- secretion, and in vitro cyst growth of human ADPKD cells stimulated by vasopressin. *Am. J. Physiol. Ren. Physiol.* **301,** F1005–F1013 (2011).

177. Gattone, V. H., Wang, X., Harris, P. C. & Torres, V. E. Inhibition of renal cystic disease development and progression by a vasopressin V2 receptor antagonist. *Nat. Med.* **9,** 1323–1326 (2003).

178. Torres, V. E. *et al.* Effective treatment of an orthologous model of autosomal dominant polycystic kidney disease. *Nat. Med.* **10,** 363–364 (2004).

179. Wang, X., Gattone, V., Harris, P. C. & Torres, V. E. Effectiveness of Vasopressin V2 Receptor Antagonists OPC-31260 and OPC-41061 on Polycystic Kidney Disease Development in the PCK Rat. *J. Am. Soc. Nephrol.* **16,** 846–851 (2005).

180. Aihara, M. *et al.* Tolvaptan delays the onset of end-stage renal disease in a polycystic kidney disease model by suppressing increases in kidney volume and renal injury. *J. Pharmacol. Exp. Ther.* **349,** 258–67 (2014).

181. Torres, V. E. *et al.* Tolvaptan in Patients with Autosomal Dominant Polycystic Kidney Disease. *N. Engl. J. Med.* **367,** 2407–2418 (2012).

182. Higashihara, E. *et al.* Kidney volume and function in autosomal dominant polycystic kidney disease. *Clin. Exp. Nephrol.* **18,** (2014).

183. Torres, V. E. *et al.* Effect of Tolvaptan in Autosomal Dominant Polycystic Kidney Disease by CKD Stage: Results from the TEMPO 3:4 Trial. *Clin. J. Am. Soc. Nephrol.* (2016).

184. Gheorghiade, M. *et al.* Effects of Tolvaptan, a Vasopressin Antagonist, in Patients Hospitalized WithWorsening Heart Failure. *Jama* **291,** 1963–1971 (2004).

185. Miyazaki, T., Fujiki, H., Yamamura, Y., Nakamura, S. & Mori, T. Tolvaptan, an Orally Active Vasopressin V2-Receptor Antagonist-Pharmacology and Clinical Trials. *Cardiovasc. Drug Rev.* **25,** 1–13 (2007).

186. Muto, S. *et al.* The effect of tolvaptan on autosomal dominant polycystic kidney disease patients: a subgroup analysis of the Japanese patient subset from TEMPO 3:4 trial. *Clin. Exp. Nephrol.* **19,** 867–877 (2015).

187. EMA, E. M. A. Jinarc tolvaptan summary. *European Medicines Agency* (2016).

188. Gansevoort, R. T. *et al.* Recommendations for the use of tolvaptan in autosomal dominant polycystic kidney disease: A position statement on behalf of the ERA-EDTA Working Groups on Inherited Kidney Disorders and European Renal Best Practice. *Nephrol. Dial. Transplant.* **31,** 337–348 (2016).

189. Horie, S. Will introduction of tolvaptan change clinical practice in autosomal dominant polycystic kidney disease? *Kidney Int.* **88,** 14–16 (2015).

190. Watkins, P. B. *et al.* Clinical Pattern of Tolvaptan-Associated Liver Injury in Subjects with Autosomal Dominant Polycystic Kidney Disease: Analysis of Clinical Trials Database. *Drug Saf.* **38,** 1103–1113 (2015).

191. Chatsudthipong, V. & Jutabha, P. Effect of Steviol on para -Aminohippurate Transport by Isolated Perfused Rabbit Renal Proximal Tubule. *J. Pharmacol. Exp. Ther.* **298,** 1120–1127 (2001).

192. Srimaroeng, C., Jutabha, P., Pritchard, J. B., Endou, H. & Chatsudthipong, V. Interactions of stevioside and steviol with renal organic anion transporters in S2 cells and mouse renal cortical slices. *Pharm. Res.* **22,** 858–866 (2005).

193. Pariwat, P., Homvisasevongsa, S., Muanprasat, C. & Chatsudthipong, V. A natural plant-derived dihydroisosteviol prevents cholera toxin-induced intestinal fluid secretion. *J. Pharmacol. Exp. Ther.* **324,** 798–805 (2008).

194. Yuajit, C., Muanprasat, C., Homvisasevongsa, S. & Chatsudthipong, V. Steviol stabilizes polycystin 1 expression and promotes lysosomal degradation of CFTR and β-catenin proteins in renal epithelial cells. *Biomed. Pharmacother.* **94,** 820–826 (2017).

195. Piontek, K., Menezes, L. F., Garcia-gonzalez, M. A., Huso, D. L. & Germino, G. G. A critical developmental switch defines the kinetics of kidney cyst formation after loss of Pkd1. *Nat. Med.* **13,** 1490–1495 (2007).

196. Lantinga-van leeuwen, I. S. et al. Kidney-specific inactivation of the Pkd1 gene induces rapid cyst formation in developing kidneys and a slow onset of disease in adult mice. *Hum. Mol. Genet.* **16,** 3188–3196 (2007).

197. Doctor, R. B., Serkova, N. J., Hasebroock, K. M., Zafar, I. & Edelstein, C. L. Distinct patterns of kidney and liver cyst growth in pkd2(WS25/-) mice. *Nephrol. Dial. Transplant.* **25,** 3496–3504 (2010).

198. Happé, H. *et al.* Toxic tubular injury in kidneys from Pkd1-deletion mice accelerates

cystogenesis accompanied by dysregulated planar cell polarity and canonical Wnt signaling pathways. *Hum. Mol. Genet.* **18,** 2532–2542 (2009).

199. Bhunia, A. K. *et al.* PKD1 induces $p21^{waf1}$ and regulation of the cell cycle via direct activation of the JAK-STAT signaling pathway in a process requiring PKD2. *Cell* **109,** 157–168 (2002).

200. Leonhard, W. N. *et al.* Curcumin inhibits cystogenesis by simultaneous interference of multiple signaling pathways: in vivo evidence from a Pkd1-deletion model. *Am. J. Physiol. Renal Physiol.* **300,** F1193–F1202 (2011).

201. Fischer, E. *et al.* Defective planar cell polarity in polycystic kidney disease. *Nat. Genet.* **38,** 21–23 (2006).

202. Luyten, A. *et al.* Aberrant Regulation of Planar Cell Polarity in Polycystic Kidney Disease. *J. Am. Soc. Nephrol.* **21,** 1521–1532 (2010).

203. Kim, I. et al. Conditional mutation of Pkd2 causes cystogenesis and upregulates beta-catenin. *J. Am. Soc. Nephrol.* **20,** 2556–2569 (2009).

204. Shibazaki, S. *et al.* Cyst formation and activation of the extracellular regulated kinase pathway after kidney specific inactivation of *Pkd1*. *Hum. Mol. Genet.* **17,** 1505–1516 (2008).

205. Jiang, S.-T. *et al.* Defining a link with autosomal-dominant polycystic kidney disease in mice with congenitally low expression of Pkd1. *Am. J. Pathol.* **168,** 205–220 (2006).

206. Wu, G. *et al.* Cardiac defects and renal failure in mice with targeted mutations in Pkd2. *Nat. Genet.* **24,** 75–78 (2000).

207. Kurbegovic, A. *et al.* Pkd1 transgenic mice: Adult model of polycystic kidney disease with extrarenal and renal phenotypes. *Hum. Mol. Genet.* **19,** 1174–1189 (2010).

208. Park, E. Y. et al. Cyst formation in kidney via B-raf signaling in the PKD2 transgenic mice. *J. Biol. Chem.* **284,** 7214–7222 (2009).

209. Lu, W. *et al.* Late onset of renal and hepatic cysts in Pkd1-targeted heterozygotes. *Nat. Genet*. **21,** 160–161 (1999).

210. Kim, K., Drummond, I., Ibraghimov-Beskrovnaya, O., Klinger, K. & Arnaout, M. A. Polycystin 1 is required for the structural integrity of blood vessels. *PNAS* **97,** 1731–1736 (2000).

211. Lu, W. *et al.* Perinatal lethality with kidney and pancreas defects in mice with a targetted Pkd1 mutation. *Nat. Genet.* **17,** 179–181 (1997).

212. Lantinga-van Leeuwen, I. S. *et al.* Transgenic Mice Expressing Tamoxifen-Inducible Cre for Somatic Gene Modification in Renal Epithelial Cells. *Genesis* **44,** 225–232 (2006).

213. Sun, Y., Zhou, H. & Yang, B. Drug discovery for polycystic kidney disease. *Acta Pharmacol. Sin.* **32,** 805–816 (2011).

214. Li, H., Yang, W., Mendes, F., Amaral, M. D. & Sheppard, D. N. Impact of the cystic fibrosis mutation F508del-CFTR on renal cyst formation and growth Impact of the cystic fibrosis mutation F508del-CFTR on renal cyst formation and growth. *Am. J. Physiol. Renal Physiol.* **303,** F1176–F1186 (2012).

215. Tradtrantip, L., Yangthara, B., Padmawar, P., Morrison, C. & Verkman, A. S. Thiophenecarboxylate Suppressor of Cyclic Nucleotides Discovered in a Small-Molecule Screen Blocks Toxin-Induced Intestinal Fluid Secretion. *Mol. Pharmacol.* **75,** 134–142 (2009).

216. Grant, M. E. *et al.* Arginine vasopressin stimulates net fluid secretion in a polarized subculture of cyst-forming MDCK cells. *J. Am. Soc. Nephrol.* **2,** 219–227 (1991).

217. Elberg, G. *et al.* EP2 receptor mediates PGE2-induced cystogenesis of human renal epithelial cells. *Am. J. Physiol. Renal Physiol.* **293,** F1622–F1632 (2007).

218. Aguiari, G. *et al.* Deficiency of polycystic kidney disease-1 gene (PKD1) expression increases A3 adenosine receptors in human renal cells: Implications for cAMP-dependent signalling and proliferation of PKD1-mutated cystic cells. *Biochim. Biophys. Acta* **1792,** 531–540 (2009).

219. Briggs, J. P. The zebrafish: a new model organism for integrative physiology. *Am. J. Physiol. Regul. Integr. Comp. Physiol.* **282,** R3–R9 (2002).

220. Lieschke, G. J. & Currie, P. D. Animal models of human disease: zebrafish swim into view. *Nat. Rev. Genet.* **8,** 353–367 (2007).

221. England, S. J., Campbell, P. C., Banerjee, S., Swanson, A. J. & Lewis, K. E. Identification and Expression Analysis of the Complete Family of Zebrafish pkd Genes. *Front. Cell Dev. Biol.* **5,** 1–36 (2017).

222. Hill, A. J., Teraoka, H., Heideman, W. & Peterson, R. E. Zebrafish as a model vertebrate for investigating chemical toxicity. *Toxicol. Sci.* **86,** 6–19 (2005).

223. Doyon, Y. *et al.* Heritable targeted gene disruption in zebrafish using designed zinc-finger nucleases. *Nat. Biotechnol.* **26,** 702–708 (2008).

224. Sander, J. D. *et al.* Targeted gene disruption in somatic zebrafish cells using engineered TALENs. *Nat. Biotechnol.* **29,** 697–698 (2011).

225. Hwang, W. Y. *et al.* Heritable and Precise Zebrafish Genome Editing Using a CRISPR-Cas System. *PLoS One* **8,** 1–9 (2013).

226. Postlethwait, J., Amores, A., Cresko, W., Singer, A. & Yan, Y. L. Subfunction partitioning, the teleost radiation and the annotation of the human genome. *Trends Genet.* **20,** 481–490 (2004).

227. Wallace, K. N. & Pack, M. Unique and conserved aspects of gut development in zebrafish. *Dev. Biol.* **255,** 12–29 (2003).

228. Hostetter, C. L., Sullivan-brown, J. L. & Burdine, R. D. Zebrafish Pronephros : A Model for Understanding Cystic Kidney Disease. *Dev. Dyn.* **228,** 514–522 (2003).

229. Rosen, J. N., Sweeney, M. F. & Mably, J. D. Microinjection of Zebrafish Embryos to Analyze Gene Function. *J. Vis. Exp.* **1,** e1115 (2009).

230. Bill, B. R., Petzold, A. M., Clark, K. J., Schimmenti, L. a & Ekker, S. C. A primer for morpholino use in zebrafish. *Zebrafish* **6,** 69–77 (2009).

231. Corey, D. R. & Abrams, J. M. Morpholino antisense oligonucleotides: tools for investigating vertebrate development. *Genome Biol.* **2,** reviews 1015.1-1015.3 (2001).

232. Gerety, S. S. & Wilkinson, D. G. Morpholino artifacts provide pitfalls and reveal a novel role for pro-apoptotic genes in hindbrain boundary development. *Dev. Biol.* **350,** 279–289 (2011).

233. Kok, F. O. *et al.* Reverse genetic screening reveals poor correlation between Morpholino-induced and mutant phenotypes in zebrafish. *Dev. Cell* **32,** 97–108 (2015).

234. Rossi, A. *et al*. Genetic compensation induced by deleterious mutations but not gene knockdowns. *Nature* **524,** 230–233 (2015).

235. Timme-Laragy, A. R., Karchner, S. I. & Hahn, M. E. Gene knockdown by morpholino-modified oligonucleotides in the zebrafish model: applications for developmental toxicology. *Methdos Mol. Biol.* **889,** 51–71 (2012).

236. Morcos, P. A., Vincent, A. C. & Moulton, J. D. Gene Editing Versus Morphants. *Zebrafish* **12,** 319 (2015).

237. Detrich III, H. W., Westerfield, M. & Zon, L.I. *The Zebrafish: Cellular and Developmental Biology - Ch9* (Academic Press, Cambridge, 2010)

238. Paavola, J. *et al.* Polycystin-2 mutations lead to impaired calcium cycling in the heart and predispose to dilated cardiomyopathy. *J. Mol. Cell. Cardiol.* **58,** 199-208 (2013).

239. Le Corre, S., Eyre, D. & Drummond, I. A. Modulation of the Secretory Pathway Rescues Zebrafish Polycystic Kidney Disease Pathology. *J. Am. Soc. Nephrol.* **25,** 1749–1759 (2014).

240. Sun, Z. *et al.* A genetic screen in zebrafish identifies cilia genes as a principal cause of cystic kidney. *Development* **131,** 4085–4093 (2004).

241. Obara, T. *et al*. Polycystin-2 Immunolocalization and Function in Zebrafish. *Am. Soc. Nephrol.* **17,** 2706–2718 (2006).

242. Bisgrove, B. W., Snarr, B. S., Emrazian, A. & Yost, H. J. Polaris and Polycystin-2 in dorsal forerunner cells and Kupffer's vesicle are required for specification of the zebrafish left-right axis. *Dev. Biol.* **287,** 274–288 (2005).

243. Mangos, S. *et al.* The ADPKD genes pkd1a/b and pkd2 regulate extracellular matrix formation. *Dis. Model. Mech.* **3,** 354–365 (2010).

244. Essner, J. J., Amack, J. D., Nyholm, M. K., Harris, E. B. & Yost, H. J. Kupffer's vesicle is a ciliated organ of asymmetry in the zebrafish embryo that initiates left-right development of the brain, heart and gut. *Development* **132,** 1247–1260 (2005).

245. Ramu, Y., Xu, Y. & Lu, Z. Inhibition of CFTR Cl- channel function caused by enzymatic hydrolysis of sphingomyelin. *PNAS* **104,** 6448–6453 (2007).

246. Park, H. *et al.* A Soluble Sulfogalactosyl Ceramide Mimic Promotes D F508 CFTR Escape from Endoplasmic Reticulum Associated Degradation. *Chem. Biol.* **16,** 461–470 (2009).

247. Caohuy, H. *et al.* Activation of 3-phosphoinositide-dependent kinase 1 (PDK1) and serum- and glucocorticoid-induced protein kinase 1 (SGK1) by short-chain sphingolipid C4-ceramide rescues the trafficking defect of ΔF508-cystic fibrosis transmembrane conductance regulator (ΔF508-CFTR). *J. Biol. Chem*. **289,** 35953–35968 (2014).

248. Bartke, N. & Hannun, Y. A. Bioactive sphingolipids: metabolism and function. *J. Lipid Res.* **50,** S91–S96 (2009).

249. Gault, C. R., Obeid, L. M. & Hannun, Y. A. An overview of sphingolipid metabolism: From synthesis to breakdown. *Adv. Exp. Med. Biol.* **688,** 1–23 (2010).

250. Kim, Y. M., Park, T.-S. & Kim, S. G. The role of sphingolipids in drug metabolism and transport. Expert Opin. Drug Metab. *Exp. Opin. Drug Metab. Toxicol.* **9,** 319–331 (2013).

251. Rao, R. P. *et al.* Sphingolipid Metabolic Pathway: An Overview of Major Roles Played in Human Diseases. *J. Lipids* **2013,** 1–12 (2013).

252. Yamaji, T. & Hanada, K. Sphingolipid Metabolism and Interorganellar Transport: Localization of Sphingolipid Enzymes and Lipid Transfer Proteins. *Traffic* **16,** 101–122 (2015).

253. Kolter, T. & Sandhoff, K. Sphingolipid metabolism diseases. *Biochim. Biophys. Acta* **1758,** 2057–2079 (2006).

254. Ziobro, R. M. *et al.* Ceramide in cystic fibrosis. *Clin. Lipidol.* **8,** 681–692 (2013).

255. Bates, I. R. *et al.* Membrane Lateral Diffusion and Capture of CFTR within Transient Confinement Zones. *Biophys.* J. **91,** 1046–1058 (2006).

256. Kowalski, M. P. & Pier, G. B. Localization of cystic fibrosis transmembrane conductance regulator to lipid rafts of epithelial cells is required for Pseudomonas aeruginosa-induced cellular activation. *J. Immunol.* **172,** 418–425 (2004).

257. Vilela, R. M., Lands, L. C., Meehan, B. & Kubow, S. Inhibition of IL-8 release from CFTR-deficient lung epithelial cells following pre-treatment with fenretinide. *Int. Immunopharmacol.* **6,** 1651–1664 (2006).

258. Teichgraber, V. *et al*. Ceramide accumulation mediates inflammation , cell death and infection susceptibility in cystic fibrosis. *Nat. Med.* **14,** 382–391 (2008).

259. Guilbault, C. *et al.* Fenretinide corrects newly found ceramide deficiency in cystic fibrosis. *Am. J. Respir. Cell Mol. Biol.* **38,** 47–56 (2008).

260. Becker, K. A., Tümmler, B., Gulbins, E. & Grassmé, H. Accumulation of ceramide in the trachea and intestine of cystic fibrosis mice causes inflammation and cell death. *Biochem. Biophys. Res. Commun.* **403,** 368–374 (2010).

261. Kimmel, C. B., Ballard, W. W., Kimmel, S. R., Ullmann, B. & Schilling, T. F. Stages of embryonic development of the zebrafish. *Dev. Dyn.* **203,** 253–310 (1995).

262. Mullins, M. C. Microinjection Techniques : Injecting through the chorion. *Zebrafish* Course **August,** (2005).

263. Mendes, F. *et al.* Establishment and Characterization of a Novel Polarized MDCK Epithelial Cellular Model for CFTR Studies. *Cell Physiol. Biochem.* **16,** 281–290 (2005).

264. Navis, A. & Bagnat, M. Loss of cftr function leads to pancreatic destruction in larval zebrafish. *Dev. Biol.* **399,** 237–248 (2015).

265. Fagerberg, L. *et al.* Analysis of the Human Tissue-specific Expression by Genome-wide Integration of Transcriptomics and Antibody-based Proteomics. *Mol. Cell. Proteomics* **13,** 397–406 (2014).

266. Eaton, S. L. *et al.* Total Protein Analysis as a Reliable Loading Control for Quantitative Fluorescent Western Blotting. *PLoS One* **8,** 1–9 (2013).

267. Oliveira, I., Lopes, S. S. & Roxo-rosa, M. Sphingolipids in kidney cyst formation - Poster session at SINAL 2017 conference(2017).

268. Ogretmen, B. *et al.* Biochemical mechanisms of the generation of endogenous long chain ceramide in response to exogenous short chain ceramide in the A549 human lung adenocarcinoma cell line. Role for endogenous ceramide in mediating the action of exogenous ceramide. *J. Biol. Chem.* **277,** 12960–12969 (2002).

269. Mikłosz, A., Łukaszuk, B., Baranowski, M., Górski, J. & Chabowski, A. Effects of inhibition of Serine Palmitoyltransferase (SPT) and Sphingosine Kinase 1 (SphK1) on palmitate induced insulin resistance in L6 myotubes. *PLoS One* **8,** 1–9 (2013).

270. Favale, N. O., Santacreu, B. J., Pescio, L. G., Marquez, M. G. & Sterin-Speziale, N. B.

Sphingomyelin metabolism is involved in the differentiation of MDCK cells induced by environmental hypertonicity. *J. Lipid Res.* **56,** 786–800 (2015).

271. Yuan, S., Zhao, L., Brueckner, M. & Sun, Z. Intraciliary calcium oscillations initiate vertebrate left-right asymmetry. *Curr. Biol.* **25,** 556–567 (2015).

272. Field, S. *et al.* Pkd1l1 establishes left-right asymmetry and physically interacts with Pkd2. *Development* **138,** 1131–1142 (2011).

273. Wilschanski, M. & Novak, I. The cystic fibrosis of exocrine pancreas. *Cold Spring Harb. Perspect. Med.* **3,** 1–17 (2013).

274. Streets, A. J., Moon, D. J., Kane, M. E., Obara, T. & Ong, A. C. M. Identification of an N-terminal glycogen synthase kinase 3 phosphorylation site which regulates the functional localisation of polycystin-2 in vivo and in vitro. *Hum. Mol. Genet.* **15,** 1465–1473 (2006).

275. Wei, L. *et al.* Functional interaction between TRP4 and CFTR in mouse aorta endothelial cells. *BMC Physiol.* **1,** 3 (2001).

276. Noe, J. *et al.* CFTR regulation of intracellular pH and ceramides is required for lung endothelial cell apoptosis. *Am. J. Respir. Cell Mol. Biol.* **41,** 314–323 (2009).

277. Robert, R., Savineau, J.-P., Norez, C., Becq, F. & Guibert, C. Expression and function of cystic fibrosis transmembrane conductance regulator in rat intrapulmonary arteries. *Eur. Respir. J.* **30,** 857–864 (2007).

278. Sun, X. & Bonanno, J. Expression, localization, and functional evaluation of CFTR in bovine corneal endothelial cells. *Am. J. Physiol. Physiol.* **282,** C673–C683 (2002).

279. Peters, W., Kusche-Vihrog, K., Oberleithner, H. & Schillers, H. Cystic fibrosis transmembrane conductance regulator is involved in polyphenol-induced swelling of the endothelial glycocalyx. *Nanomed. Nanotech. Biol. Med.* **11,** 1521–1530 (2015).

280. Tousson, A., Tine, B. A. V. A. N., Naren, A. P., Shaw, G. M. & Schwiebert, L. M. Characterization of CFTR expression and chloride channel activity in human endothelia. *Am. J. Physiol. Cell Physiol.* **275,** C1555–C1564 (1998).

281. Totani, L. *et al.* Mechanisms of endothelial cell dysfunction in cystic fibrosis. Biochim. *Biophys. Acta.* **1863**, 3243-3253 (2017).